NAVAL POSTGRADUATE SCHOOL
Monterey, California

THESIS

Flow Visualization of Time-Varying Structural Characteristics of Dean Vortices in a Curved Channel

by

David Wayne Bella

December 1988

Thesis Advisor: Phillip M. Ligrani
Co-Advisor: Chelakara S. Subramanian

Approved for public release; distribution is unlimited.

REPORT DOCUMENTATION PAGE

1a REPORT SECURITY CLASSIFICATION UNCLASSIFIED	1b RESTRICTIVE MARKINGS
2a SECURITY CLASSIFICATION AUTHORITY	3 DISTRIBUTION/AVAILABILITY OF REPORT Approved for public release; distribution is unlimited
2b DECLASSIFICATION/DOWNGRADING SCHEDULE	
4 PERFORMING ORGANIZATION REPORT NUMBER(S)	5 MONITORING ORGANIZATION REPORT NUMBER(S)
6a NAME OF PERFORMING ORGANIZATION Naval Postgraduate School 6b OFFICE SYMBOL (If applicable) Code 69	7a NAME OF MONITORING ORGANIZATION
6c ADDRESS (City, State, and ZIP Code) Monterey, California 93943-5000	7b ADDRESS (City, State, and ZIP Code) Monterey, California 93943-5000
8a NAME OF FUNDING/SPONSORING ORGANIZATION 8b OFFICE SYMBOL (If applicable)	9 PROCUREMENT INSTRUMENT IDENTIFICATION NUMBER MIPR No. C-80019-F
8c ADDRESS (City, State, and ZIP Code) U.S. Army Aviation Res & Tech Activity AVSCOM NASA-Lewis Res. Center, Cleveland 45433	10 SOURCE OF FUNDING NUMBERS PROGRAM ELEMENT NO / PROJECT NO / TASK NO / WORK UNIT ACCESSION NO.

11 TITLE (Include Security Classification)

Flow Visualization of Time-Varying Structural Characteristics of Dean Vortices in a Curved Channel

12 PERSONAL AUTHOR(S) BELLA, David Wayne

13a TYPE OF REPORT	13b TIME COVERED	14 DATE OF REPORT (Year, Month, Day)	15 PAGE COUNT
Master's Thesis	FROM _____ TO _____	1988 December	110

16 SUPPLEMENTARY NOTATION
The view expressed in this thesis are those of the author and do not reflect the official policy or position of the Department of Defense or the U. S. Government

17 COSATI CODES			18 SUBJECT TERMS (Continue on reverse if necessary and identify by block number)
FIELD	GROUP	SUB-GROUP	Visualization, Dean Vortices, Centrifugal Instabilities, Rocking motion

19 ABSTRACT (Continue on reverse if necessary and identify by block number)

The time varying development and structure of Dean vortices were studied using flow visualization. Observations were made over a range of Dean numbers from 40 to 200 using a transparent channel with mild curvature, 40:1 aspect ratio, and an inner to outer radius ratio of 0.979. Seven flow visualization techniques were tried but only one, a wood burning smoke generator, produced usable results. Different vortex characteristics were observed and documented in sequences of photographs spaced one quarter of a second apart at locations ranging from 85 to 135 degrees from the start of curvature. Evidence is presented that supports the twisting/rocking nature of the flow.

20 DISTRIBUTION/AVAILABILITY OF ABSTRACT ☒ UNCLASSIFIED/UNLIMITED ☐ SAME AS RPT ☐ DTIC USERS	21 ABSTRACT SECURITY CLASSIFICATION UNCLASSIFIED
22a NAME OF RESPONSIBLE INDIVIDUAL Professor Ligrani	22b TELEPHONE (Include Area Code) (408) 646-3382 22c OFFICE SYMBOL 69Li

DD FORM 1473, 84 MAR 83 APR edition may be used until exhausted
All other editions are obsolete

SECURITY CLASSIFICATION OF THIS PAGE
UNCLASSIFIED

Approved for public release; distribution is unlimited.

Flow Visualization of Time-Varying Structural Characteristics of Dean Vortices in a Curved Channel

by

David Wayne Bella
Lieutenant, United States Navy
B. S., University of California, Riverside, 1978

Submitted in partial fulfillment of the requirements for the degree of

MASTER OF SCIENCE IN MECHANICAL ENGINEERING

from the

NAVAL POSTGRADUATE SCHOOL
December 1988

Author: David Wayne Bella
David Wayne Bella

Approved: Phillip M. Ligrani
Phillip M. Ligrani, Thesis Advisor

C Subramanian
Chelakara S. Subramanian, Co-Advisor

Anthony J. Healey
Anthony J. Healey, Chairman,
Department of Mechanical Engineering

G E Schacher
Gordon E. Schacher, Dean of
Science and Engineering

ABSTRACT

The time varying development and structure of Dean vortices were studied using flow visualization. Observations were made over a range of Dean numbers from 40 to 200 using a transparent channel with mild curvature, 40:1 aspect ratio, and an inner to outer radius ratio of 0.979. Seven flow visualization techniques were tried but only one, a wood burning smoke generator, produced usable results. Different vortex characteristics were observed and documented in sequences of photographs spaced one quarter of a second apart at locations ranging from 85 to 135 degrees from the start of curvature. Evidence is presented that supports the twisting/rocking nature of the flow.

TABLE OF CONTENTS

LIST OF FIGURES

ACKNOWLEDGEMENT

This work was sponsored by AVSCOM (The U.S. Army Aviation Research and Technology Activity) through the Lewis Research Center of NASA, MIPR Grant No. C-80010-F. Dr. Kestitus C. Civinskas was the program monitor.

I would like to express my sincere gratitude to those who supported me throughout this endeavor. My two thesis advisors were always there for me. Professor Ligrani provided me with guidance and encouragement. Professor Subramanian's quiet reassurance and willingness to talk things out, helped me through the rough spots. The Mechanical Engineering shop personnel, specifically, Tom McCord, Charles Crow and Jim Schofield always were there with excellent craftmanship. The Educational Media Department's Photographic Division personnel, specifically Andy Sarakom and Mitch Nichols were outstanding in their support and quick turn-around times, without which completion of this thesis would have been nearly impossible. Finally, to my wife Lynn, whose love, patience and ability to keep things in perspective made this work possible. To you Lynn I can never find the words to say how truely grateful I am.

I. INTRODUCTION

A. BACKGROUND

A study was made of counter-rotating vortices which form as a result of centrifugal instabilities. The centrifugal instabilities were induced in a 40 to 1 aspect ratio curved channel with mild streamwise curvature. Of interest here is the influence of concave curvature on the flow and the resulting vortex pairs as well as their subsequent affects on boundary layer structure and the initiation and development of transition from laminar to turbulent flow. Understanding the nature of these vortices and their impact is expected to lead to design improvements for heat exchangers, gas turbine blade cooling configurations, and other components where concave curvature has an important influence on flow behavior.

Figure 1 [Ref. 1] shows the secondary flow from the vortices in the curved channel. The structure and time varying development of these vortices at different

channel Reynolds numbers, $RE_c = Ud/\nu$, was investigated using flow visualization techniques. A specially designed transparent channel was used to view flow structure at different streamwise locations and at varying Dean numbers.

W. R. Dean [Ref. 2] first analyzed flow in a curved channel in 1928. From this study, he determined that the magnitude of the concave wall curvature was the major factor in the formation and development of flow instabilities. The magnitude of curvature is expressed as a dimensionless parameter which is now called the Dean number, De. The Dean number is the product of the channel Reynolds number, Re_c, and the radius ratio $\sqrt{d/r_i}$ such that $De = Re_c, \sqrt{d/r_i}$. Here, U is the mean streamwise velocity, d is the channel height, is the kinematic viscosity and r_i is the radius of curvature of the convex channel surface. Dean found that, channels having $r_i/r_o \sim 1$, flow is unstable to small disturbances if the Dean number is greater than 35.92. Dean's work was verified by the further analytical work of Reid [Ref. 3] and Hammerlin [Ref. 4] and by experimental study of Brewster et al., [Ref. 5].

For flows in a rectangular curved channel with Dean numbers less than 35.92 the flow is entirely azimuthal and is known as curved channel Poiseille flow (CCPF).

For Dean numbers greater than this critical value, the flow becomes non-azimuthal due to centrifugal forces imposed by the concave curvature. Fluid particles at the center of the flow move with higher velocities than particles closer to either wall and thus are subjected to greater centrifugal forces. These high velocity and centrifugally unstable particles displace the fluid near the concave wall. The particles originally occupying the concave surface are moved, first in a spanwise direction and then normal to and away from the wall. This process is continually repeated, resulting in spanwise periodic regions of high and low speed flow which eventually form into pairs of counter-rotating vortices. Today these are known as Dean vortices.

The works previously cited by Dean, Reid and Hammerlin, were focused on flows between concentric cylinders. Studies by Cheng et al., [Ref. 6] have shown the effect of low aspect ratios (breath to depth up to 12) on the curved channel flow. To date, little work has been done to study flows in large aspect ratio curved channels. The first published experimental work was by Kelleher et al., [Ref. 7]. The results of this experiment show spanwise velocity traces from the concave side of the midplane of the channel which are 180 degrees out of phase with velocity

traces from the convex side of the midplane of the channel. Results are presented for Dean numbers ranging from 79 to 113.

Numerical simulations of curved channel flow with geometry similiar to the Kelleher experiment were performed by Finlay et al., [Ref. 8, 9] using the three-dimensional, incompressible Navier-Stokes equations. Some results of this simulation were verified by the flow visualization work of Ligrani and Niver [Ref. 10] and Niver [Ref. 11]. The channel used in this study had a 40 to 1 aspect ratio and a radius ratio of 0.979. The channel was geometrically similar but twice the size of the channel used by Kelleher et al., [Ref. 7]. These investigators found generally symmetric vortex pairs in the range of Dean numbers 40 to 100. For Dean numbers greater than 160, the vortices were non-symmetric with a twisting mode of oscillation. For all cases, the behavior of the vortex pairs depended upon the radial location from the start of curvature and the Dean number. The curved channel used in this study was also used by Siedband [Ref. 12] and Baun [Ref. 13]. These two investigators used flow visualization techniques to study Dean Vortes structure and development. Baun [Ref. 13] also made velocity surveys, vorticity surveys, and measured spectra of hot-wire voltage signals.

In the present study, smoke was introduced into the channel allowing flow patterns to be photographed at specific and preset time intervals in order to document the time varying aspect of flow structure development. The present study expands upon previous works in order to obtain a better understanding of the time sequence of the events in the channel. Measurements were made for Dean numbers varying from 40 to 200 and angular positions from the start of curvature ranging from 85 to 135 degrees.

As a continuing study, the effects of these Dean vortices on heat transfer characteristics is also pursued. To that end, some initial setup and calibration tests were performed on heat transfer surfaces to be used in a second curved channel.

B. OBJECTIVES

The objectives of this thesis are:

a. Provide extensive photographic evidence of visualized flow patterns as they vary with time in the curved channel as a function of the radial location and Dean number.

b. To conduct contact resistance measurement and conductance loss calibration for heat transfer surfaces for a second curved channel to be used for heat transfer measurements.

C. ORGANIZATION

Subsequent to this introduction, Chapter II discusses experimental facilities and procedures. Chapter III presents the results of the flow visualization tests and compares the results with other works. Chapter IV details the procedures and results for the measurement of the contact resistance and conduction loss for the heat transfer surfaces to be used in a second curved channel. Chapter V presents conclusions and recommendations.

II. EXPERIMENTAL APPARATUS AND PROCEDURES

A. RECTANGULAR CURVED CHANNEL

The rectangular curved channel used in this study is shown schematically in Figure 2 [Ref. 11]. Front and side photographs of the channel are presented in Figures 3 and 4, respectively. This apparatus was specifically designed and constructed for flow visualization studies, and is part of the laboratory facilities of the Department of Mechanical Engineering of the Naval Postgraduate School. Niver [Ref. 11], Siedband [Ref. 12] and Baun [Ref. 13] present the details of the design and construction of the facility. To ensure completeness, a discussion of the curved channel is also presented here.

A one-third horsepower blower is used to create a pressure lower than atmospheric inside plenum number two [Fig. 2]. This low pressure plenum is connected to the outlet plenum via a 5.08 cm diameter pipe. Throttling of the flow and mass flow measurement is accomplished by a globe valve and an orifice plate, respectively. Both devices are located in the connecting pipe.

After being drawn into the channel at the inlet, the air passes through a flow management section. This section consists of an aluminium honeycomb and three successive screens, whose purpose is to reduce the spatial non-uniformities of the flow. This results in a more stable laminar flow. Immediately, following the flow management section is a 20:1 contraction ratio nozzle which serves to accelerate the flow. The nozzle also serves to reduce spatial non-uniformities by inducing longitudinal strain. After the nozzle, the flow enters a 2.44 m long straight and transparent duct constructed of a polycarbonate material (commercial name, Lexan). With this length, the flow is fully developed prior to the curved section for Dean numbers up to 640 [Ref. 10]. The convex wall of the curved duct has a radius of 59.69 cm and a concave wall radius of 60.96 cm. These radii are maintained by traverse and longitudinal supports. These supports maintain the cross sectional area at 1.27 cm by 50.8 cm (0.5 in. X 20 in.) within $\pm$ 0.015 cm for channel depth and $\pm$ 0.05 cm for channel width [Ref. 10]. Exiting the curved section, the flow enters another 2.44 m long straight duct and then another screen and honeycomb system, followed by an outlet plenum.

B. SELECTION OF SMOKE SOURCE

In the course of this study, a total of seven different sources of smoke were tried prior to final selection. These consisted of (1) cigars and cigarettes, (2) incense of both stick and conical form, (3) a helium bubble generator, (4) a theatrical fog-fluid machine manufactured by Roscoe, (5) a second commercial device called Cloudmaker, manufactured by Testing Machines Inc., which vaporizes mineral oil, (6) a device which produces a vapor from dry ice (solid CO_2) and (7) a wood burning device. The wood burning device was finally selected. The first two methods, cigars, cigarettes and incense were impractical due to the limited amount of smoke produced relative to the dimensions of the channel. The helium bubble generator was not used because the quantity of bubbles was insufficient, and the optical density of the bubbles did not allow for sufficient contrast.

The remaining smoke sources were not as easily dismissed. The first commercial smoke generator tried was the Roscoe theatrical fog fluid machine used by Baun [Ref. 13]. Numerous problems were encountered with the vapor produced by this device. The main problem was the deposition of fluid droplets on the inside walls of the channel. In addition three other problems were noted.

First, the pump action of the machine at low flow rates was sufficient to disturb the flow. Second, fluid droplets had a wide variety of sizes and only the smaller ones were entrained by the flow. The last problem encountered with this system was the optical quality of the smoke. Despite numerous camera settings and lighting combinations, satisfactory photographs of the vapor patterns were difficult to obtain.

The second commercial smoke generator, Cloudmaker by Testing Machines Inc. was not used due to mechanical problems. These problems consisted of oil leaks which occasionally resulted in small fires within the apparatus. Both the quantity and optical characteristics of smoke were promising, but the device never operated over a long enough period to be useful.

The solid CO_2 (dry ice) system consisted of a sealed container of water in which the dry ice was allowed to sublimate. The container was heated to encourage sublimation. The major drawback to this system was the large amount of condensation which occurred on the inner walls of the channel for Dean numbers less than 200. For higher Dean numbers less condensation seemed to be present.

The last method investigated was the burning of wood chips. The chips were either Mesquite or Hickory. The burning of these resulted in a dense white smoke which was then cooled. The drawback to this system was the odor introduced into the lab and a buildup of soot on channel walls. The film deposited on the walls of the channel was not as thick and more uniform than any of the other methods. The smoke was also believed to be the least disruptive to the flow because its density was close to that of air. This was the smoke generation system chosen for this study. Additional details are given in the next section.

C. SMOKE GENERATION SYSTEM EMPLOYED

The smoke generator selected was the same as the one used by Ligrani and Niver [Ref. 10], Niver [Ref. 11] and originally by Morrison [Ref. 14]. Figure 5 [Ref. 11] shows a schematic. The system consists of a vertical, 3 inch diameter, 16 inch long steel pipe forming a combustion chamber in which wood chips are burned. The top of the pipe is sealed by a flange from which a 1 inch pipe extends. The piping serves to channel the smoke to a sealed glass jar where combustion particles and water vapor are removed. The smoke is then cooled

in two standard Pyrex 24/40 glass distillation tubes which use water as the cooling medium. After being cooled the smoke is ducted, via rubber tubing to a smoke rake located at the curved channel inlet. A vent valve in the tubing allows for regulation of the amount of smoke introduced into the channel. Combustion was initiallized by a nichrome heating coil in the combustion chamber base. Alternatively, combustion could be induced by burning alcohol, but for safety reasons use of this method was minimized. After the wood begins to burn from the coil, a high rate of combustion and smoke flow are maintained. Runs made without a coil produced less smoke than those made with the coil energized. Compressed air at 4-5 psig is also supplied to ensure combustion and to force the smoke through the system. Small chips of Mesquite wood were used as fuel since it produces a dense white smoke. The small size of the chips was important to maximize the surface area exposed to air. When larger wood chunks were employed, less smoke was produced. Hickory wood chips that had been soaked in water for 15 minutes prior to burning were also occasionally, used in the smoke generator.

D. LIGHTING AND PHOTOGRAPHY

Visual observations of the flow were made using the technique of Ligrani and Niver [Ref. 10] and Niver [Ref. 11]. A focused light source was aimed at a 2 mm X 46.0 mm slit in a black construction paper liner which covers the outside of the convex part of the channel surface. Each slit is located 5 cm off channel center-line on either side. The liner serves to minimize reflections and stray light.

Photographs of the radial spanwise plane were taken with the same equipment as Niver [Ref. 11], but with a slightly modified approach. The primary difference between his study and the present one was that pictures were taken using a manual drive mode for the camera in order to obtain photos in sequence spaced at equal time intervals. In both studies, KODAK TRI-X 400 film was used. The camera used was a Nikon F3 body with a 55 mm, f2.8 lens. Attached to the camera body was a Nikon MD-4 motor drive and a Nikon SB-16 zoom flash. All photographs were taken in sequence at a rate of four frames a second, the maximum speed of the motor drive.

Figure 6 [Ref. 10] shows how the camera and flash were orientated with respect to the channel. Photos were taken with the camera pointed in the downstream

direction. In doing so, the camera was mounted on a tripod and the flash replaced the light source used for visual observation. Photographs with high contrast and sharp detail were obtained with the following camera and flash settings: aperture of f4.0, shutter speed of 30, and ASA of 400, flash set to motor drive mode and the flash zoom head to the "T" or 85 degree position. The flash was located four inches from the convex channel wall, and focused on the individual slit openings in the liner attached to the outside of the convex wall.

E. DEAN NUMBER DETERMINATION

Mass flow and Dean number were determined using procedures similar to those of Baun [Ref. 13]. Those procedures are presented here.

The pressure measurement system consisted of an electrical pressure transducer and a small scale water manometer connected in parallel. A Celesco model LCVR variable reluctance differential pressure transducer was connected to tubing leading from the pressure taps on each side of an ASME 1.5 in. orifice plate. A Meriam Model 40G010 WM 1.27 cm horizontal manometer was "T" connected in parallel to the transducer to provide a means to calibrate the transducer and to verify its

output. A final check on the accuracy of the calibration coefficient is given by reading the manometer presssure during the run and comparing it to the computer determined value for the orifice differential pressure. The range of these Celesco transducers is 0-2 cm of water. Celesco DC10D carrier demodulators are used to convert the transducer electrical output to DC voltage.

The transducer/demodulator system was calibrated by first adjusting the zero such that the output with no applied pressure was less than .01 volts. This offset voltage was determined from the average of 100 samples recorded by the data acquisition system, and then included in later data reduction. Next, a calibration coefficient was determined. This coefficient is the ratio of the manometer pressure and the difference between the average voltage and the offset voltage. With the blower running, the manometer pressure was entered and the coefficient calculated. This procedure was repeated five times and averaged to reduce experimental uncertainty at each anticipated flow rate. A final check on the accuracy of the calibration coefficient was made by reading the manometer pressure during the run and comparing it to the computer determined value for the orifice differential pressure.

The flow was allowed to stablize for five minutes before the Dean number was calculated after each flow rate adjustment. With the flow stabilized, smoke was then introduced into the channel. The smoke layer in the channel was allowed to build slowly until approximately the bottom half of the inlet nozzle was filled. When the smoke was visible in the curved section of the channel, six photographs were taken in sequence. The camera was then relocated so that a survey of different streamwise locations was completed as the Dean number was held constant.

The signal from the transducer/demodulator is sent to a Hewlett-Packard Series 300, Model 9836S computer via a HP3498A extender which is in turn controlled by a HP3497 data acquisition/control unit. The sensitivity of the HP3497A digital voltmeter is 1μV. The sampling rate is approximately 5 HZ. Actual calculation of Dean number is accomplished by a HP Basic program, called "DEAN", used by Baun [Ref. 13]. This program calculates the density of air from ambient temperature and pressure readings and the perfect gas relationship. The expansion coefficient,

Y, is calculated from Holman and Gajda [Ref. 15]. A first guess at the Dean number is made by interpolating pressure drop versus Dean number data from Niver [Ref. 11; p. 33]. From this initial guess of a mass flow rate, the pipe Reynolds number, Re_p, is calculated using

$$Re_p = \dot{m} d_p / \rho \nu A$$

Where $\dot{m}$ is the mass flow rate, d is the diamerer, A is the cross-sectional area. The subscript p indicates the measured parameters of the pipe. The flow coefficient, K, is then interpolated from ASME Tables [Ref. 16]. The mass flow is then updated using

$$\dot{m} = K A_{or} Y \sqrt{2 \rho \Delta P_{or}}$$

Here the subscript or indicates parameters measured at the orifice. This iterative process is continued until the mass flow rate converges to a variation not greater than one percent for two successive calculations. The program finally concludes by calculating the Dean number using an equation of the form

$$De = (\dot{m} / \rho A_{ch}) \; X \; (d / \nu) \; X \sqrt{d / r_i}$$

III. FLOW VISUALIZATION

Photographs showing smoke patterns over a range of Dean numbers at different streamwise locations are presented. For each experimental condition, all photographs were taken in sequence 0.25 seconds apart. In each figure, photographs are placed such that time increases moving down the page.

The top of each photo depicts the convex wall of the channel. A centimeter scale was taped to the outer part of the concave wall and appears at the bottom of the picture. Photographs always show the flow moving downstream (away from the observer). The illuminated field of view is 1.27 cm by 4.6 cm with the spanwise direction horizontal and the radial direction vertical. All photographs were taken on the left hand side of the channel, except where noted. In these photographs the right hand side of each picture is located 5.08 cm off the channel centerline. Table I is a summary of the photos taken. In the majority of cases, less than one minute was required to relocate and refocus the camera as photographic sequences at different streamwise locations were obtained.

TABLE I. PHOTOGRAPHIC SURVEY RESULTS

Dean Number	85 Degrees	95 Degrees	105 Degrees	115L Degrees	115R Degrees	125 Degrees	135 Degrees
40			Fig. 7	Fig. 8		Fig. 9	
60	Fig. 10	Fig. 11	Fig. 12	Fig. 13	Fig. 14	Fig. 15	Fig. 16
80	Fig. 17	Fig. 18	Fig. 19	Fig. 20	Fig. 21	Fig. 22	
100	Fig. 23	Fig. 24	Fig. 25	Fig. 26	Fig. 27	Fig. 28	Fig. 29
120	Fig. 30	Fig. 31	Fig. 32	Fig. 33		Fig. 34	Fig. 35
141	Fig. 36	Fig. 37	Fig. 38	Fig. 39	Fig. 40	Fig. 41	Fig. 42
160	Fig. 43	Fig. 44	Fig. 45	Fig. 46			
170	Fig. 47	Fig. 48	Fig. 49				
180	Fig. 50	Fig. 51	Fig. 52				
201	Fig. 53	Fig. 54	Fig. 55				

Figures 7, 8, and 9 present sequences of photographs taken at De=40 at locations of 105, 115, and 125 degrees from the start of curvature, respectively. All of these show the presence of a smoke layer near the convex surface. The layer exists in the way because smoke was injected at the bottom half of the channel inlet. It then remained in the bottom half of the straight section. As smoke then entered the curved section, the majority of it remained near the convex wall. In Figures 7-9, there is no evidence of vortices, even though the Dean number was greater than the critical value of 36. A careful examination of the patterns was necessary at these low Dean numbers not to misinterpret a buoyant smoke effect.

Evidence of vortex motion is indicated in Figure 10 which presents a sequence of photos taken at De=60 and at a streamwise location 85 degrees from the start of curvature (θ). Semicircular shaped patterns are present which show movement in the radial and spanwise directions as time increases. Further, the shapes do not occupy the full channel width. Figures 11-16 follow the flow in the streamwise direction at the same Dean number for θ locations of 95, 105, 115, 125, and 135 degrees. By the time the flow has reached the 95 degree location [Fig. 11], mushroom shaped smoke patterns provide evidence of

intermittently present Dean Vortex pairs. These patterns form as a result of the spanwise variation caused by the upwash and downwash regions associated with pairs of counter-rotating vortices. The upwash from the concave surface to the convex surface results in the stem of the mushroom shape. Figure 12 shows the conditions which exist at the 105 degree location for De=60. Here no clear vortex pairs are visible, and both radial and spanwise movement are seen. Well developed vortex pairs are present and exhibit a rocking motion at the 115 degree location [Fig. 13, 14]. Less spanwise motion is seen at the 125 degree location [Fig. 15]. At the 135 degree location, vortex pairs are well developed, occupy full channel width, and have virtually no spanwise movement [Fig. 16].

If the Dean number is increased to 80, photographic results such as the ones shown in Figures 17-22 are obtained. Similar phenomena are present as observed for De=60, except that the Dean vortices seem to be present at θ as small as 85 degrees. By the time the flow reaches the 115 degree location [Fig. 20, 21], the shapes are spanwise periodic and relatively stable.

Figures 23 through 29 were obtained at De=100. At 85 degrees [Fig. 23] semicircular patterns appear which are relatively stable in the spanwise direction, yet vary in height from one half to three quarters of the channel width. At the 95 degree location [Fig. 24], the patterns occupy more of the channel width, and mushroom-shaped smoke patterns are occasionally visible. This sequence also shows significant movement in the spanwise direction which reverses itself within three frames (0.75 seconds). Figure 25 shows the conditions which exist at the 105 degree location for De=100. Here, the patterns are seen to have less uniform spacing in the spanwise direction, probably because of the periodic appearance of additional secondary vortex pairs near the concave surface. At the 115 degree location [Fig. 26, 27], the mushroom shapes are clearly visible, and occupy the full channel height with spanwise movement. This movement includes distortion of the stem as it periodically leans from left to right with spanwise displacement of the corresponding vortex pair. In Figure 28, where results from the 125 degree location are shown, this motion becomes more pronounced. Here, well defined vortex pairs exist, which show so much movement that pairs are barely discernable. The final frame in the sequence again captures a set of

well defined vortex pairs. Figure 29 for Θ =135 degrees provides evidence of vortex pairs with the maximum amount of movement observed in the present study for a Dean number equal to 100.

Figures 30-35 show sequences of photographs taken at De=120. Vortex pairs are visible and occupy most of the channel width as early as the 85 degree location [Fig. 30]. The vortex pairs occupy the full channel width and show both radial and spanwise movement at the 95 degree location [Fig. 31]. At the 105 degree location [Fig. 32], four to five vortex pairs are generally present in each field of view. Figure 33 shows mushroom patterns with significant distortion. This distortion increases for the 125 degree [Fig. 34] and 135 degree [Fig. 35] locations, however, vortex pairs are still visible.

Photographs of flow characteristics of De=141 are shown in Figures 36-42. Figure 36 shows that the vortex pairs are fully developed and occupy the full channel width at the 85 degree location. The smoke patterns show evidence of spanwise movement. Rocking motion is evident for the center vortex pair in all frames of Figure 37, which shows results for 95 degree location. At the 105 degree location [Fig. 38] the rocking motion is evident in all vortex pairs, in all frames. This is evidence of

twisting Dean vortex flow. Figure 39 for Θ =115 degrees and the left side of the channel shows less spanwise movement than previously seen at lesser angular positions. The rocking motion has decreased at the 115 degree right location [Fig. 40]. Here, the spacing between vortex pairs has also decreased. At the 125 degree [Fig. 41] location the rocking motion has returned and at the 135 degree location [Fig. 42] the rocking motion is further amplified.

Figures 43-46 show conditions for De=160. Results for the 85 degree location are given in Figure 43, which shows evenly spaced semicircular regions that occupy the full channel height. There is little spanwise motion. At the 95 degree location [Fig. 44], rocking is clearly shown by the changing inclination of the stem of the left most vortex pair. Vortex pairs seem to have increased in spanwise width over those seen at the 85 degree location. Photographs in Figure 46 show significant motion and distortion of smoke patterns compared to those seen at smaller Θ .

Sequences of photographs presented in Figures 47-49 were taken at De=170. The semicircular regions seen at Θ=85 degrees [Fig. 47], increase in size at the 95 degree location [Fig. 48]. At the 105 degree location [Fig. 49], spanwise rocking can be seen.

De=180 results are shown in Figures 50-52, where the same phenomena are present as observed for De=170. The main difference is that phenomena are occurring at smaller streamwise angular positions. In all photographs spanwise rocking movement can be seen. At the 85 degree location [Fig. 50] there is also some radial movement in addition to the rocking motion.

Photographs of flow characteristics at De=201 are shown in Figures 53-55. At Θ =85 degrees [Fig. 53] both spanwise and radial movement can be seen. For a Θ of 95 degrees [Fig. 54], the patterns occupy full channel height and show evidence of rocking.

IV. CURVED HEAT TRANSFER CHANNEL

This section describes the qualification of the heat transfer surfaces used in a second curved channel designed and constructed for heat transfer studies. This new apparatus is dimensionally similar to the channel used for flow visualization, but has heat transfer surfaces applied to both walls of the straight and curved portions of the channel. The channel was designed and constructed to allow for thermal expansion resulting from the heated test sections.

Qualification tests were conducted consisting of: (1) conduction heat loss measurements and (2) contact resistance measurements. To facilitate the tests, a full scale model of the curved heated section was constructed. This model consisted of a wooden framework which supported curved heat transfer surfaces developed especially for these qualifications tests. The arrangement of components within each heat transfer surface is shown in Figure 56 [Ref. 17; Fig. 232]. Tests were also conducted with the surface layed out flat and outside of the curved support section to simulate the arrangement used for the straight inlet portion of the channel.

The thin foil heaters that comprise the heat transfer surfaces are designed to provide uniform heat flux boundary conditions to the walls of the channel. With the thermocouples attached beneath the Lexan surface of the channel interior, temperatures of the channel walls can be measured and the convective heat transfer coefficients determined.

A. CONDUCTION LOSS PROCEDURES AND RESULTS

Under ordinary operating conditions, with the flow in the channel, the backs of the heat transfer surfaces are insulated. The purpose of performing an energy balance is to determine the conductive heat loss through this insulation for normal operating conditions. To do this, the heater is turned on and the side which would ordinarily be exposed to the convective environment is covered with three layers of foam insulation. Thermocouples are then placed between the layers to determine the heat transfer through these layers. Thus, the front surface which is normally subject to a convective environment had the insulation applied for purposes of the energy balance test.

With the temperature difference between the three layers of foam insulation, heat transfer via conduction could be estimated. A one-dimensional form of Fourier's conduction equation was used for this purpose.

$$q_w = KA\ (\Delta T/\Delta X)$$

For the insulation, K=.04 $W/m^2\ ^\circ C$, A=0.5806 m^2, Δ X=0.0254 m and ΔT is the temperature drop in the X direction in $^\circ C$. Measurement of all temperatures necessary for this test were made using copper-constantan thermocouples, manufactured by Omega Engineering Inc. The thermocouples measuring the wall temperature of the heat transfer surface were from the same batch as those installed in the curved heat transfer channel itself. These thermocouples were calibrated with a quartz crystal thermometer. The results of the calibration test yielded a polymonial of the form

$$T_w = -(1.30903E^3) + 4.63671E^2 + 19.45009E + 2.29788$$

Here, T_w is the Lexan surface temperature and E is 1000 times the input voltage measured in millivolts by the thermocouple. The thermocouples used to measure the

temperatures between the layers of foam insulation and the ambient temperature ($T_{ambient}$) were manufactured of larger diameter wire and had a different calibration polynomial

$$T = 1.05678E^3 - 6.00904E^2 + 34.14124E - 3.59415$$

Conduction through the insulation mounted behind the test surface (used under normal conditions) was then measured as a function of ($T_w - T_{ambient}$) using

$$q_c = VI - q_w$$

Here, the power into the test surface is VI and q_w is the conduction loss through the front insulation. Tests were conducted to achieve the same levels of q_c encountered during normal operation, 6-25 watts.

Figure 57 plots the combined results of both straight and curved section tests in the form of q_c versus $T_w - T_{ambient}$. A second order polynomial was then fitted to this data in order to predict conduction losses during heat transfer measurements.

$$q_c = -0.0294 + 0.4222(T_w - T_{ambient}) - 0.0015(T_w - T_{ambient})^2$$

This equation is valid for a temperature range of 10-20 °C. When exposed to convection in the curved channel, conduction losses are less than three percent of the total power. Therefore, a 25 percent error in the estimate of the conduction losses will cause less than 1/2 percent error in the total estimate of the heat transfer by convection.

B. CONTACT RESISTANCE PROCEDURES AND RESULTS

Thermocouples were attached to the test surface using a method similar to the one used by Schwartz [Ref. 17]. Because the thermocouples were in mechanical contact with the foil heater, a thermal contact resistance, CR, exists between the foil heater and the thermocouples. The temperature difference, ΔT, between the actual surface and that measured by the thermocouples is then given by

$$\Delta T = q''_w \, (CR)$$

where CR is the thermal contact resistance in $^\circ Cm^2/watt$. The experimental procedures used to determine CR are now described.

Surface temperatures were determined using Chameleon encapsulated liquid crystals applied to the test surface. The crystals were manufactured by the Appleton Papers

Division of NCR with a range of 41 to 46 °C. To create a convective environment a household fan was used to cool the heated test section. An average power input of 288 watts generated a surface temperature of 45 °C, with $T_w - T_\infty = 25$ °C. At this power level an average of 1.5 °C difference was noted between the temperature recorded by the thermocouples and that indicated by the liquid crystals (ΔT). The temperatures of the liquid crystals were determined from visual observations. For consistancy the same observer determined the color changes of the crystals on the heat transfer surface as well as color changes of the crystals when they were calibrated using a liquid bath of known temperature.

To determine the contact resistance, the convective heat flux was first estimated using

$$q_w = IV - q_c - q_r$$

and

$$q''_w = (q_w/A)$$

Here $A = 0.5806 m^2$, the surface area of the heater, q_w is the convective heat transfer at the wall and q_r is the radiation heat transfer from the surface. Next the contact resistance follows from $CR = \Delta T/q''_w$

The results of the contact resistance measurements are presented in Table II. A forced convective environment was used for all runs except for the first listed in Table II, which accounts for its higher value of CR. Disregarding the first run, the average of the contact resistance is $3.4 \times 10^{-3}\,^{\circ}Cm^2/Watt$. The values obtained for the curved section were slightly lower than those for the straight section. The present value for the contact resistance is less than 40 percent of the value reported by Joseph [Ref. 18]. This can be attributed to the fact that Joseph used foil next to the convective field, whereas a Lexan sheet was used in the present study.

TABLE II. CONTACT RESISTANCE RESULTS

Surface Geometry	Power (Watts)	q_c (Watts)	q_w (Watts)	$T_{t.c.}$ (°C)	$T_{L.C.}$ (°C)	T_∞ (°C)	CR ($^\circ Cm^2$/Watt)
Curved	298.9	9.47	289.43	45.6	43.55	24.67	4.10×10^{-3}
Curved	298.9	9.26	289.64	45.04	43.35	24.06	3.38×10^{-3}
Curved	288.0	9.81	278.19	44.97	43.40	25.64	3.28×10^{-3}
Flat	237.6	8.54	229.0	43.70	42.34	22.03	3.45×10^{-3}
Flat	257.6	9.80	247.8	44.87	43.39	20.19	3.46×10^{-3}

V. SUMMARY AND CONCLUSIONS

The time varying structural characteristics of Dean vortices in a curved channel were studied using flow visualization techniques. Of seven flow visualization techniques employed, only the wood burning smoke generator yielded satisfactory results for use in a large aspect ratio curved channel.

Photographs of visualized patterns were obtained for Dean numbers from 40 to 200, and streamwise angular locations from 85 to 135 degrees. These Dean numbers corresponded to mean velocities ranging from 0.33 to 1.68 m/sec. At each location and Dean number, a timed sequence of 6-7 photographics was collected. One and one-half seconds to one and three-quarters of a second of time elapsed during each sequence, with photographs spaced one-quarter of a second apart.

Smoke patterns showed significant spanwise and radial unsteadiness at most experimental condition. Vortex pairs were clearly visible in many of the sequences. Spanwise spacing of vortex pairs seemed to be generally maintained in spite of significant unsteadiness.

Radial unsteadiness was observed to be greatest at the lower angular streamise positions (85 and 95 degrees) and for Dean numbers between 60 and 80. Spanwise unsteadiness and rocking was greater for larger angular streamwise locations (125 and 135 degrees) and for Dean numbers between 140 and 200. In some cases, transient disturbances in the channel were believed to be responsible for some of the observed unsteadiness for several Dean numbers tested.

Qualification tests were also conducted on prototypes used to model portions of a second curved channel to be used for heat transfer measurements. A polynominal was fitted to data:

$$q_c = -0.0294+0.4222\ (T_w-T_{ambient})-0.0015\ (T_w-T_{ambient})^2$$

This equation can be used in estimating the conduction losses of the heat transfer channel. Contact resistance measurements were also conducted for the same heat transfer surface. Contact resistance is used to calculate the temperature difference between thermo-couples and the surface of the Lexan. An average value of 3.4×10^{-3} $^{\circ}Cm^2/Watt$ was obtained from these tests.

Further studies are recommended using video cameras to provide more information on the unsteady types of motion recorded in this study.

APPENDIX A

FIGURES

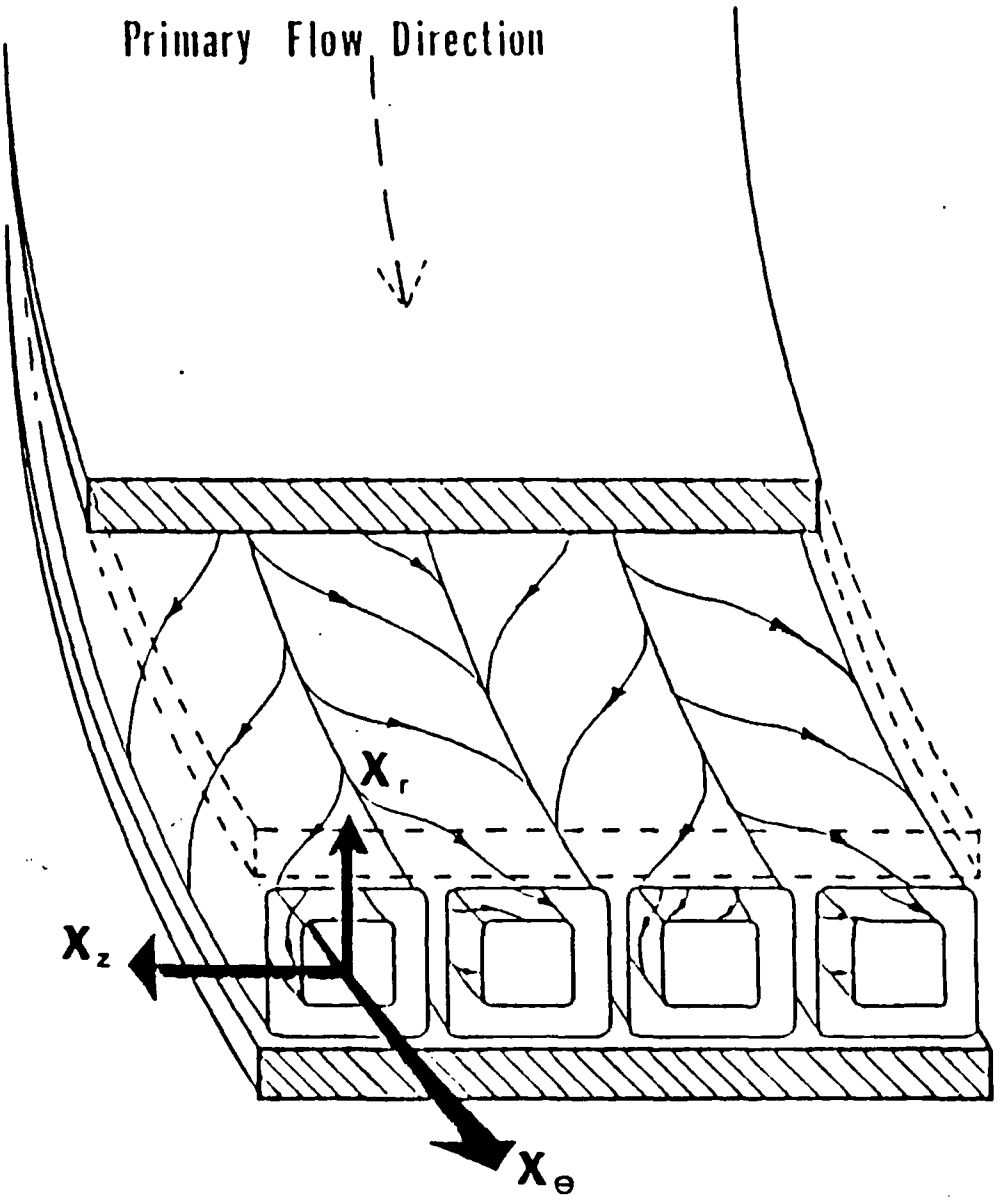

Figure 1 Schematic Of Dean Vortices
In A Curved Channel

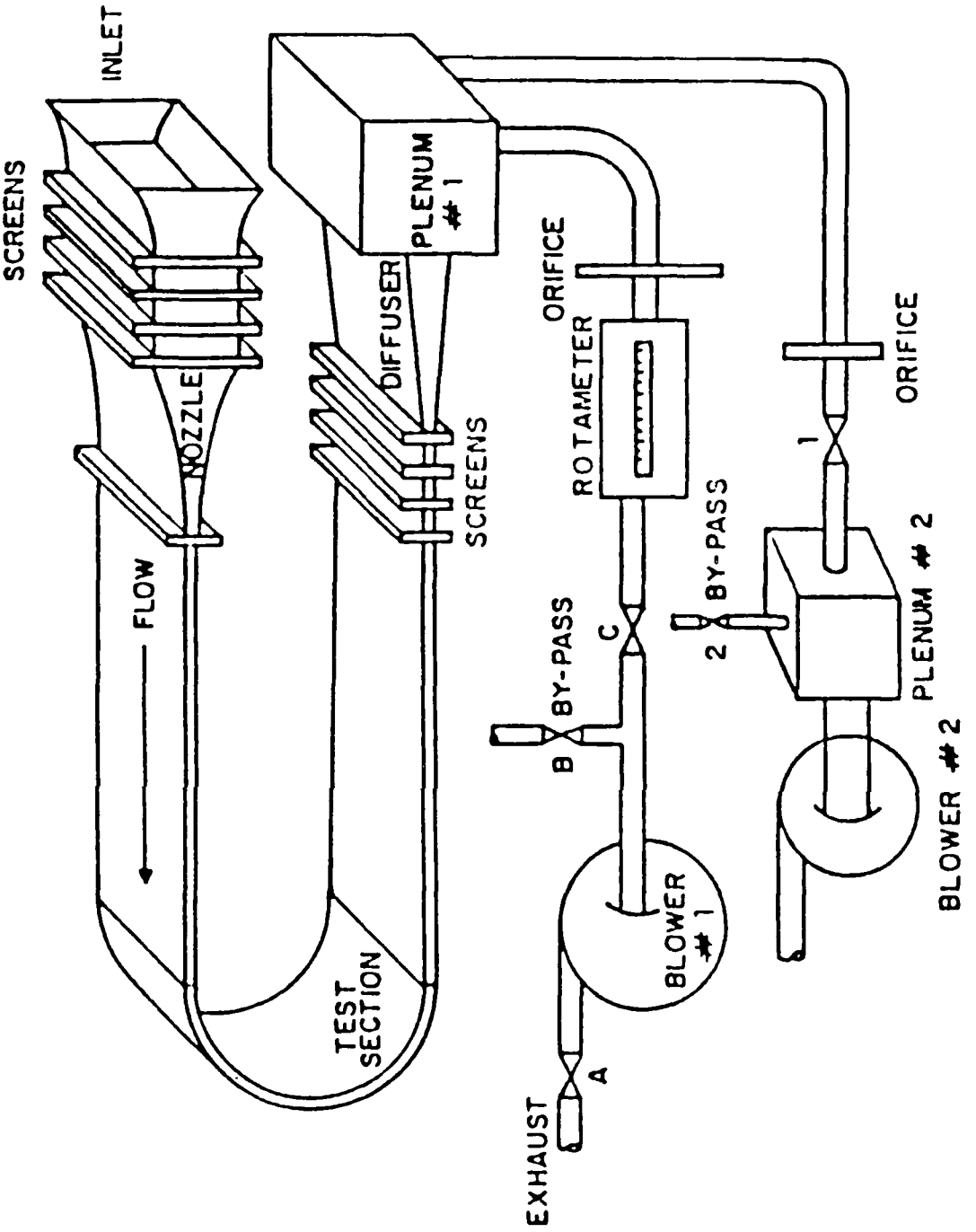

Figure 2 Schematic Of Test Facility

Figure 3 Test Facility (Front View)

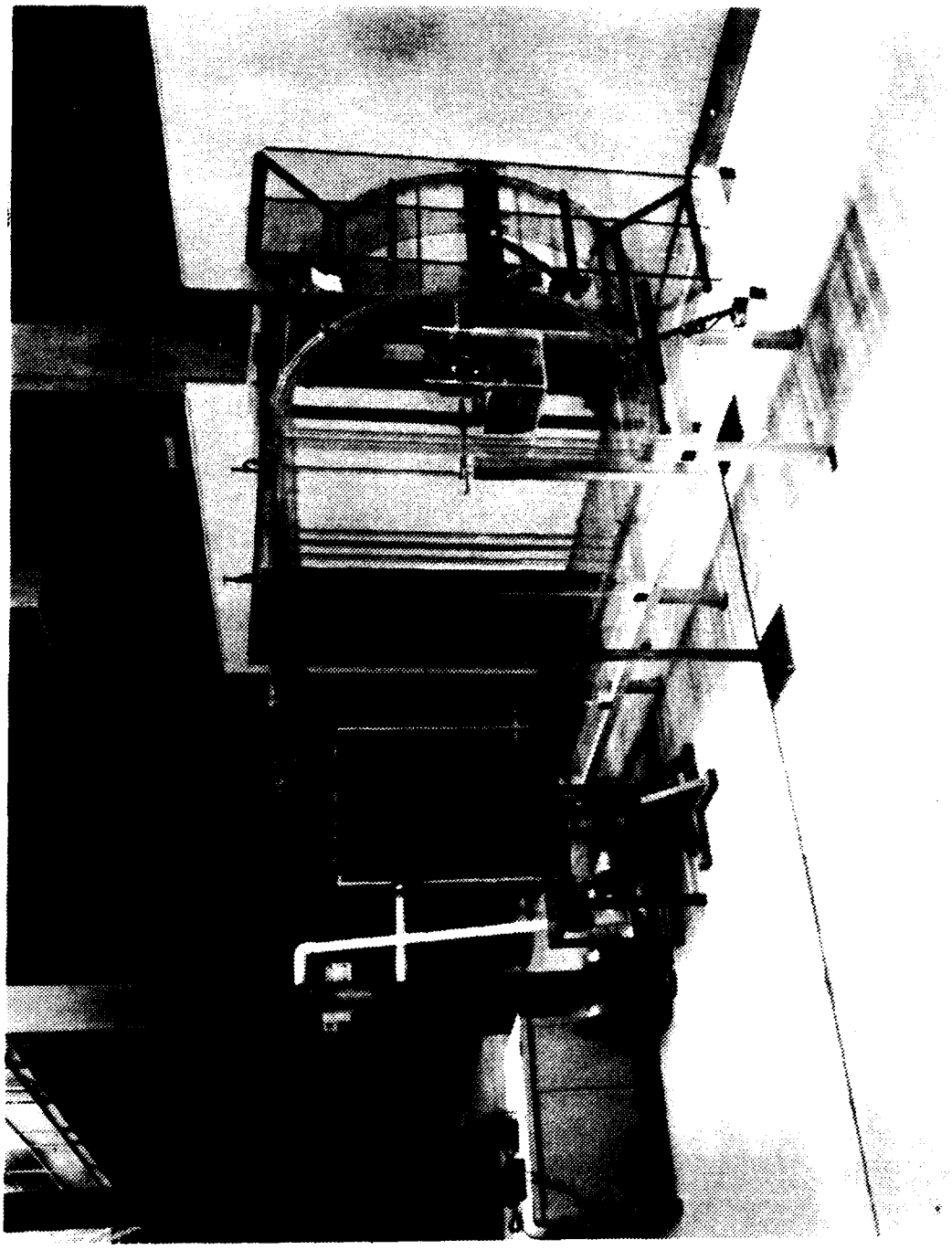

Figure 4 Test Facility (Side View)

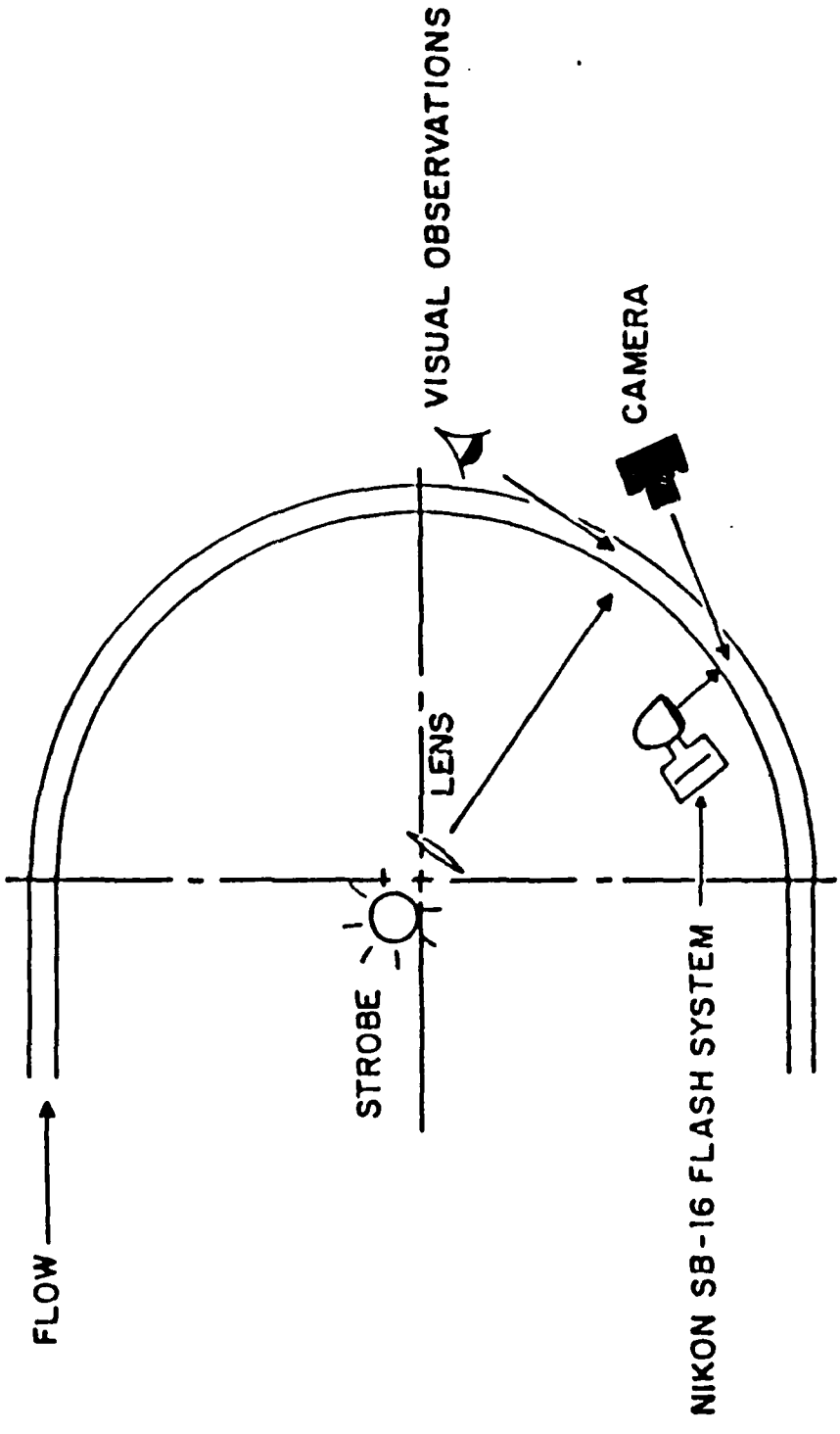

Figure 5 Radial-Spanwise Plane Flow Visualization

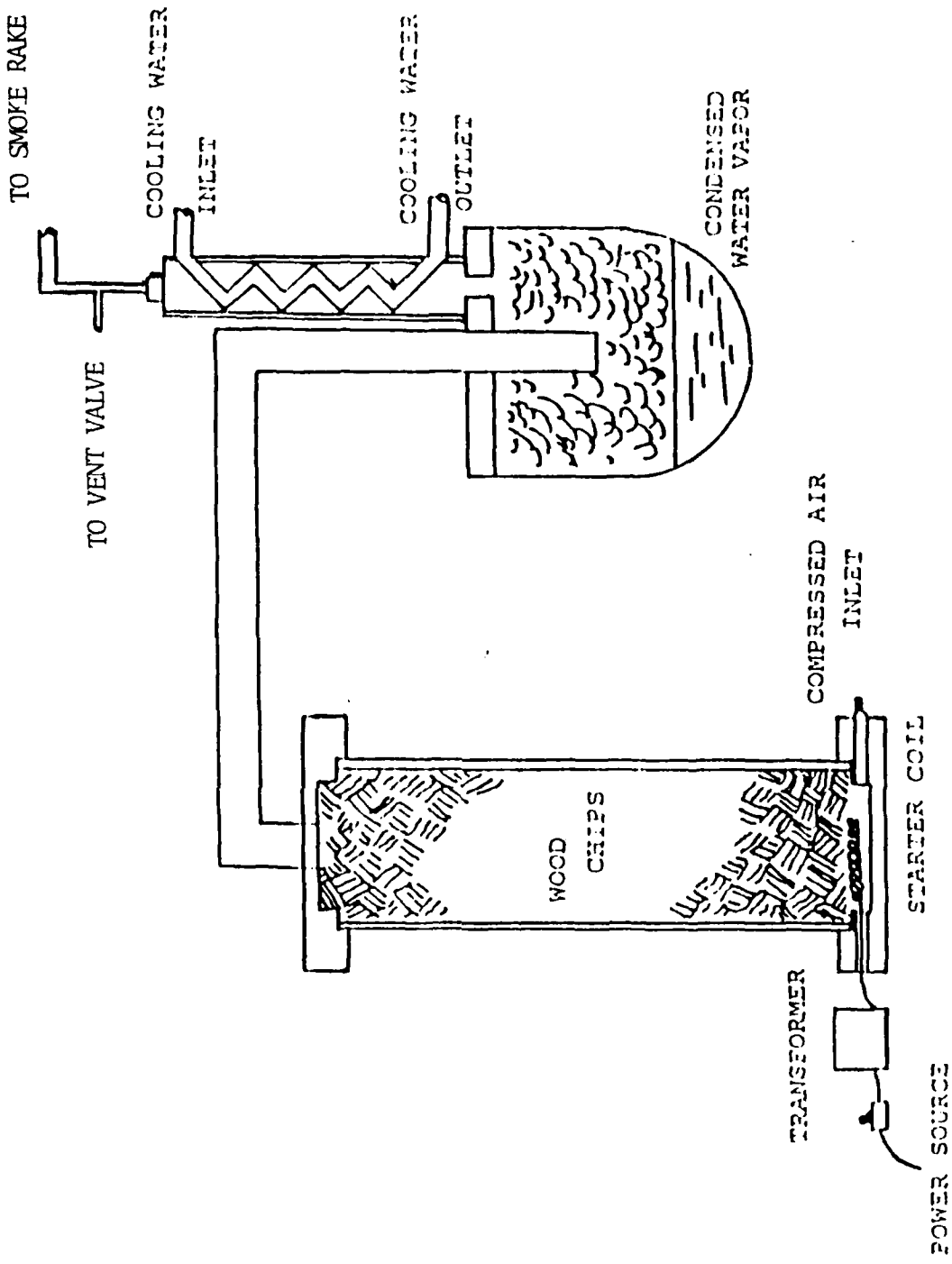

Figure 6 Schematic Of The Smoke Generator

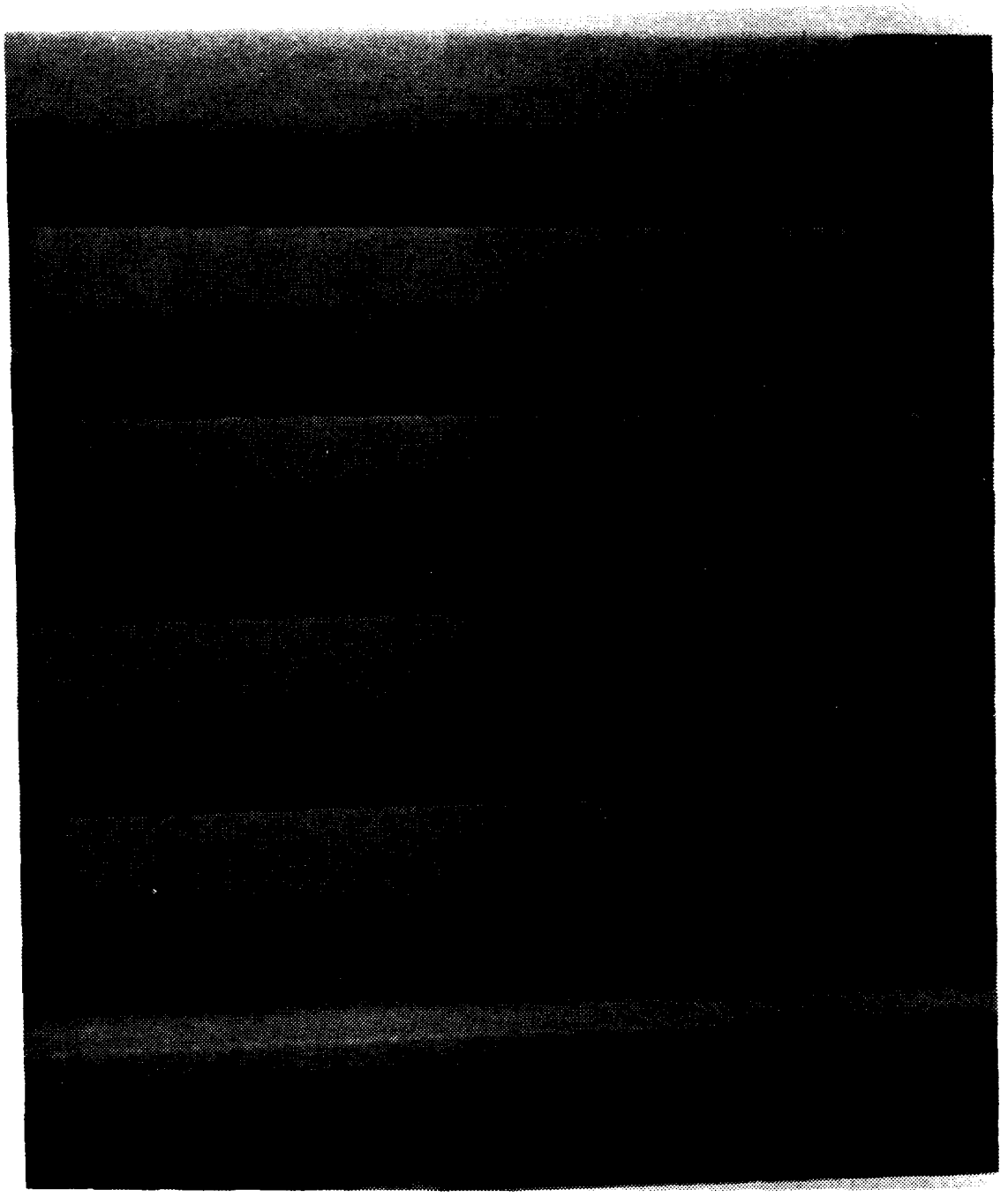

Figure 7 Flow Visualization At DE=40
And 105 Degrees From Start
Of Curvature

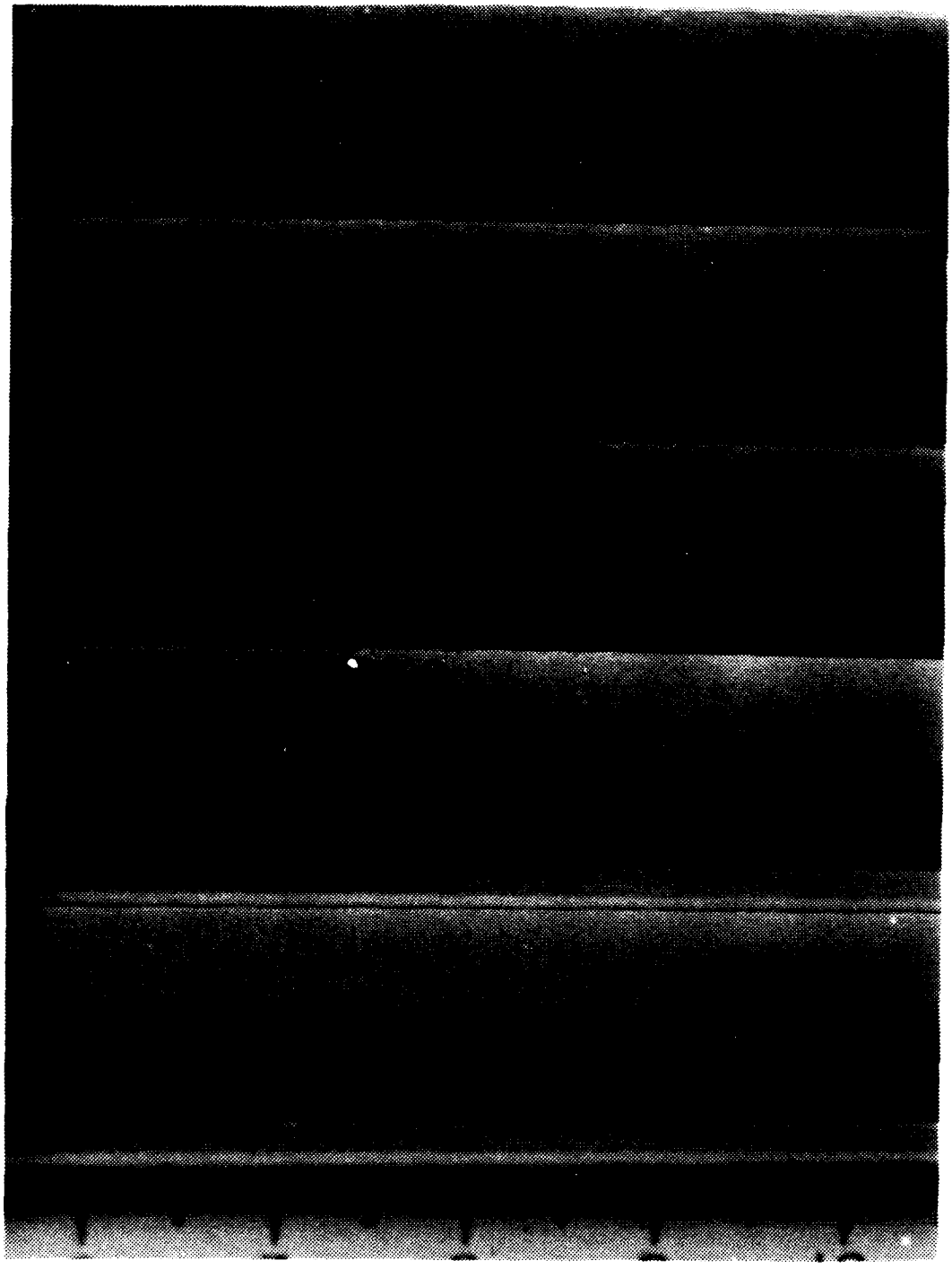

Figure 8 Flow Visualization At De=40
115 Degrees From Start
Of Curvature

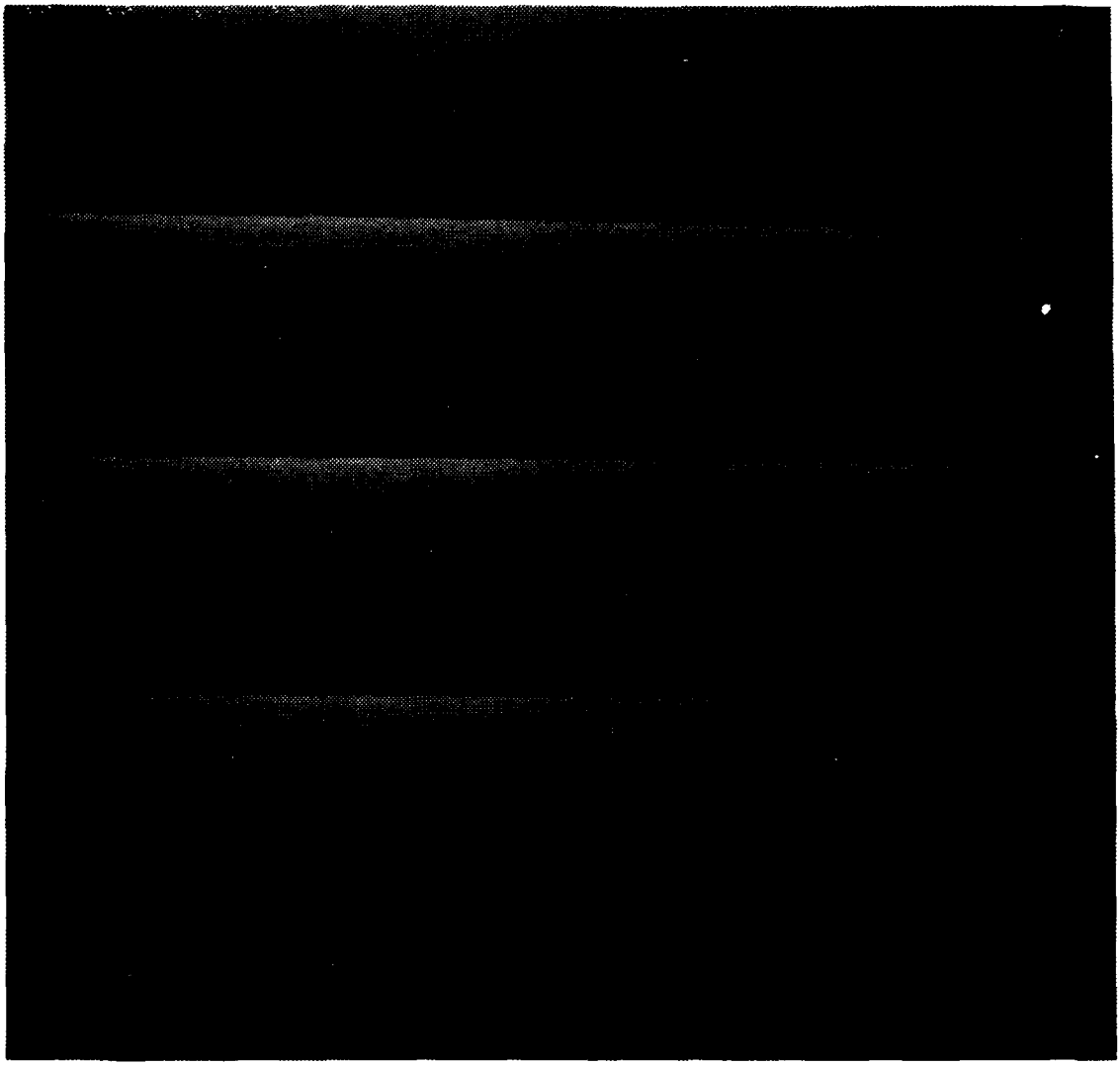

Figure 9 Flow Visualization At De=40 And 125 Degrees From Start Of Curvature

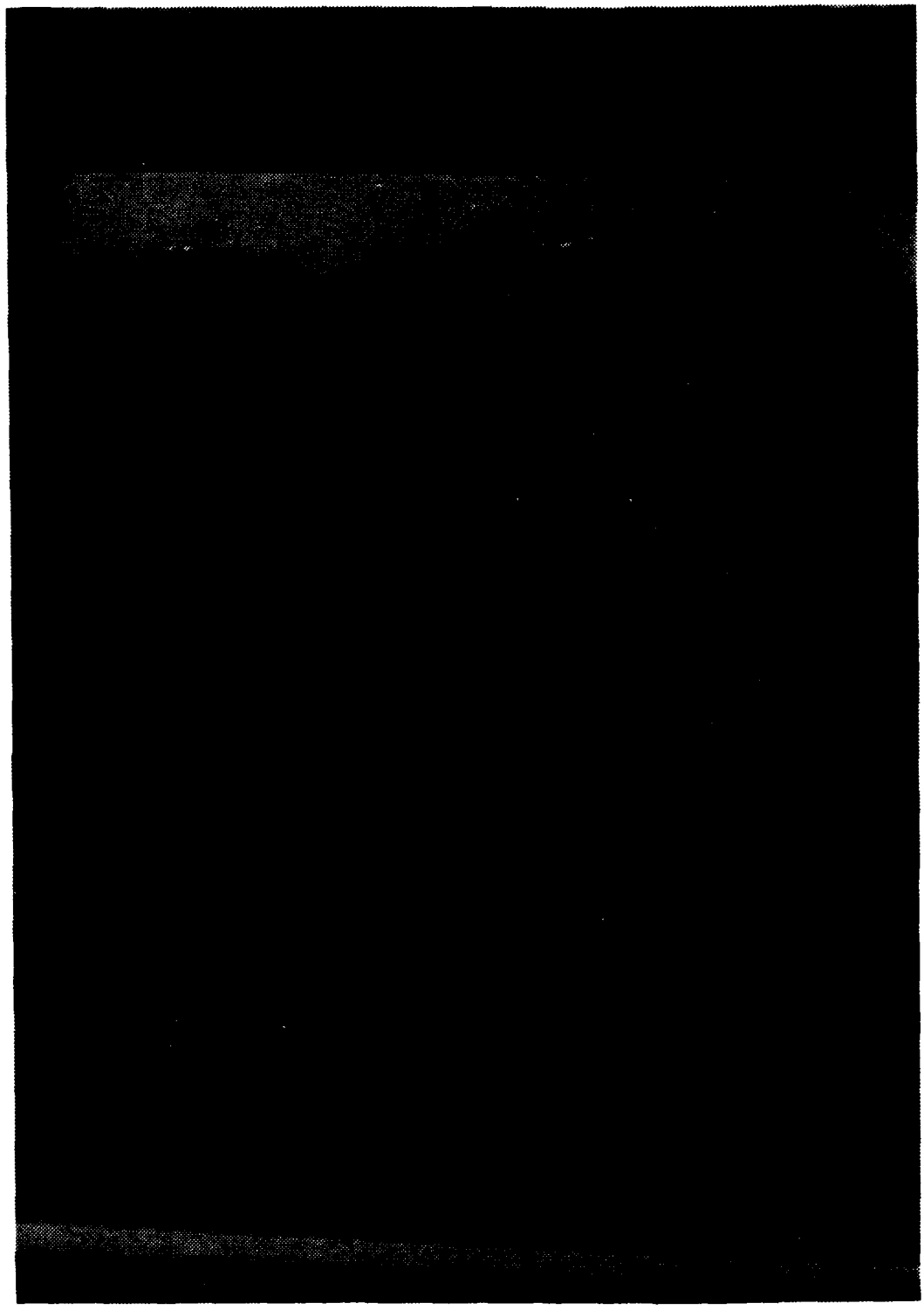

Figure 10 Flow Visualization At De=60 And 85 Degrees From Start Of Curvature

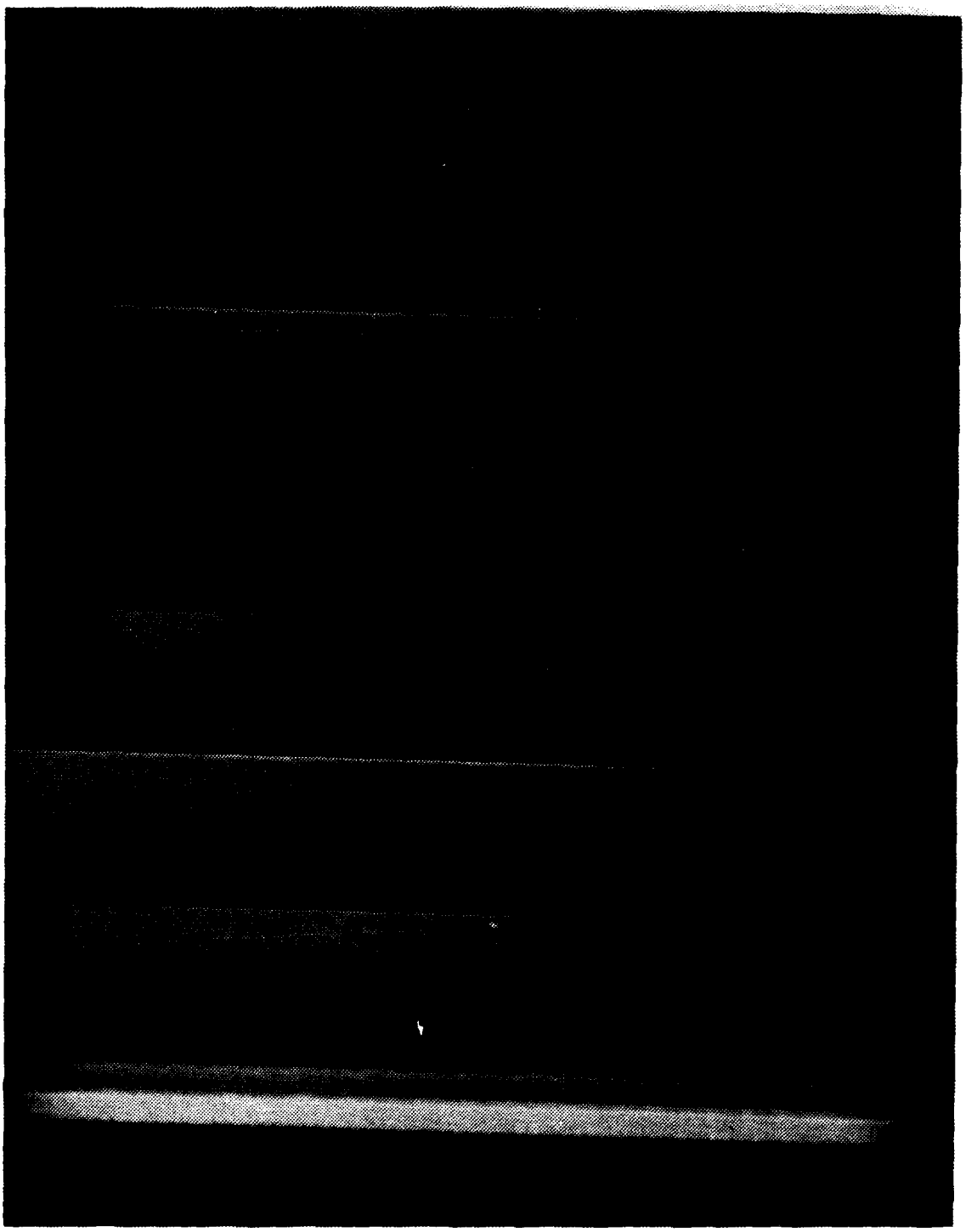

Figure 11 Flow Visualization At De=60
And 95 Degrees From Start
Of Curvature

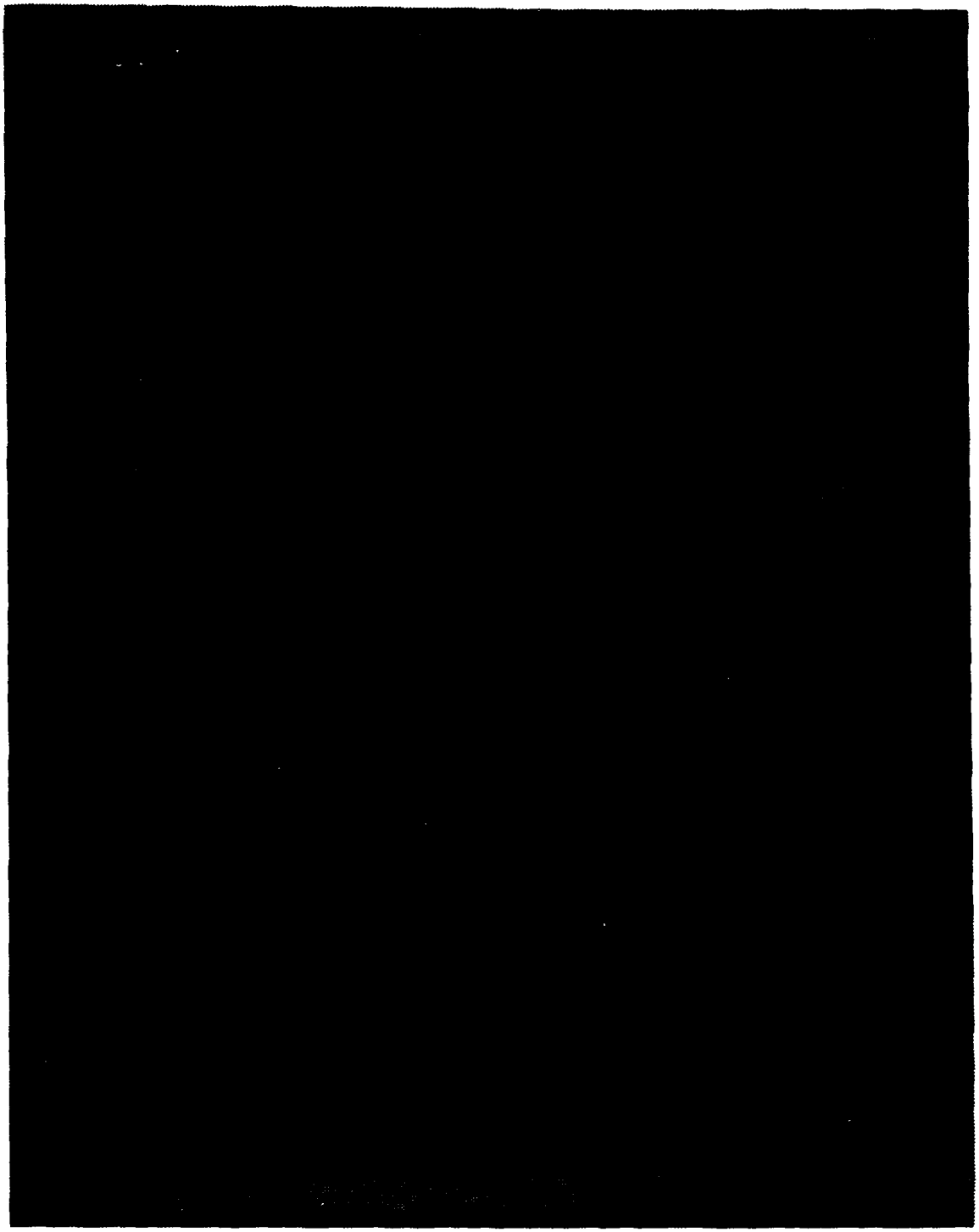

Figure 12 Flow Visualization At De=60 And 105 Degrees From Start Of Curvature

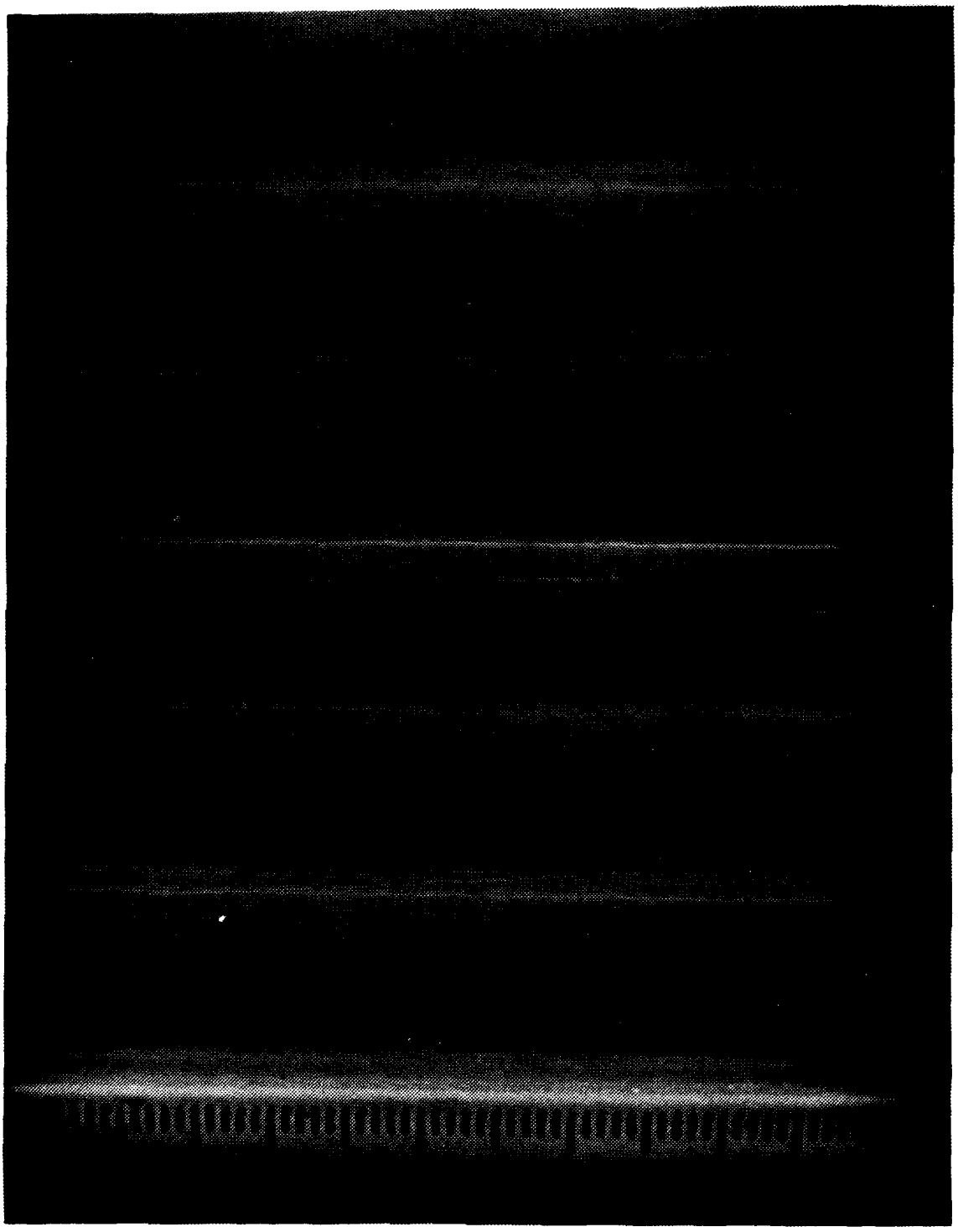

Figure 13 Flow Visualization At De=60 And 115 L Degrees From Start Of Curvature

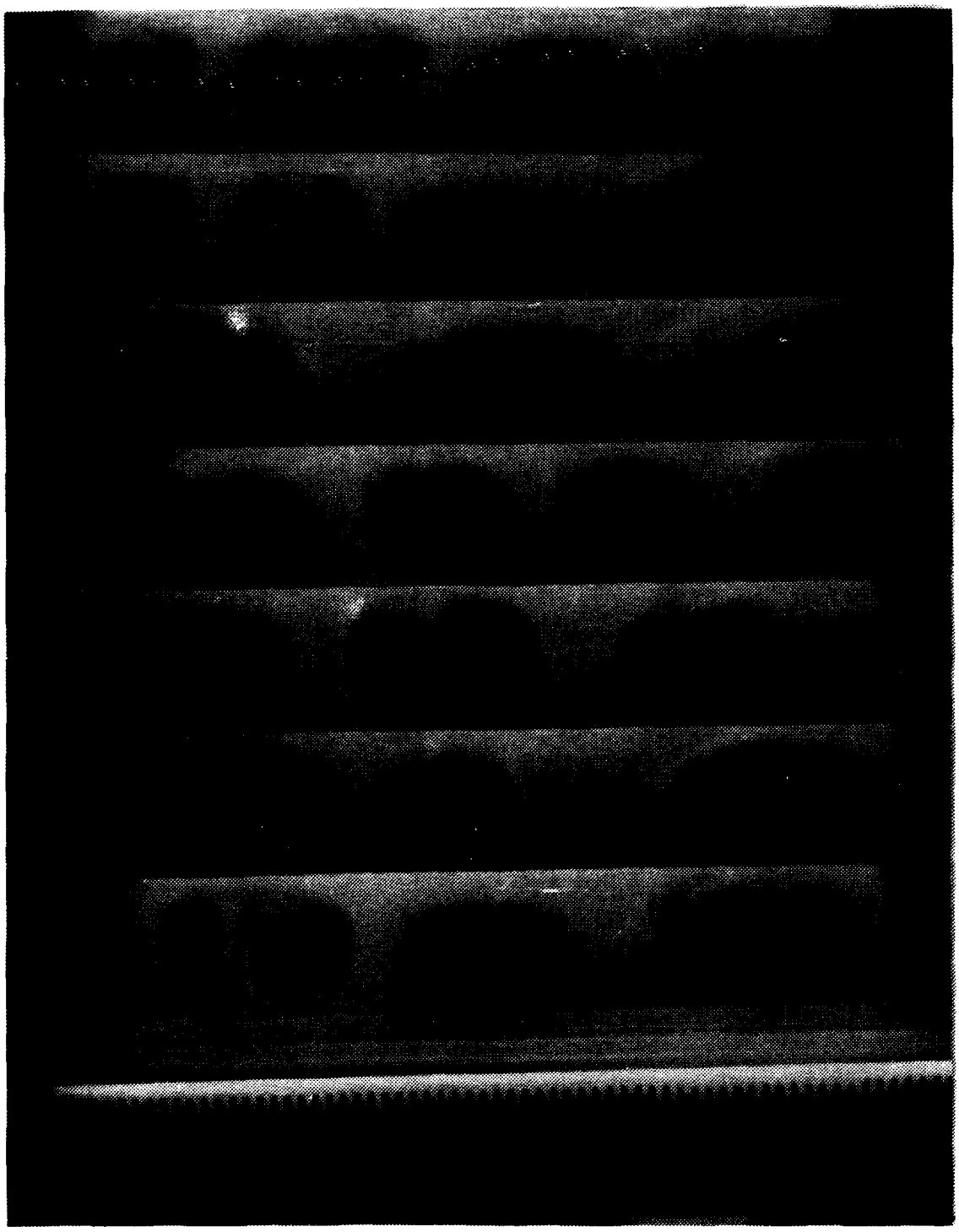

Figure 14 Flow Visualization At De=60 And 115 R Degrees From Start Of Curvature

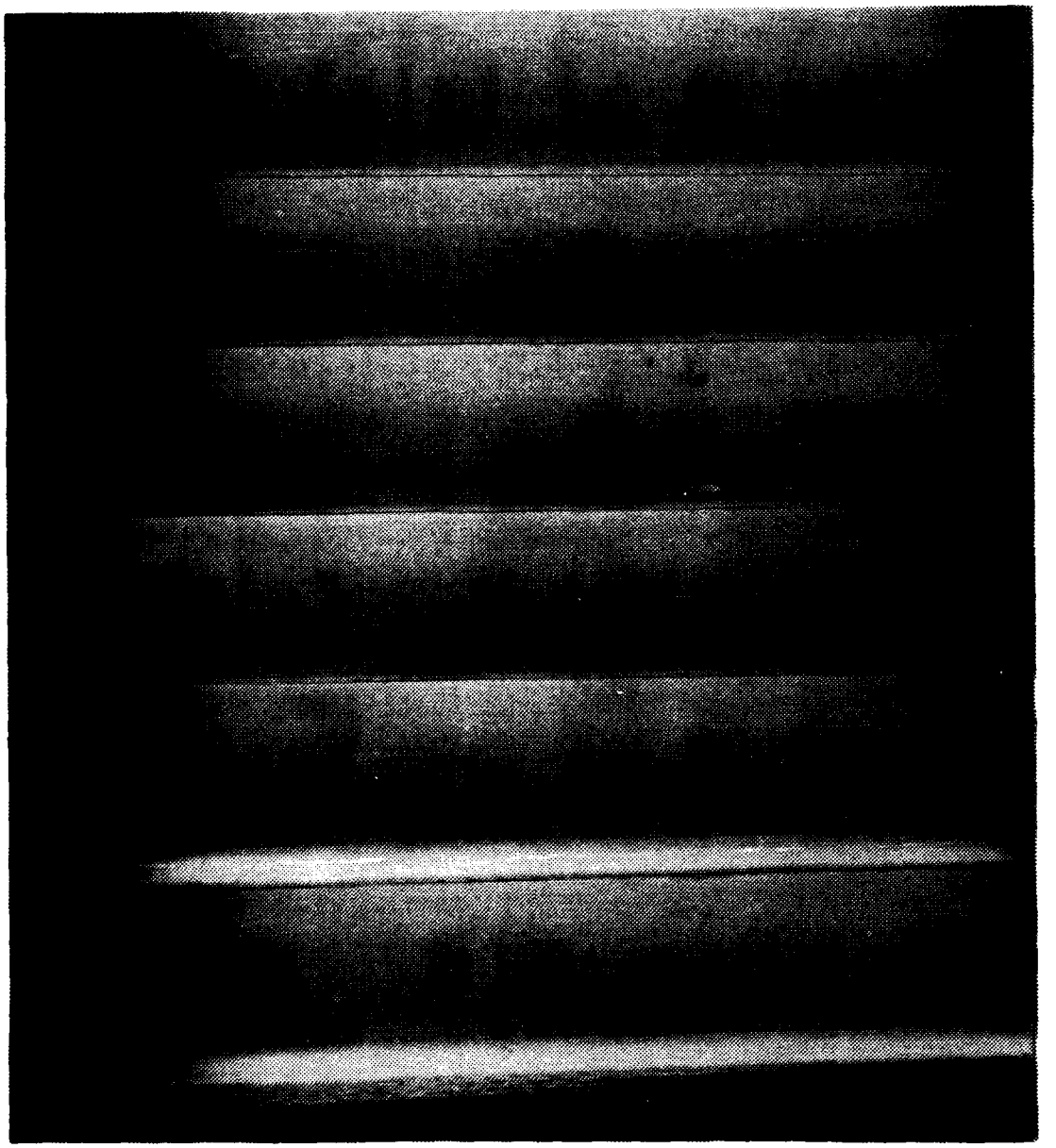

Figure 15 Flow Visualization At De=60 And 125 Degrees From Start Of Curvature

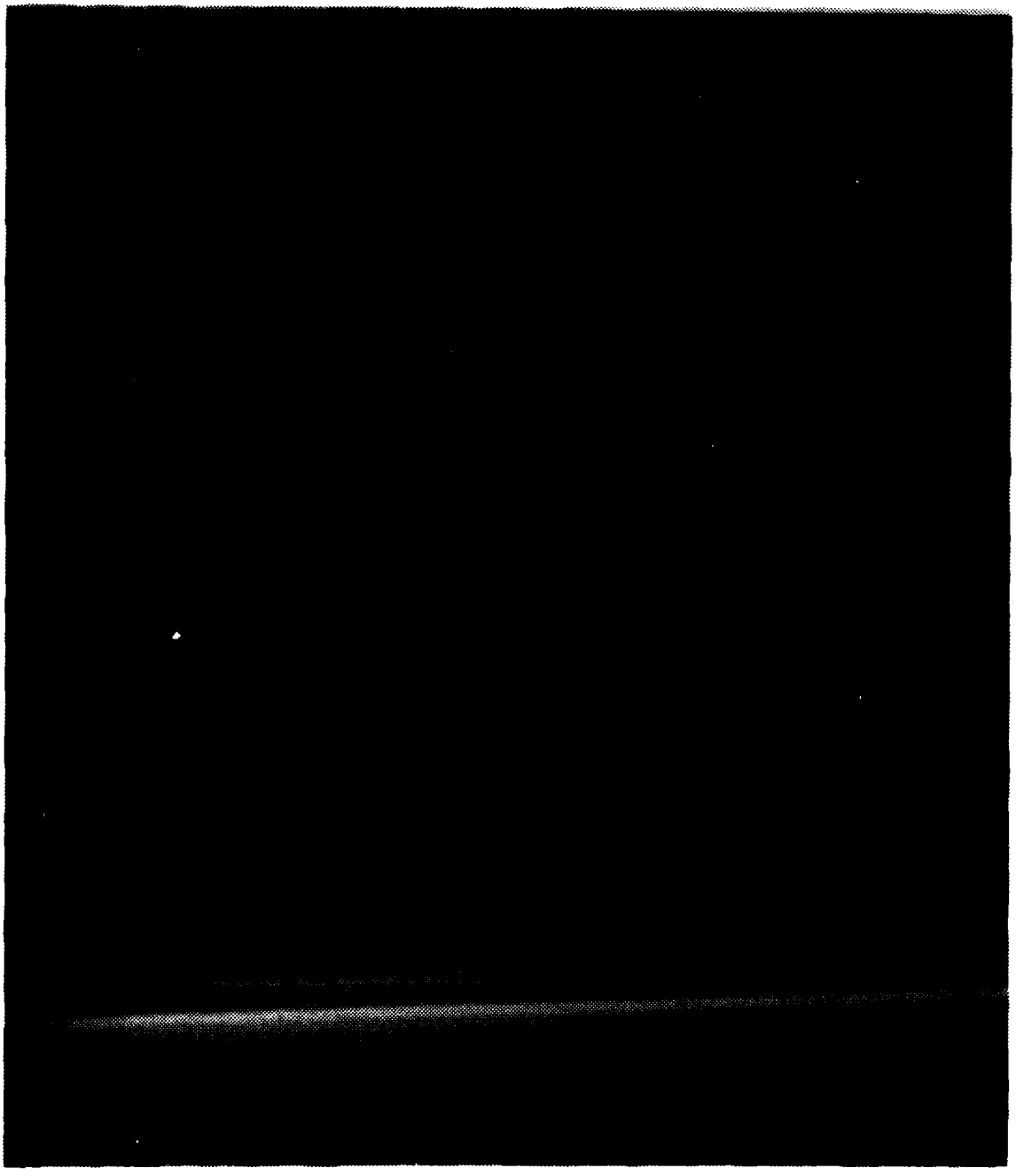

Figure 16 Flow Visualization At De=60 And 135 Degrees From Start Of Curvature

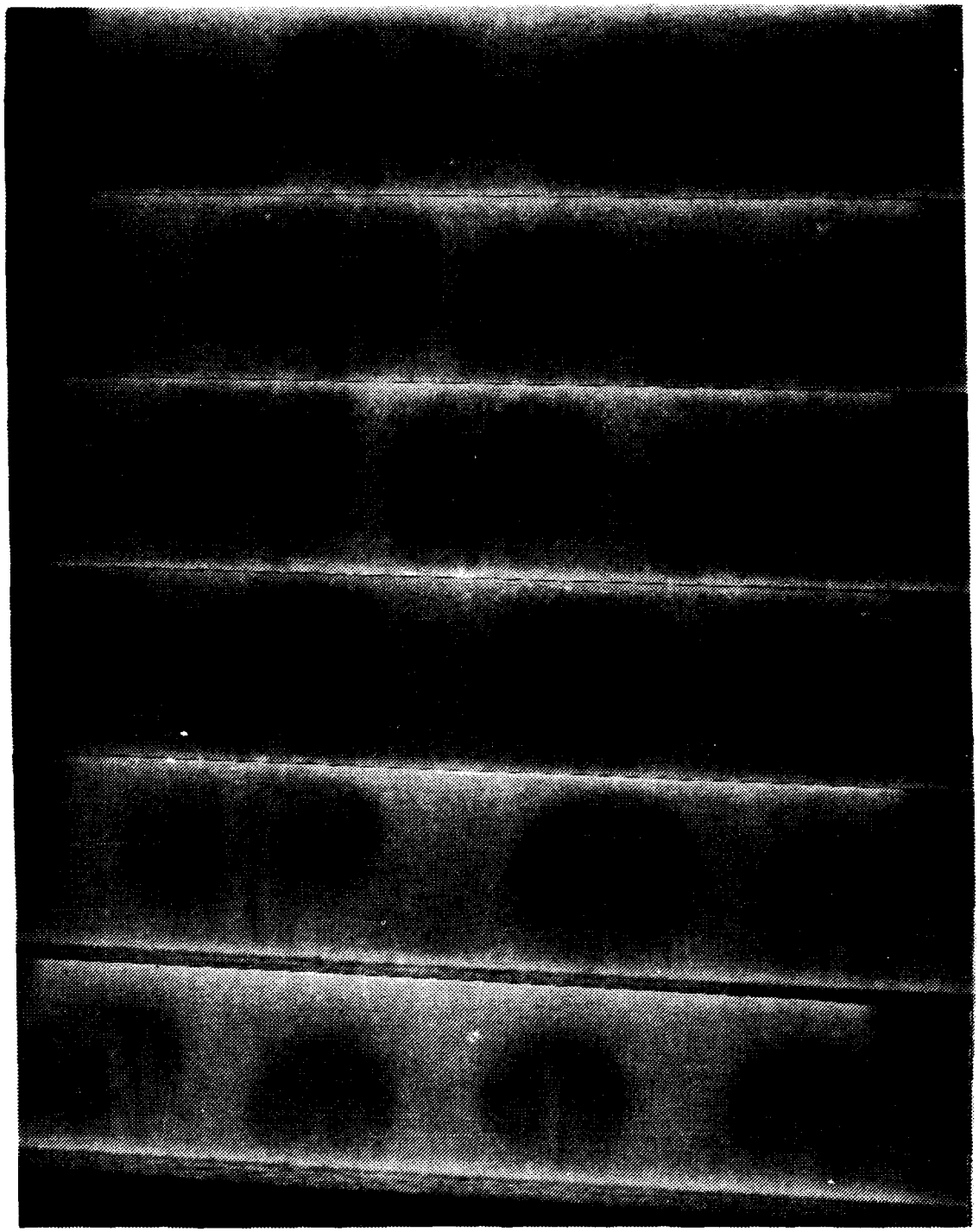

Figure 17 Flow Visualization At De=80 And 85 Degreess From Start Of Curvature

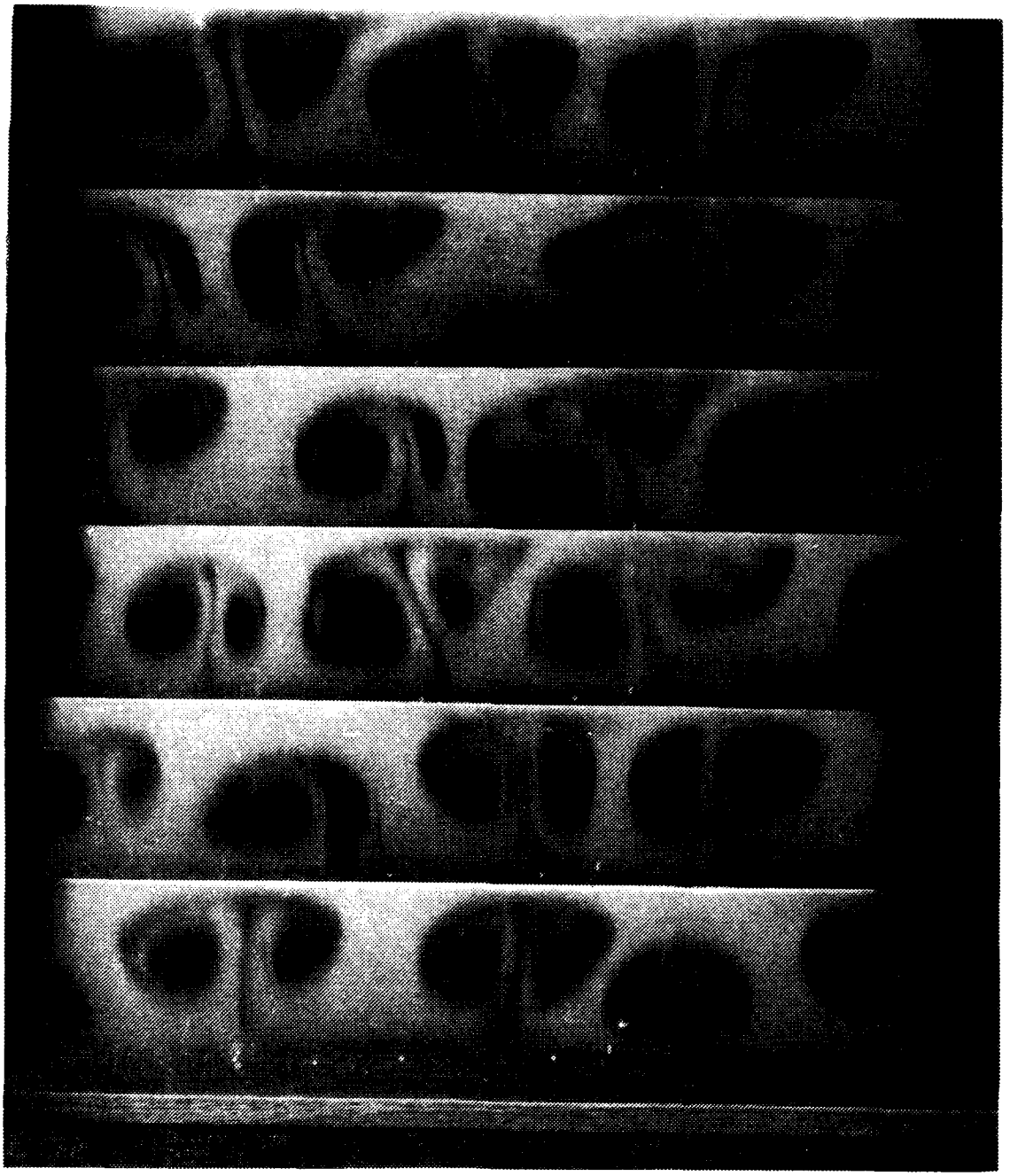

Figure 18 Flow Visualization At De=80
And 95 Degrees From Start
Of Curvature

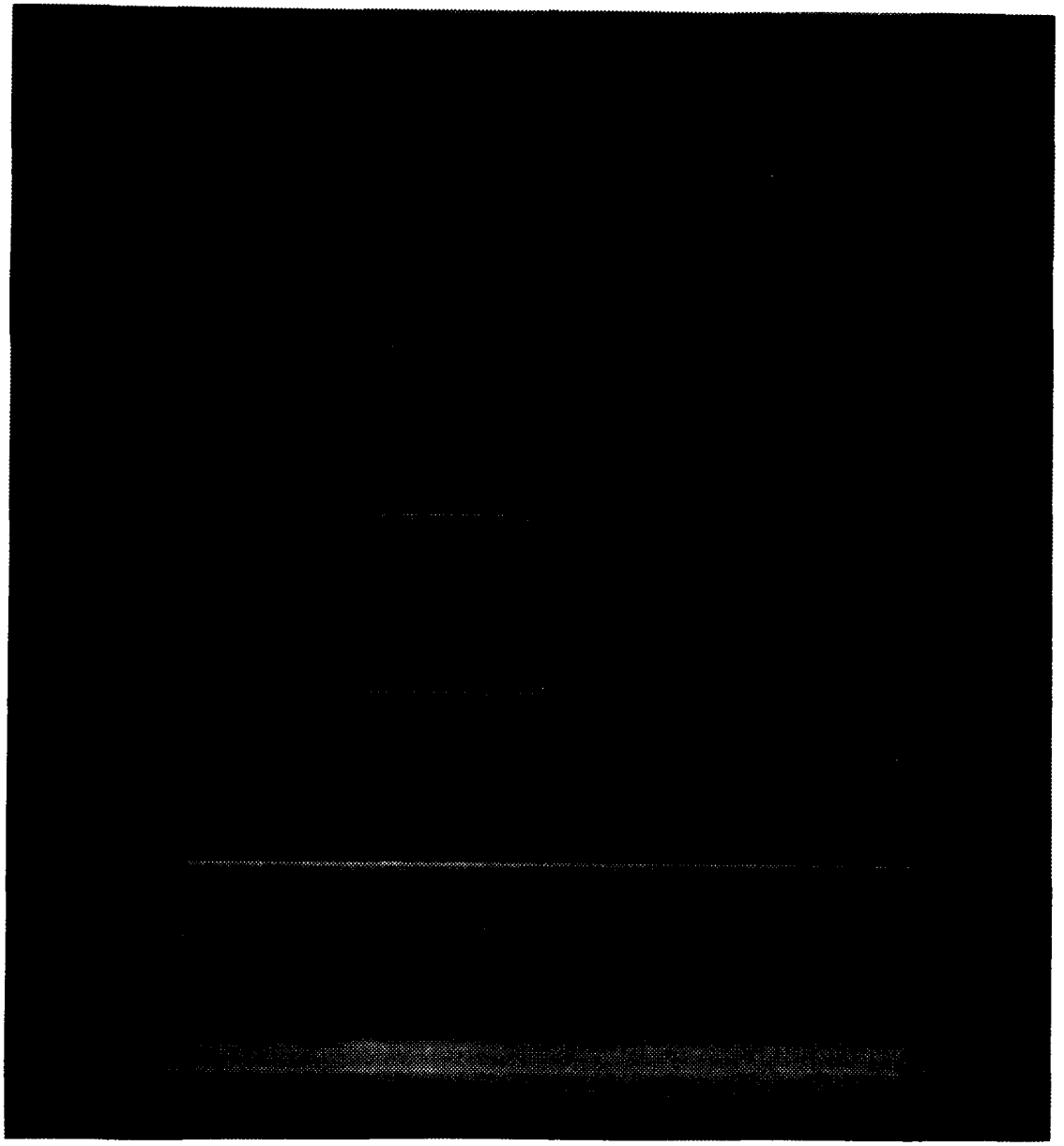

Figure 19 Flow Visualization At De=80 And 105 Degrees From Start Of Curvature

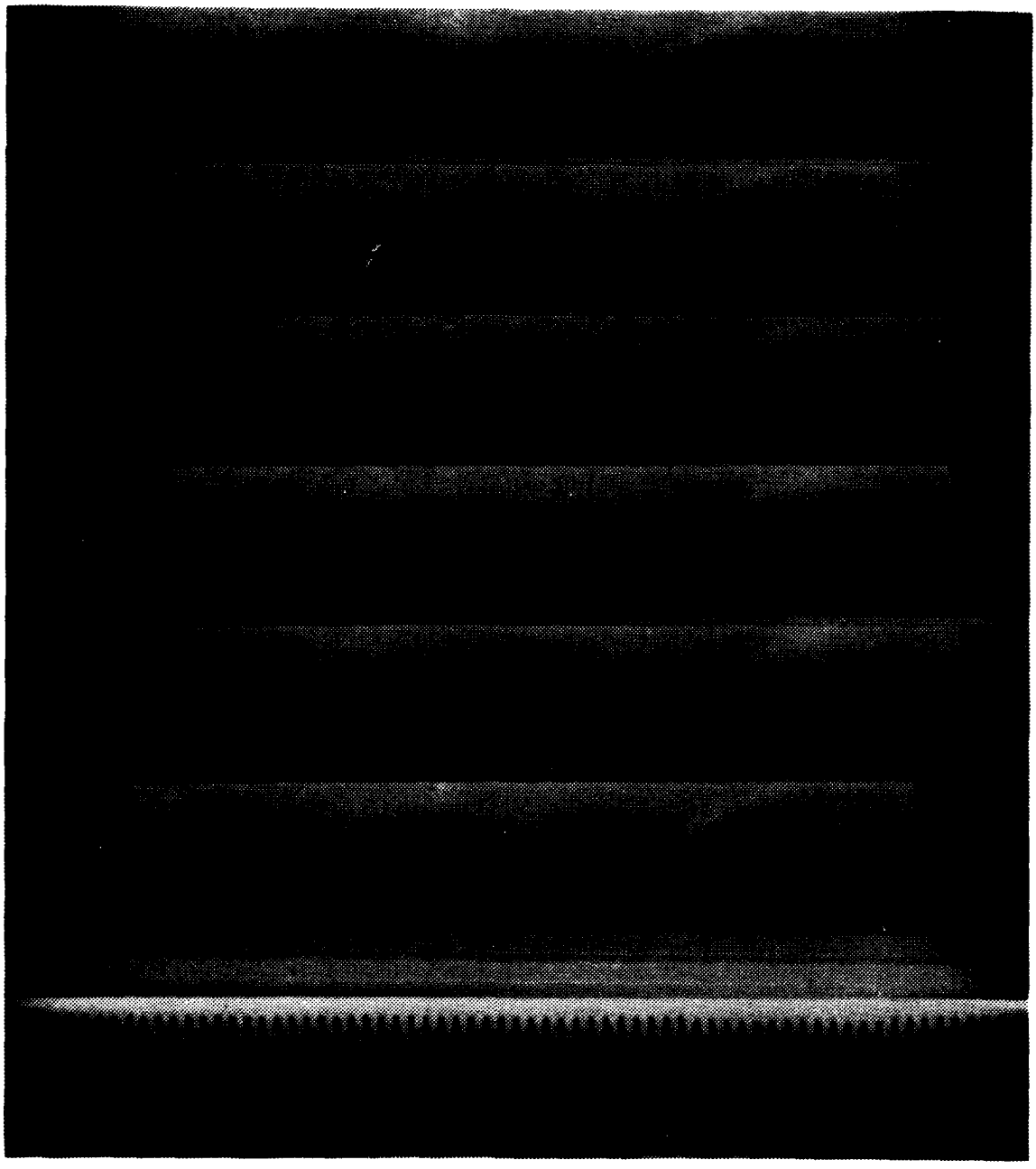

Figure 20 Flow Visualization At De=80
And 115 L Degrees From Start
Of Curvature

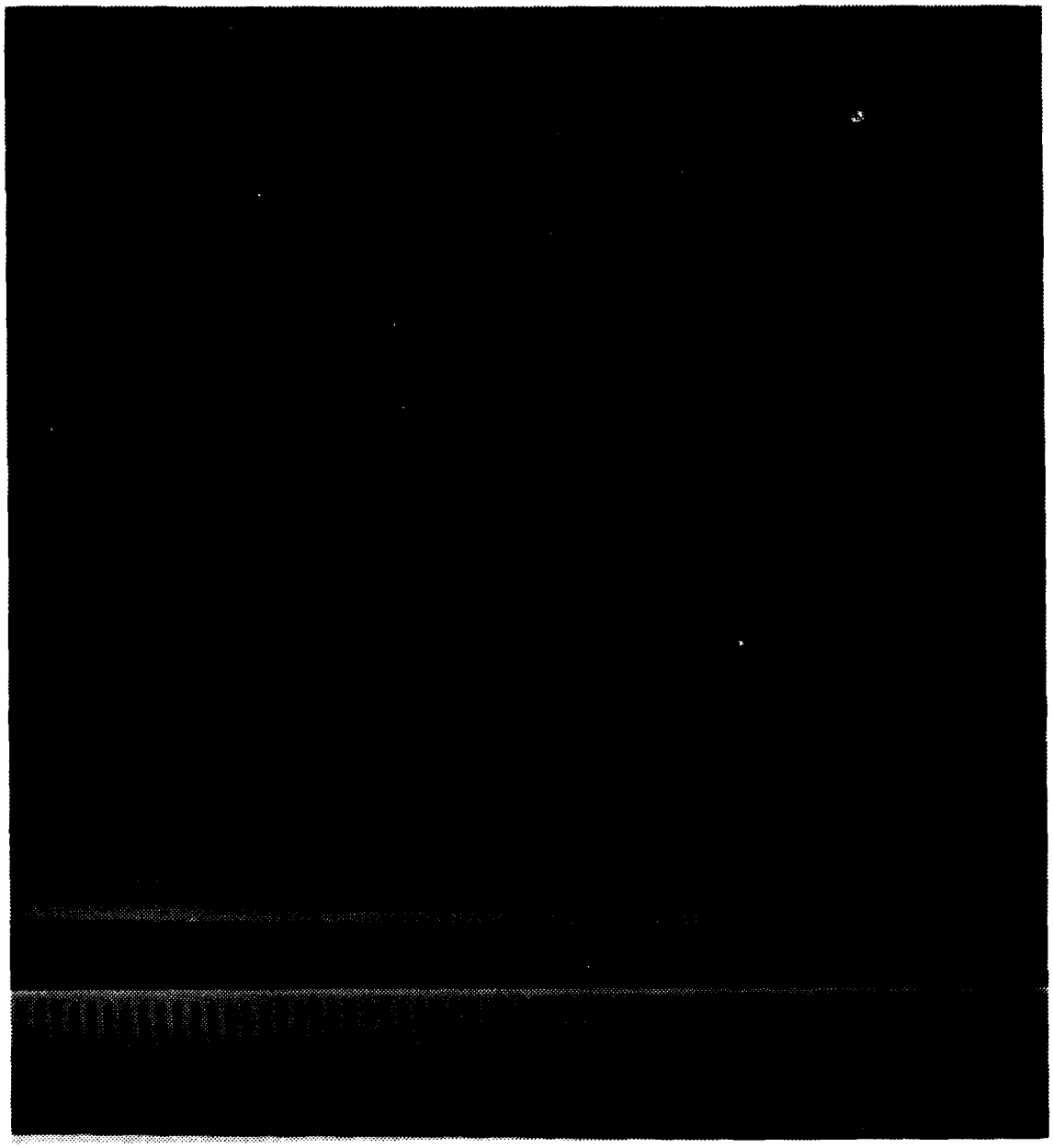

Figure 21 Flow Visualization At De=80 And 115 R Degrees From Start Of Curvature

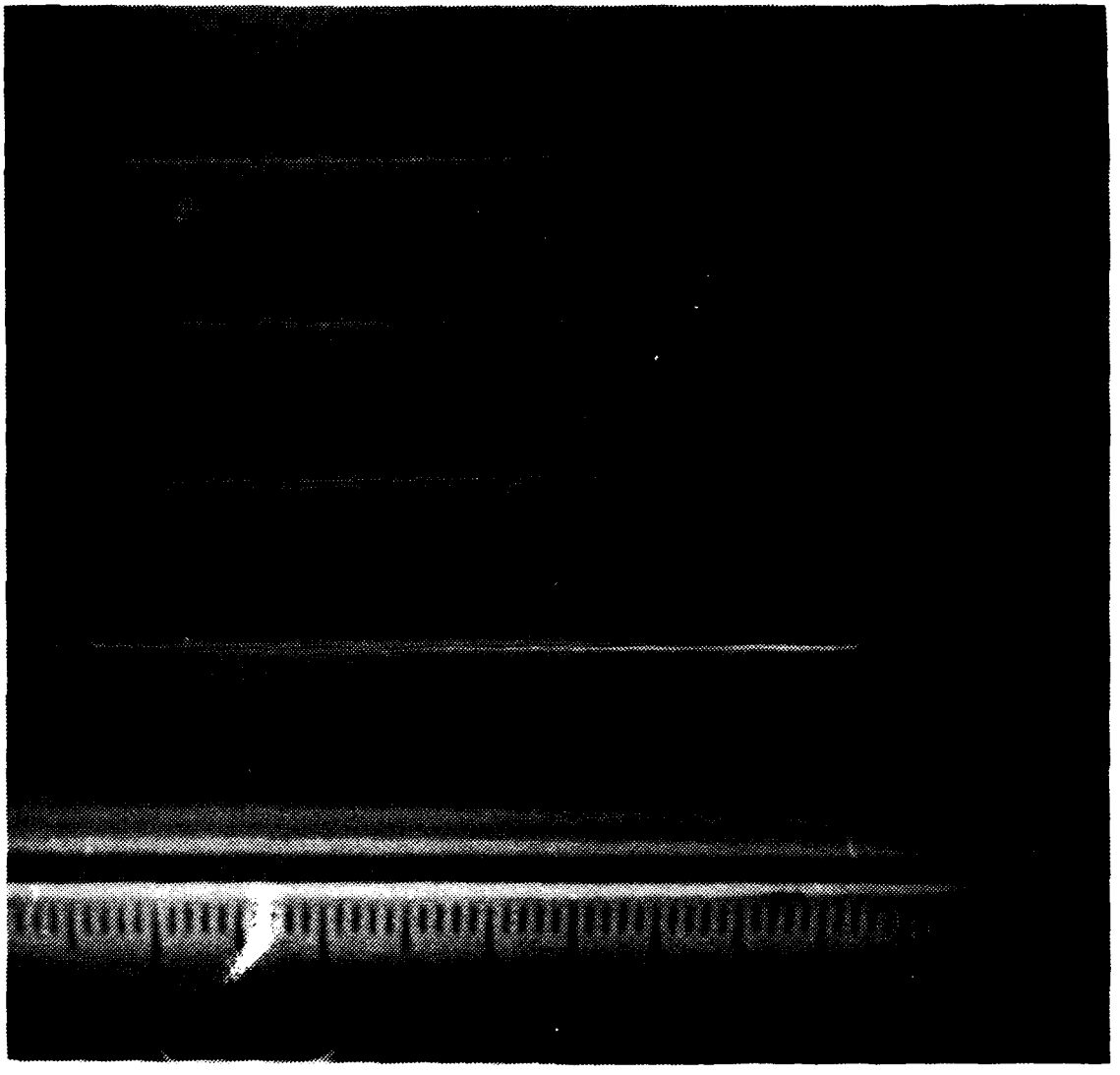

Figure 22 Flow Visualization At De=80 And 125 Degrees From Start Of Curvature

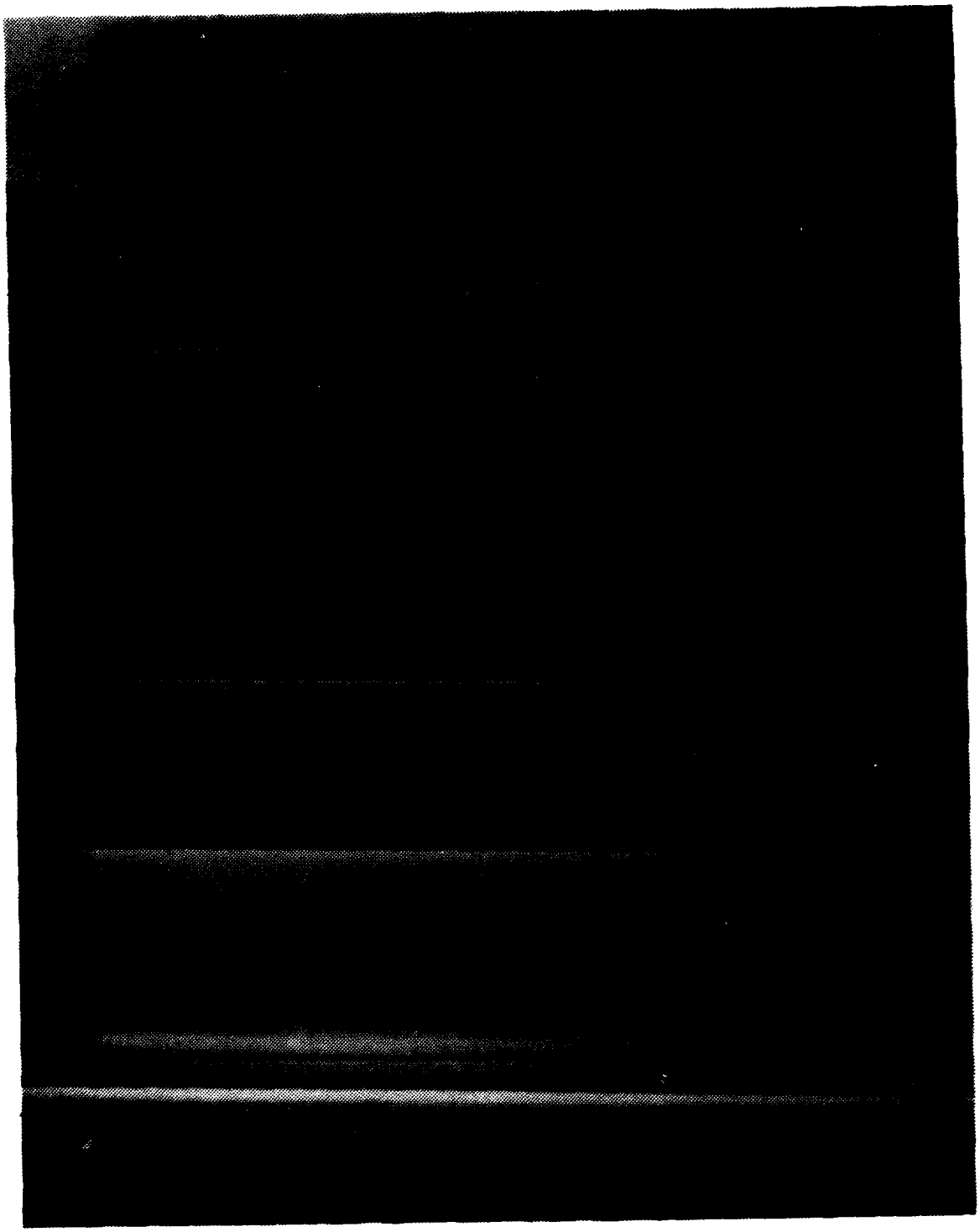

Figure 23 Flow Visualization At De=100 And 85 Degrees From Start Of Curvature

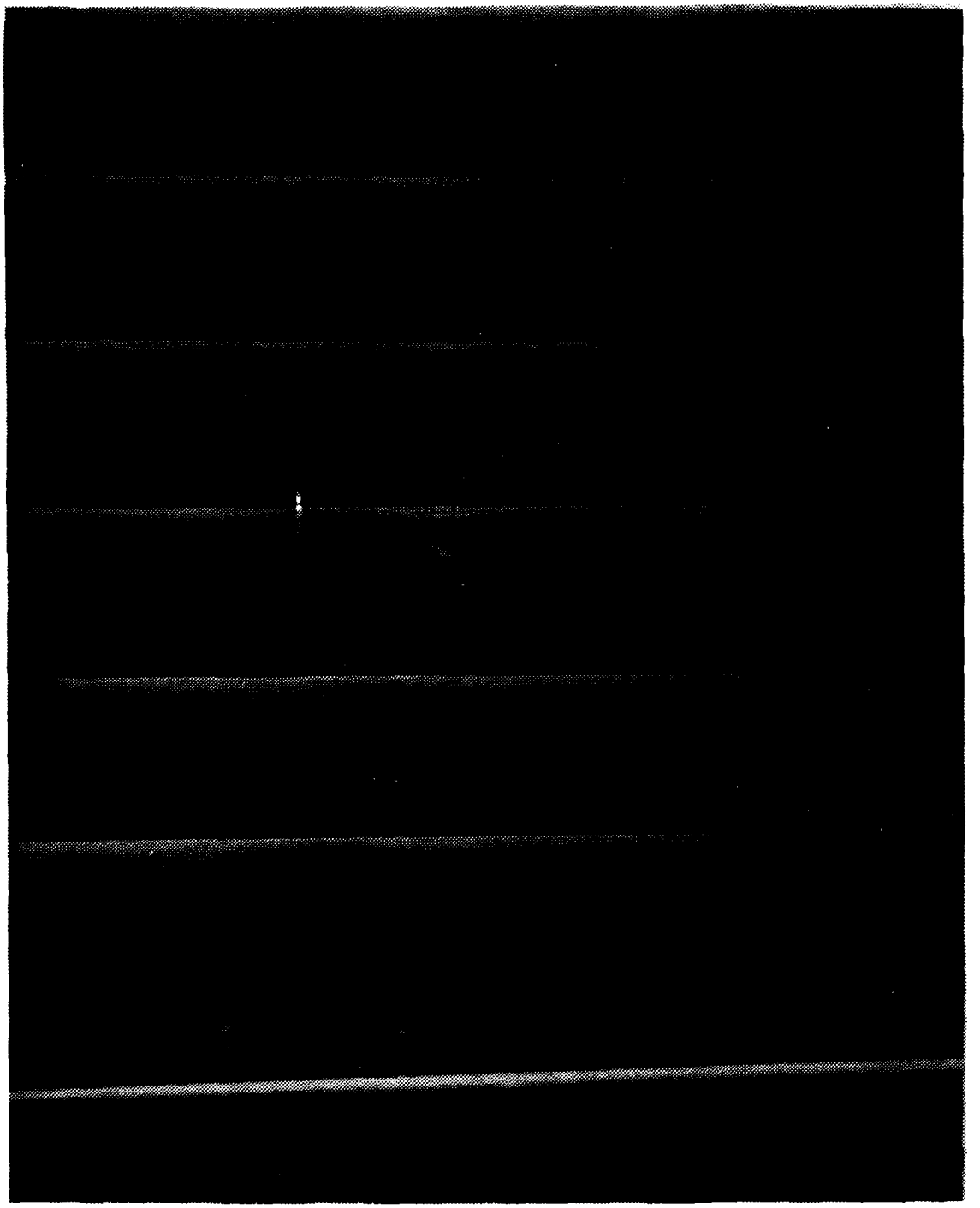

Figure 24 Flow Visualization At De=100 And 95 Degrees From Start Of Curvature

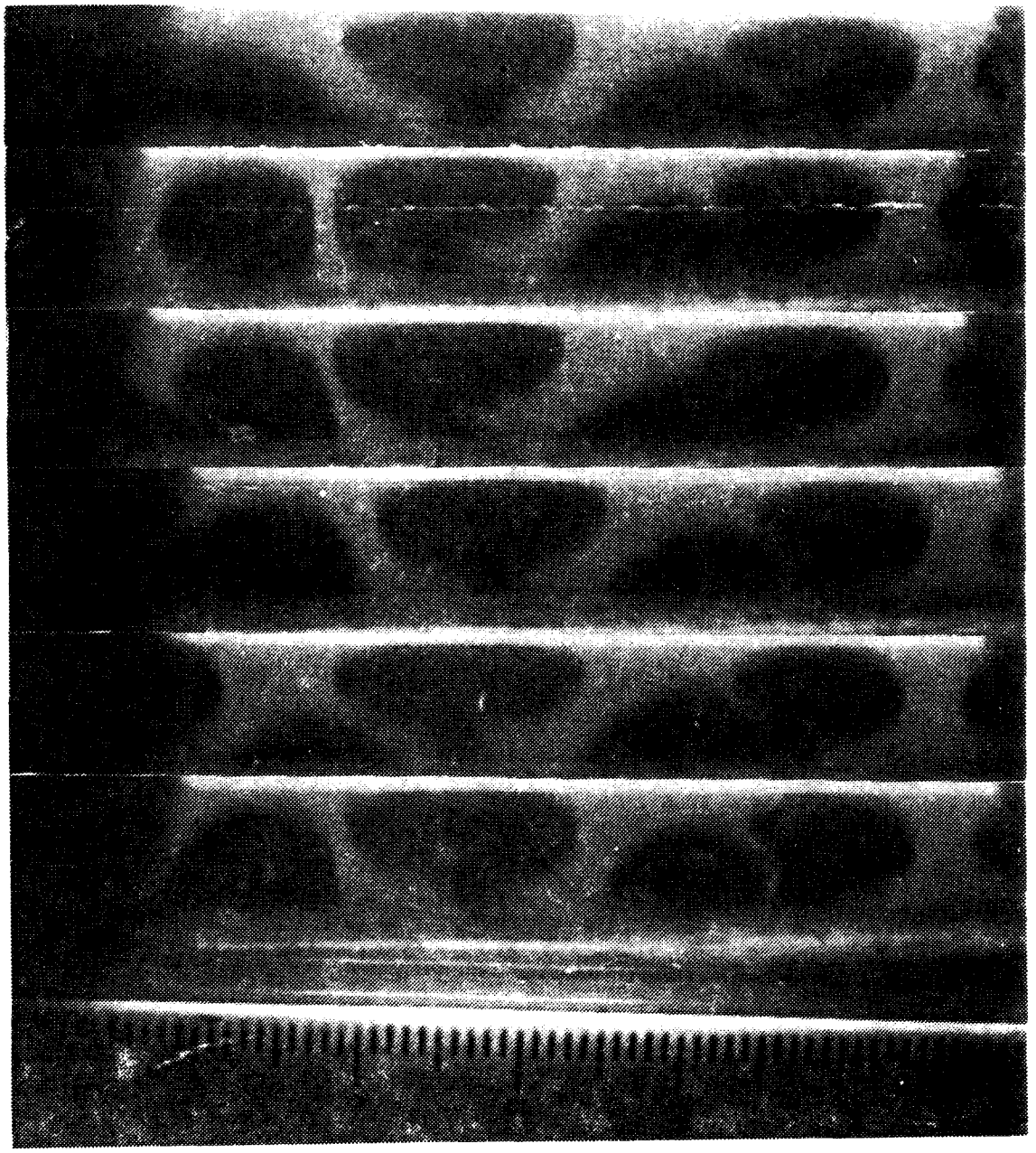

Figure 25 Flow Visualization At De=100
And 105 Degrees From Start
Of Curvature

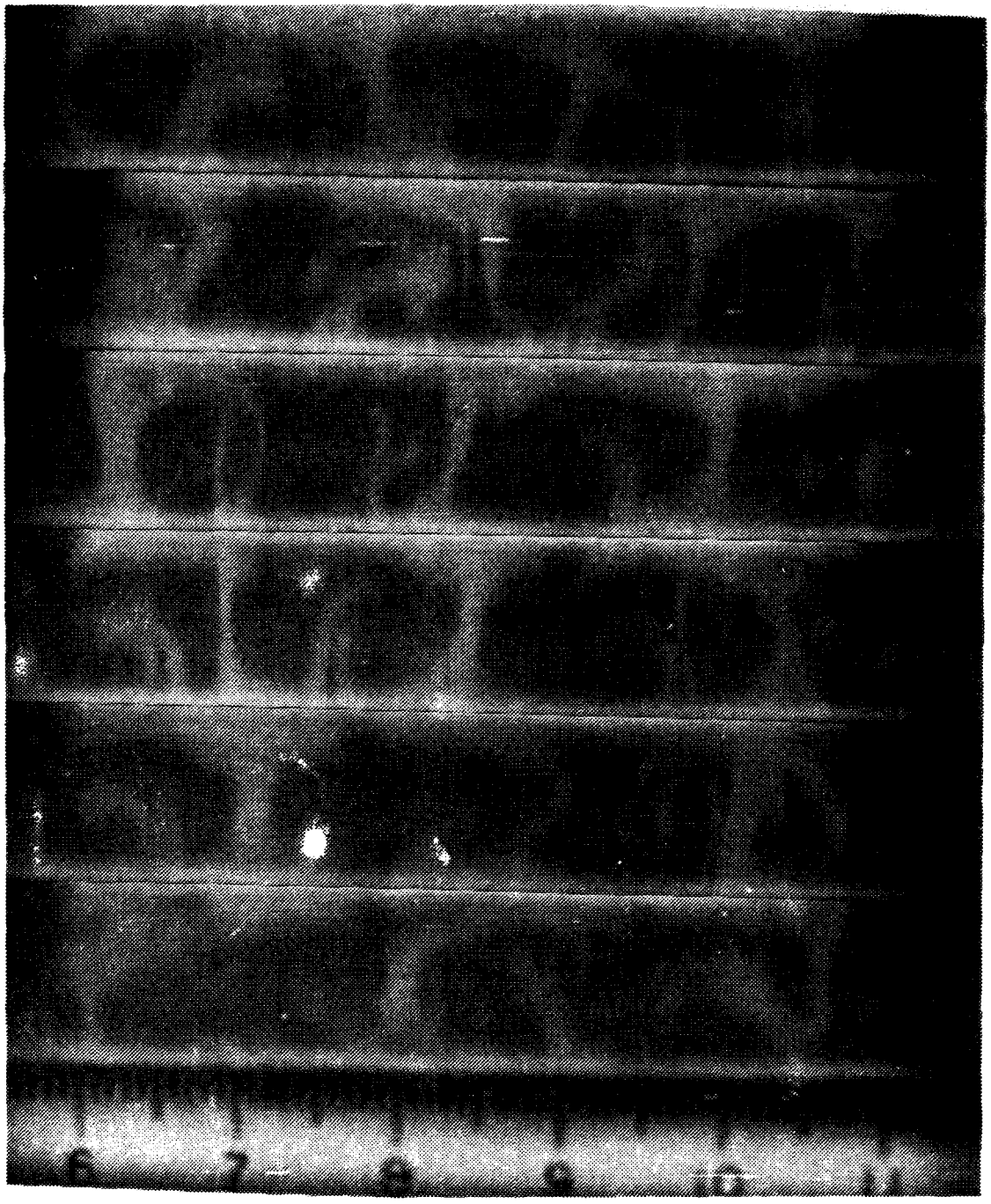

Figure 26 Flow Visualization at De=100 And 115 L Degrees From Start Of Curvature

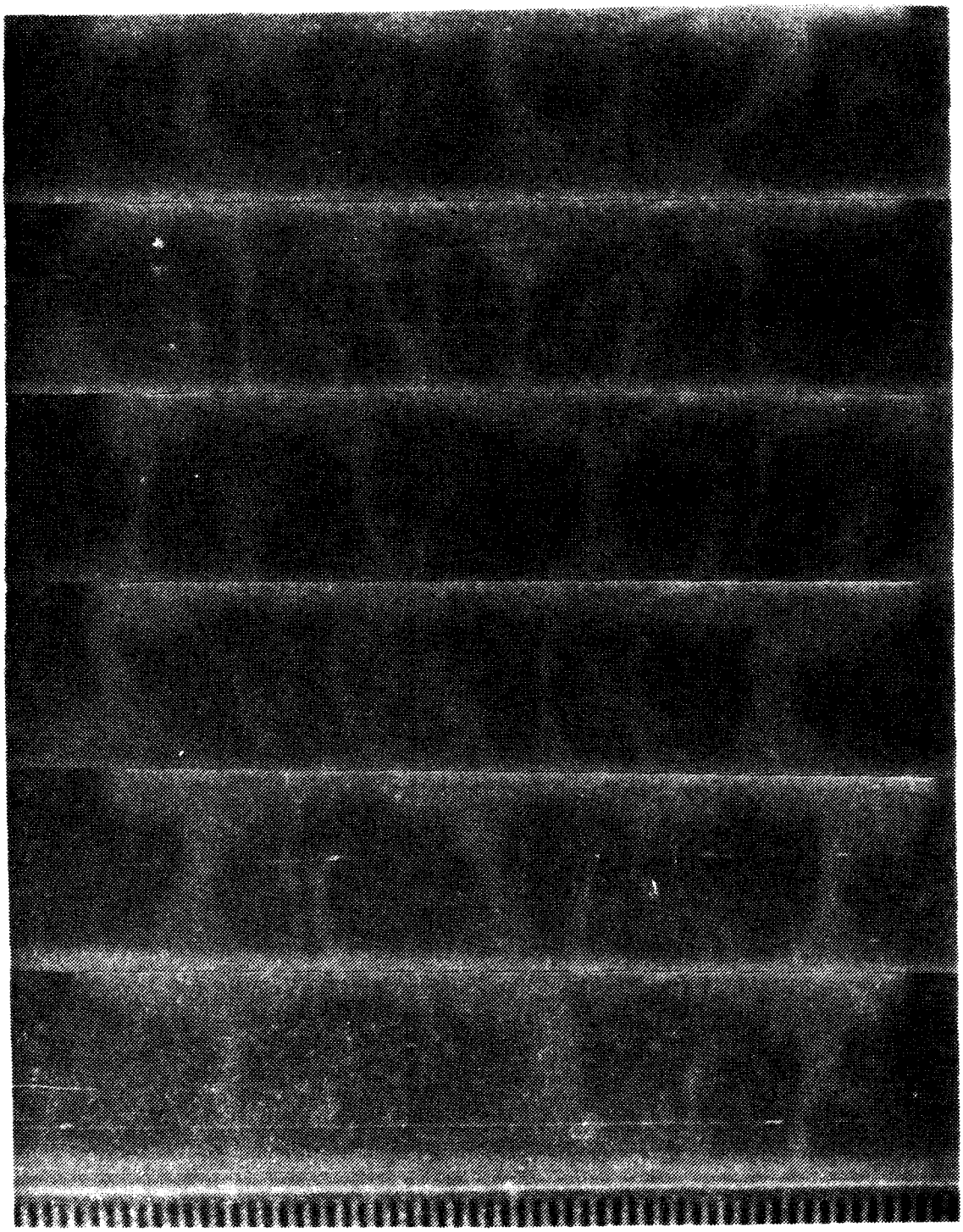

Figure 27 Flow Visualization At De=100 And 115 R Degrees From Start Of Curvature

Figure 28 Flow Visualization At De=100 And 125 Degrees From Start Of Curvature

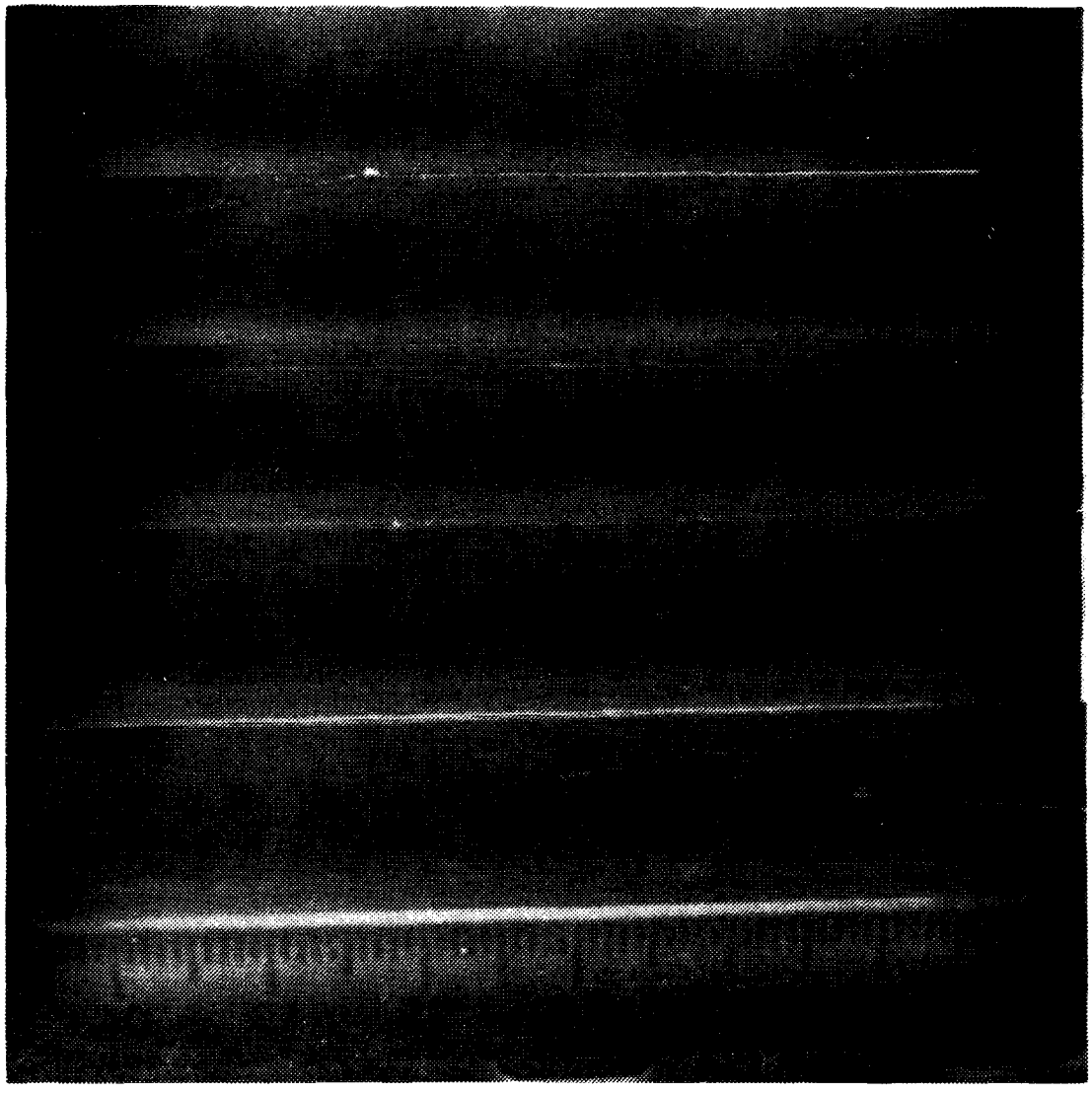

Figure 29 Flow Visualization At De=100
And 135 Degrees From Start
Of Curvature

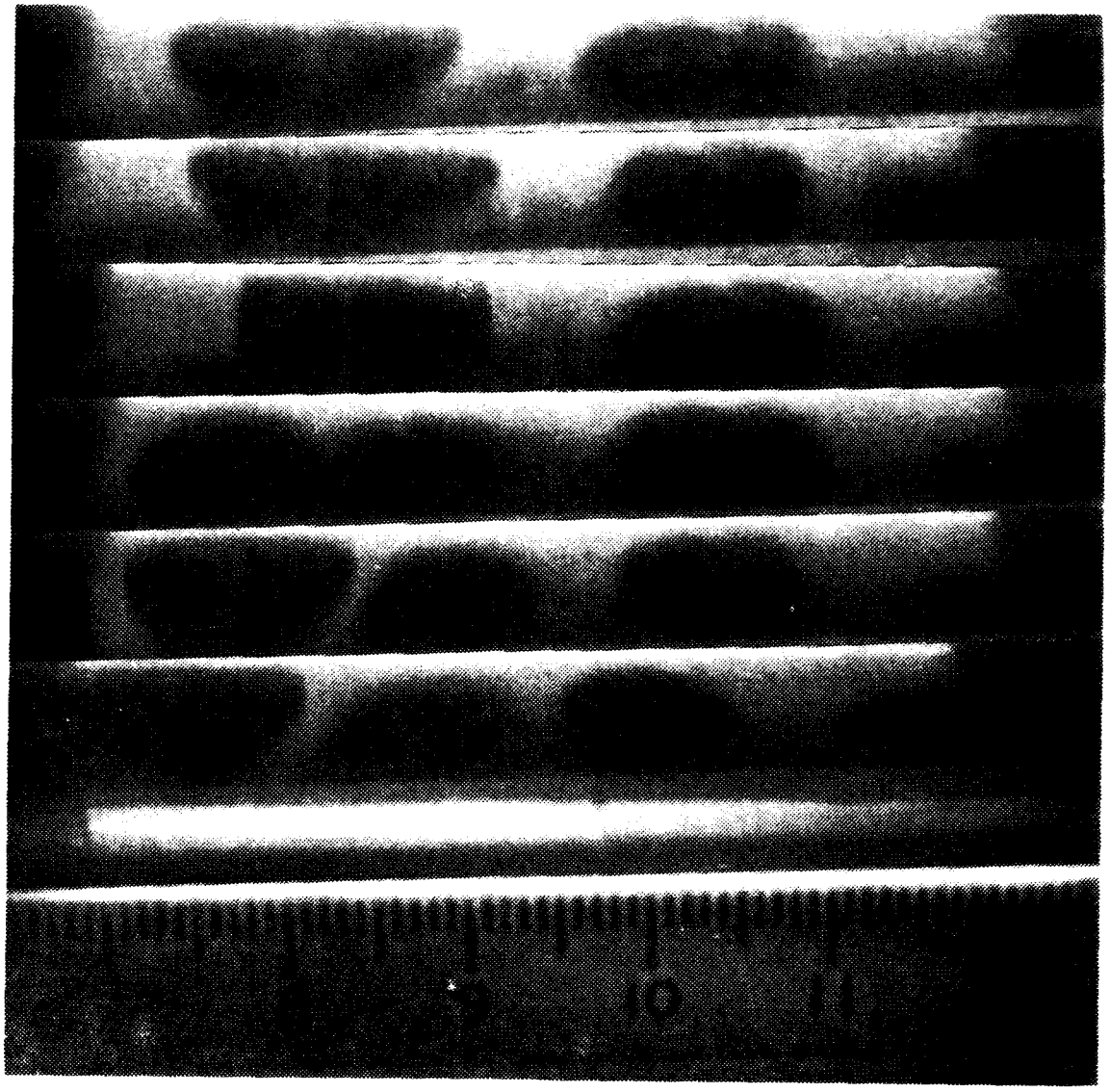

Figure 30 Flow Visualization At De=120
And 85 Degrees From Start
Of Curvature

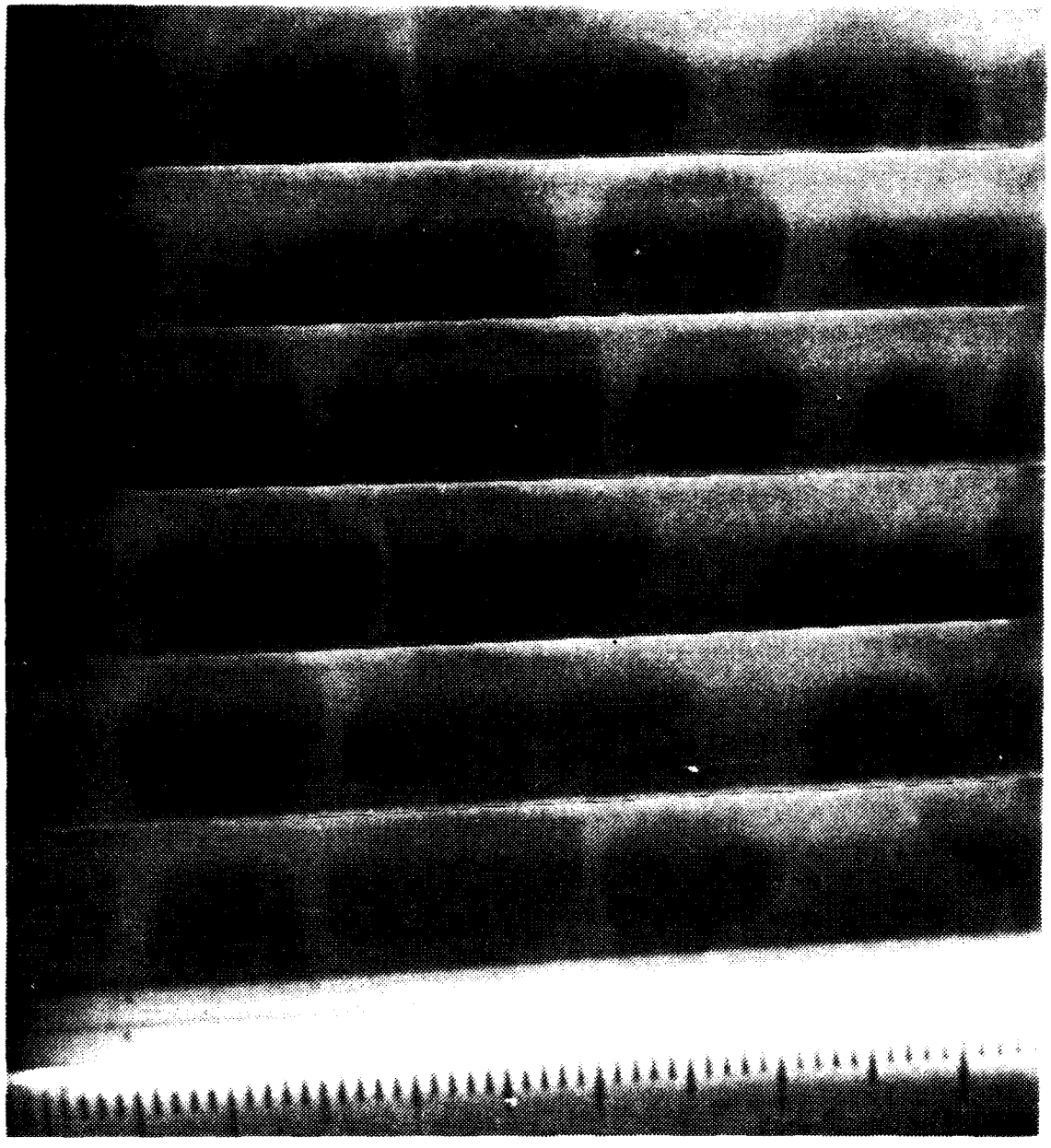

Figure 31 Flow Visualization At De=120
And 95 Degrees From Start
Of Curvature

Figure 32 Flow Visualization At De=120
And 105 Degrees From Start
Of Curvature

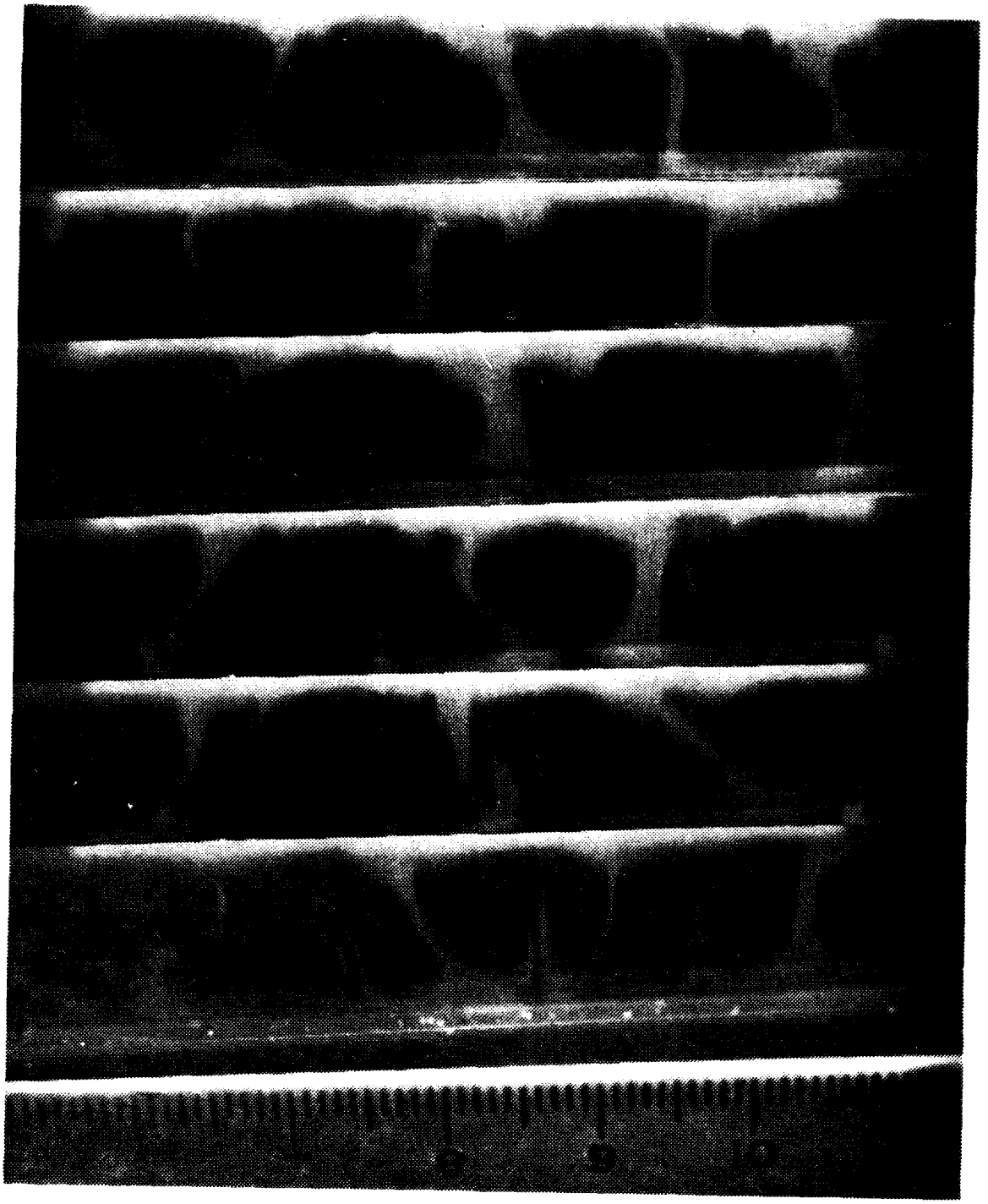

Figure 33 Flow Visualization At De=120
And 115 L Degrees From Start
Of Curvature

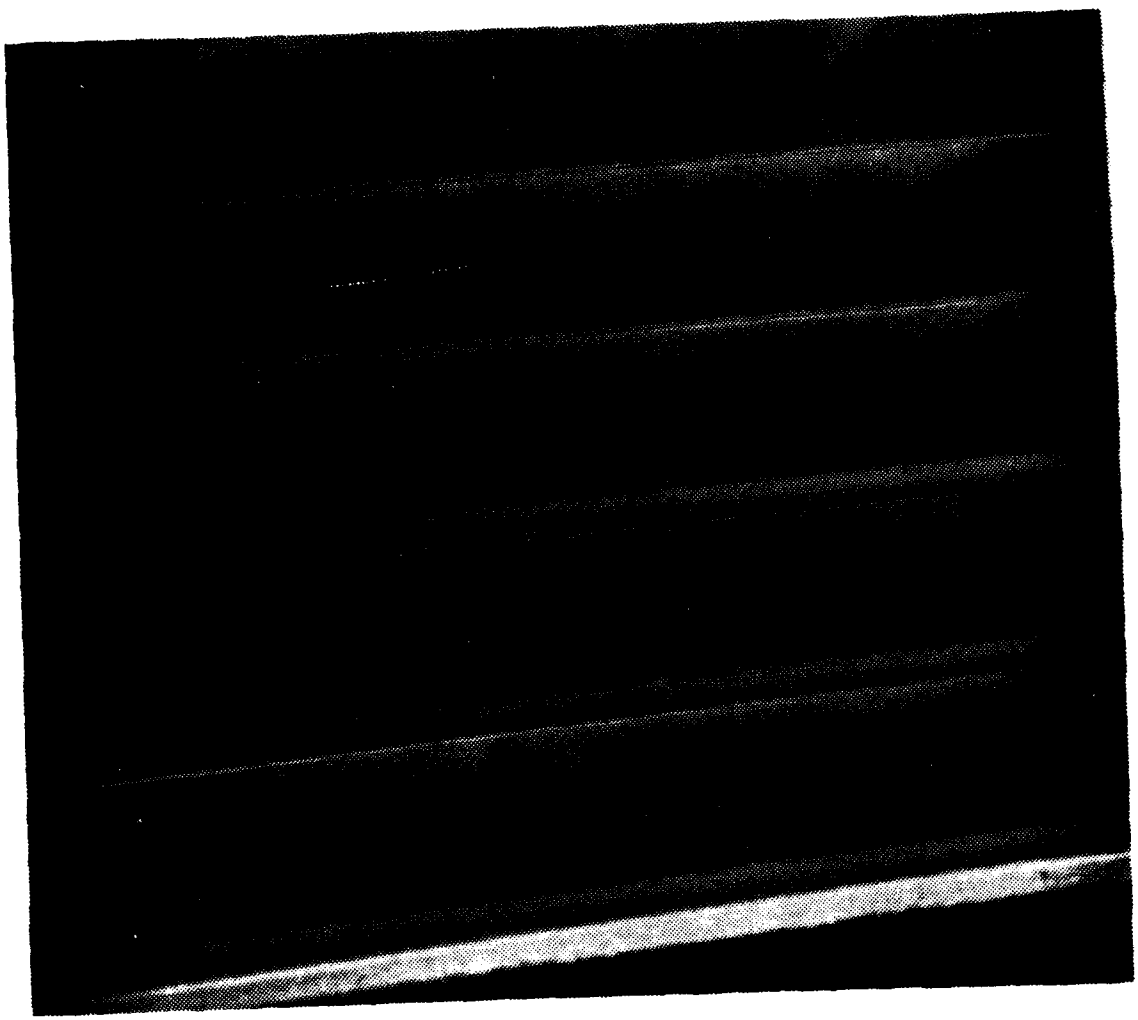

Figure 34 Flow Visualization At De=120
And 125 Degrees From Start
Of Curvature

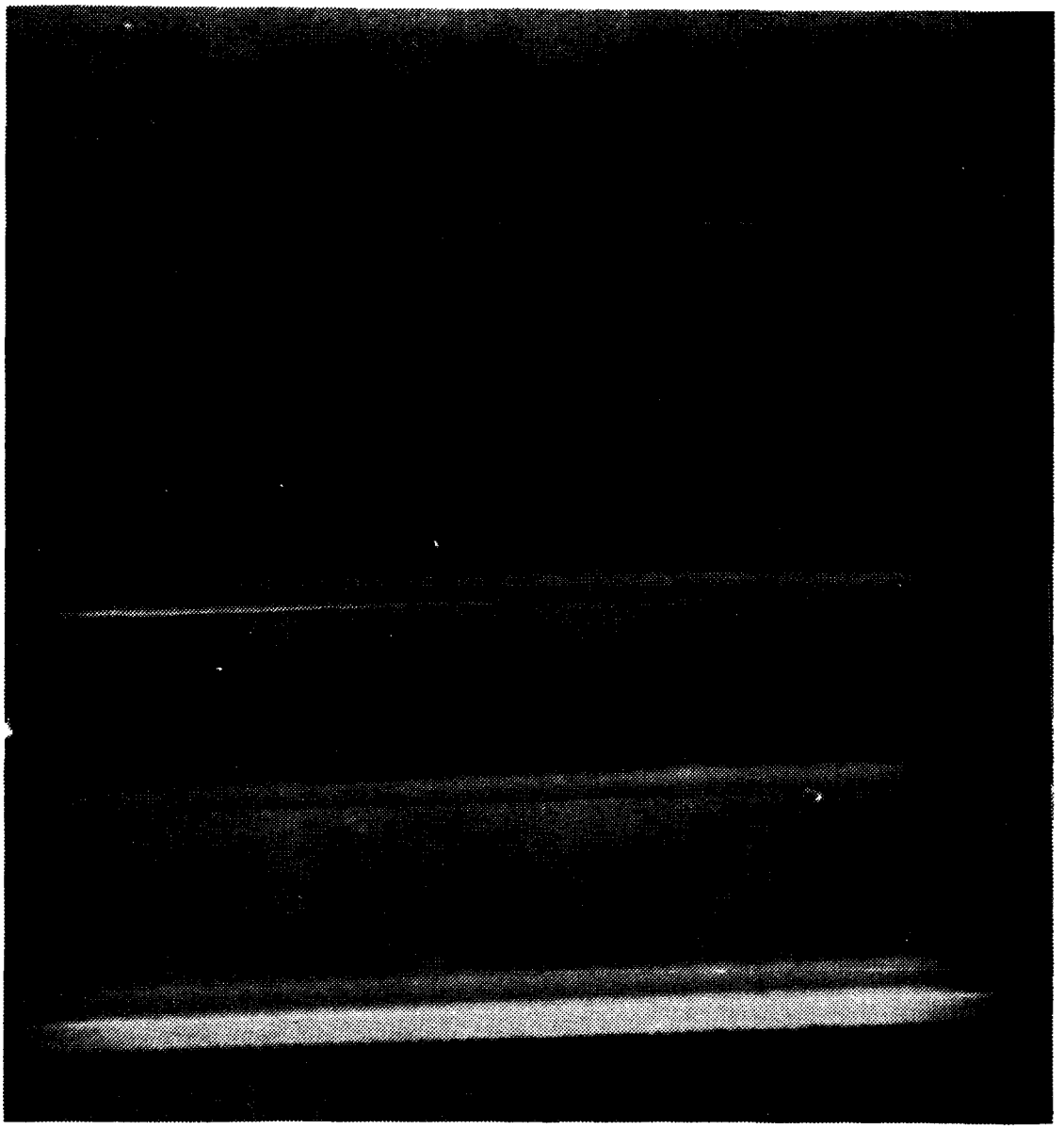

Figure 35 Flow Visualization At De=120 And 135 Degrees From Start Of Curvature

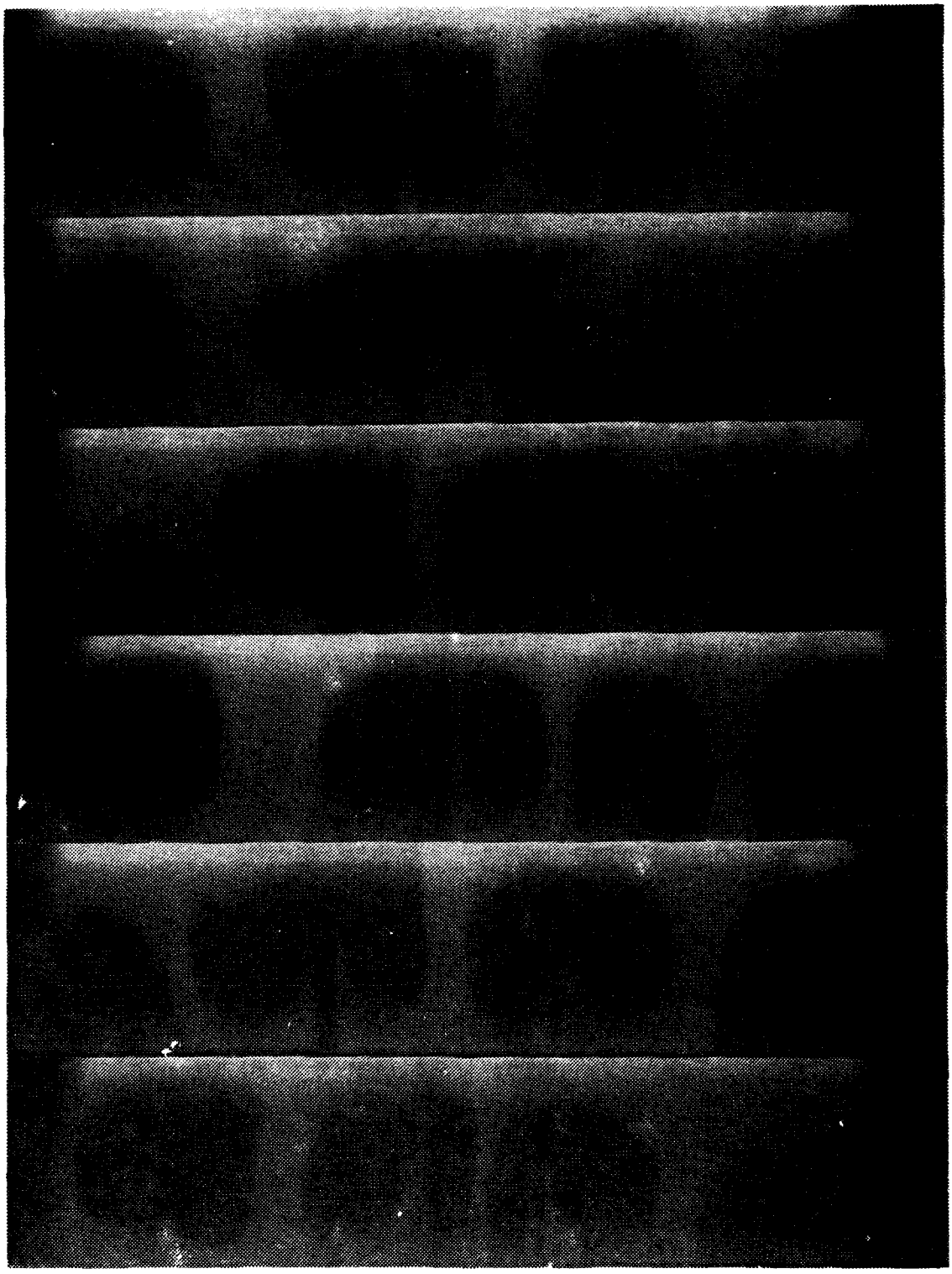

Figure 36 Flow Visualization At De=141
And 85 Degrees From Start
Of Curvature

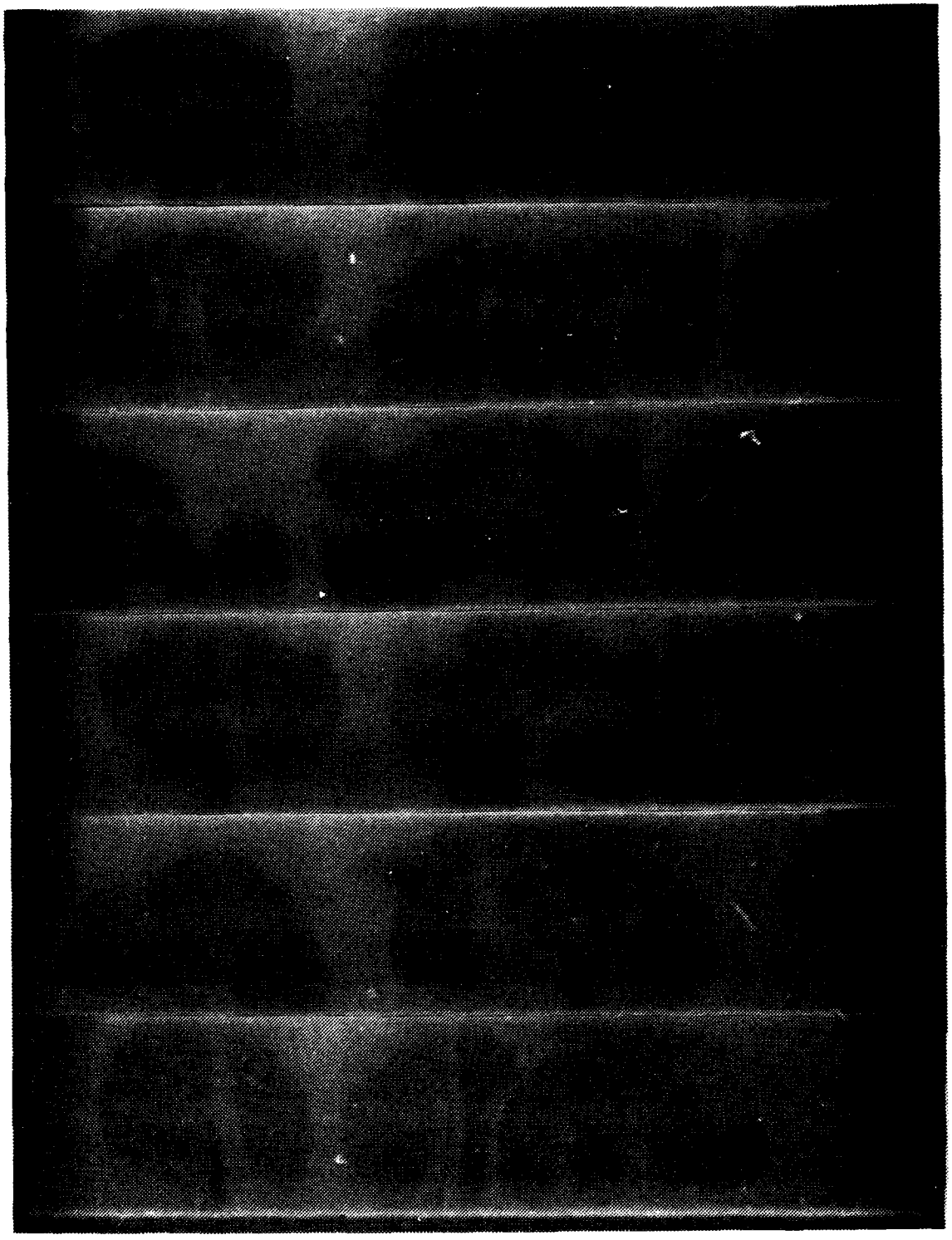

Figure 37 Flow Visualization At De=141
And 95 Degrees From Start
Of Curvature

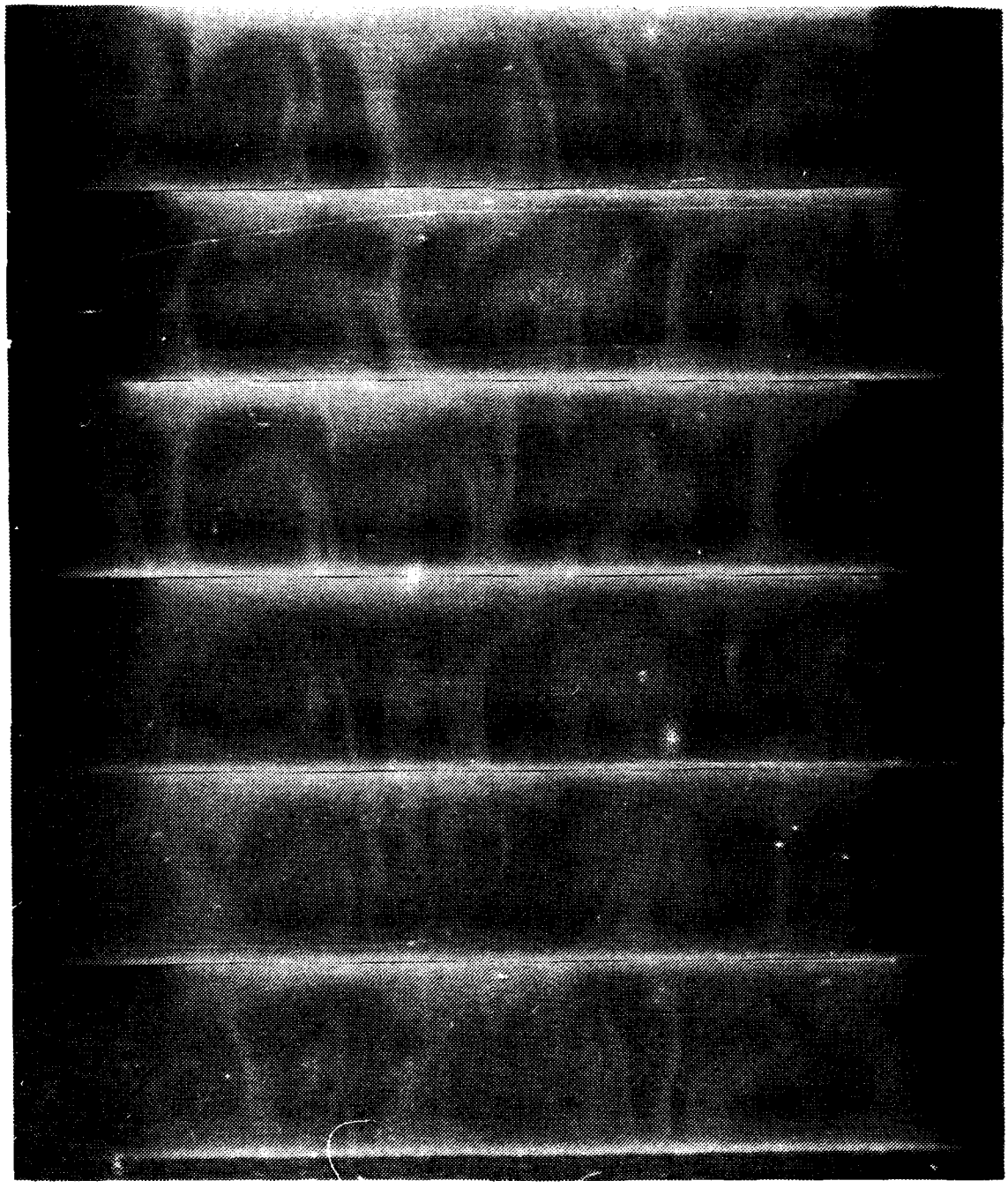

Figure 38 Flow Visualization At De=141
And 105 Degrees From Start
Of Curvature

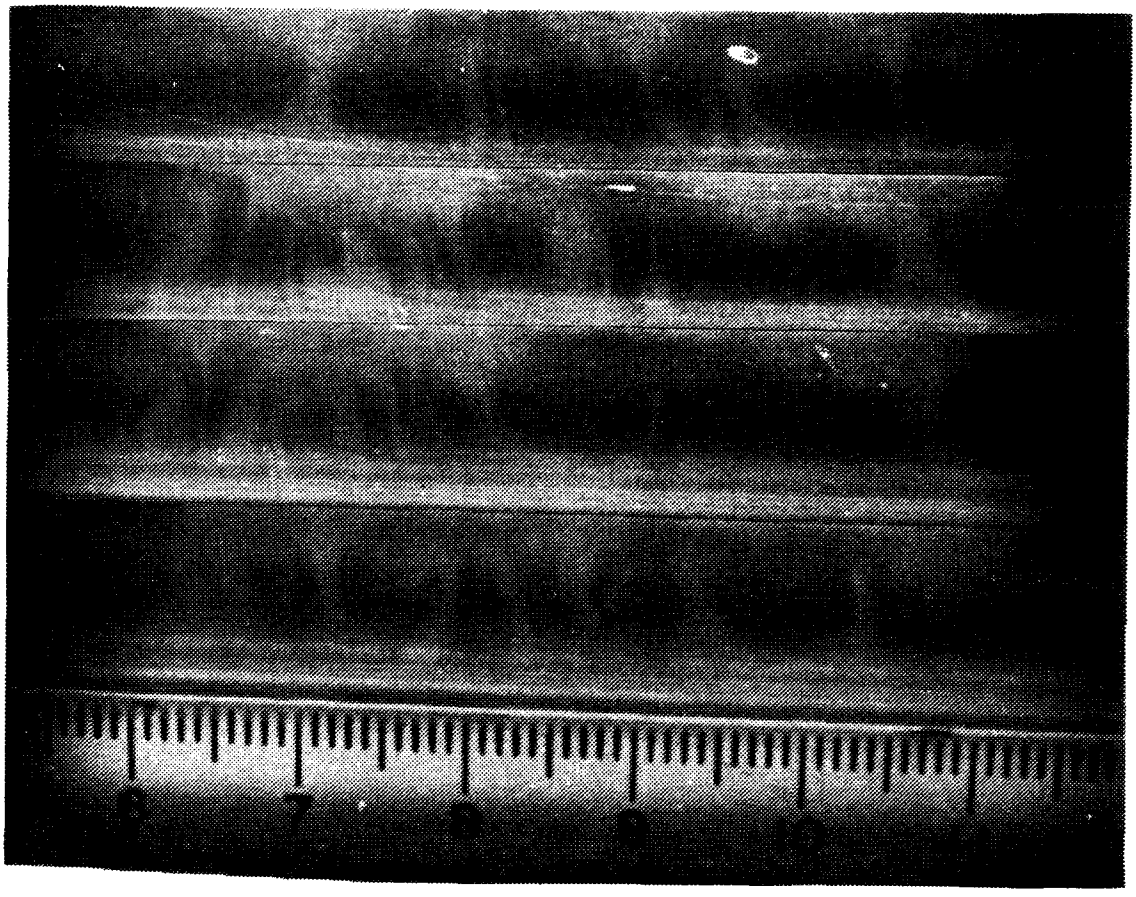

Figure 39 Flow Visualization At De=141
And 115 L Degrees From Start
Of Curvature

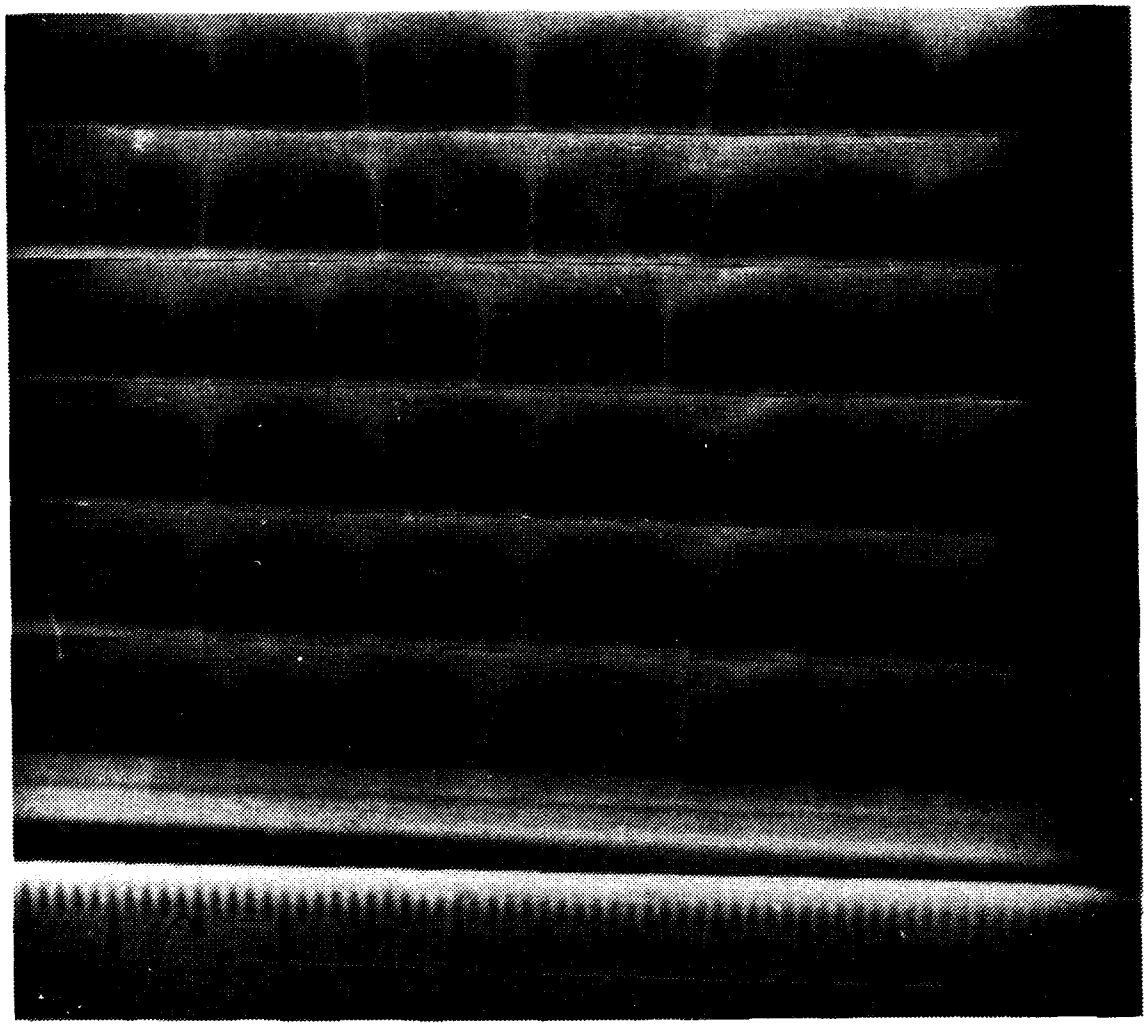

Figure 40 Flow Visualization At De=141
And 115 R Degrees From Start
Of Curvature

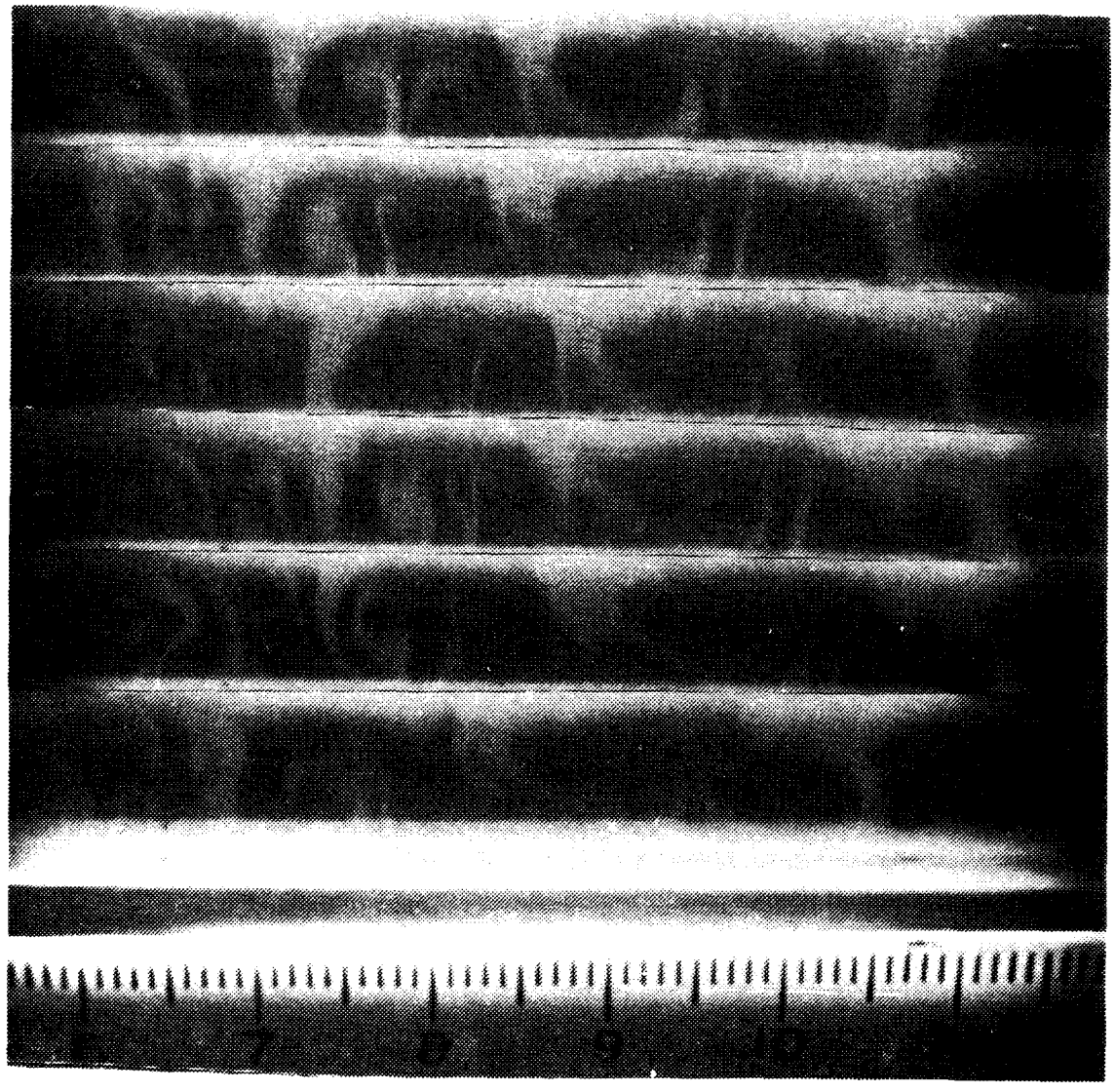

Figure 41 Flow Visualization At De=141
And 125 Degrees From Start
Of Curvature

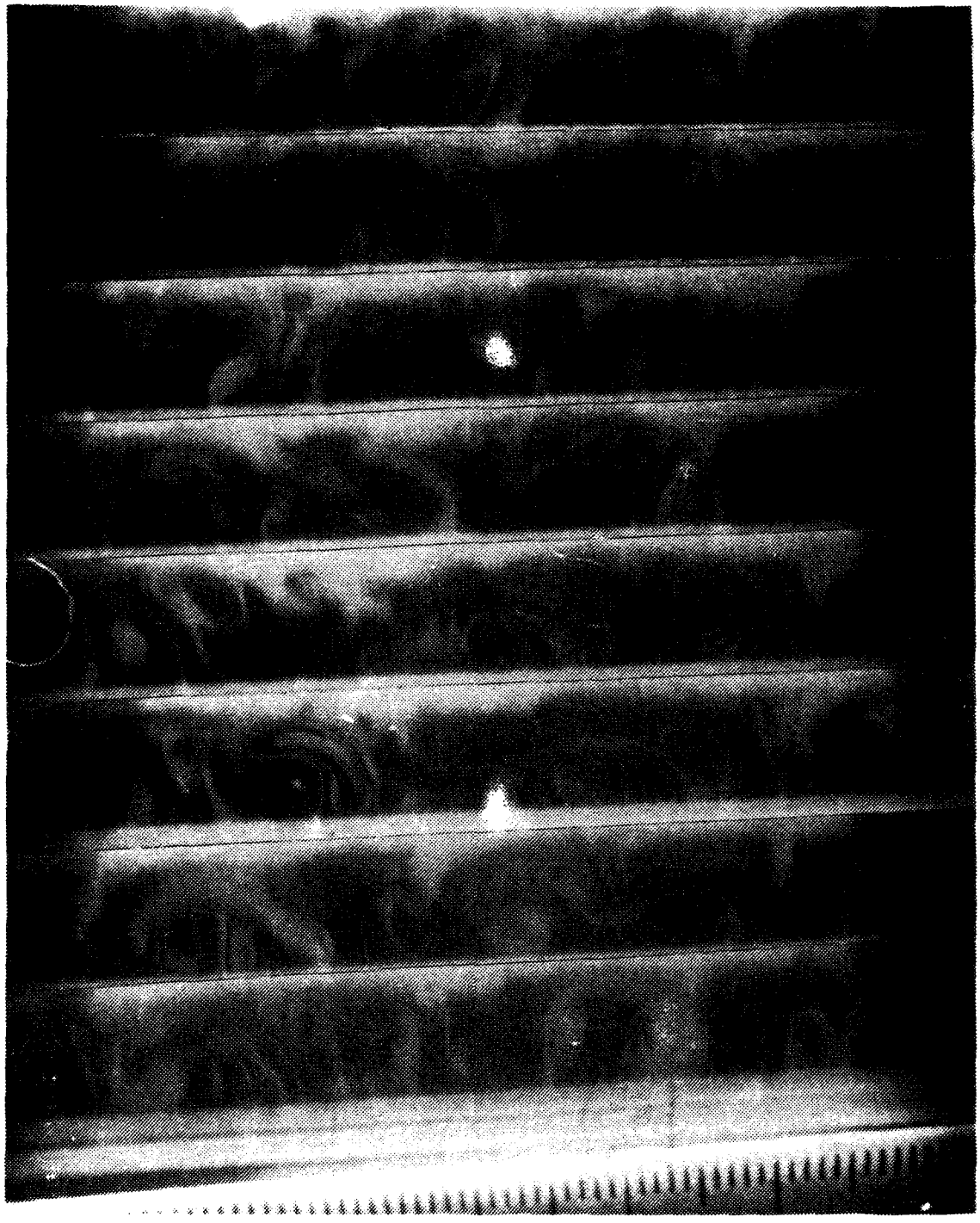

Figure 42 Flow Visualization At De=141
And 135 Degrees From Start
Of Curvature

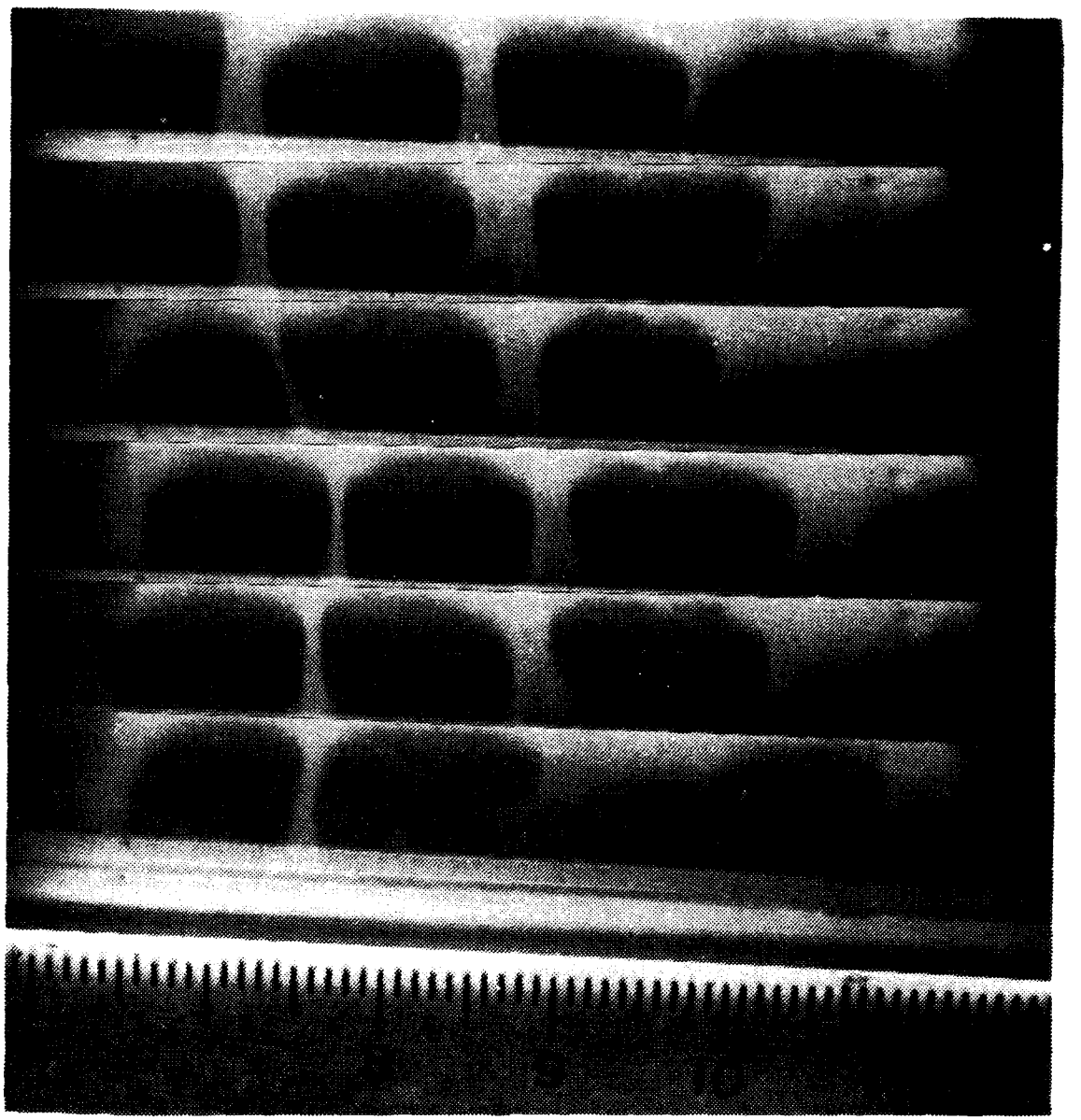

Figure 43 Flow Visualization At De=160
And 85 Degrees From Start
Of Curvature

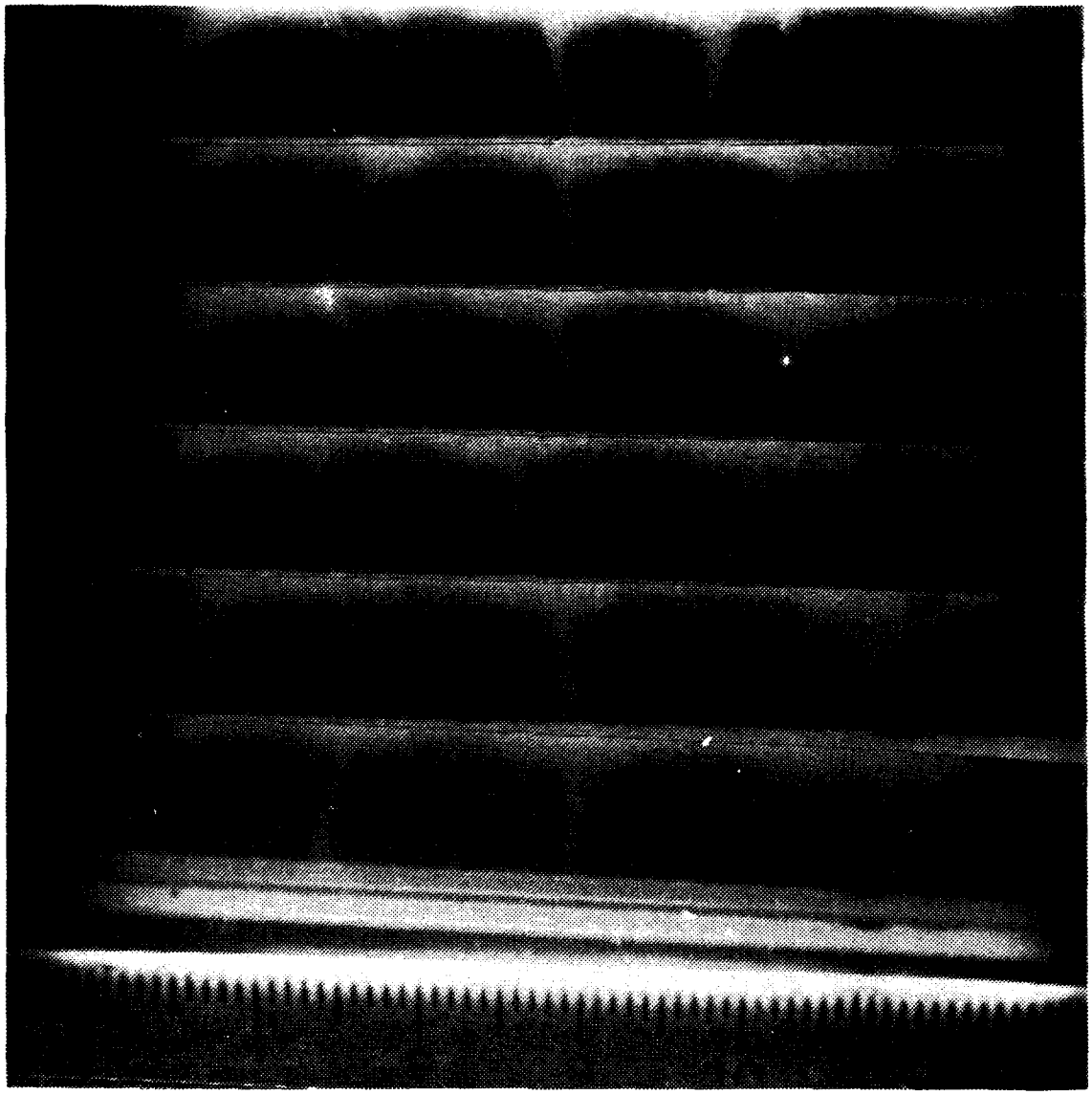

Figure 44 Flow Visualization At De=160
And 95 Degrees From Start
Of Curvature

Figure 45 Flow Visualization At De=160
And 105 Degrees From Start
Of Curvature

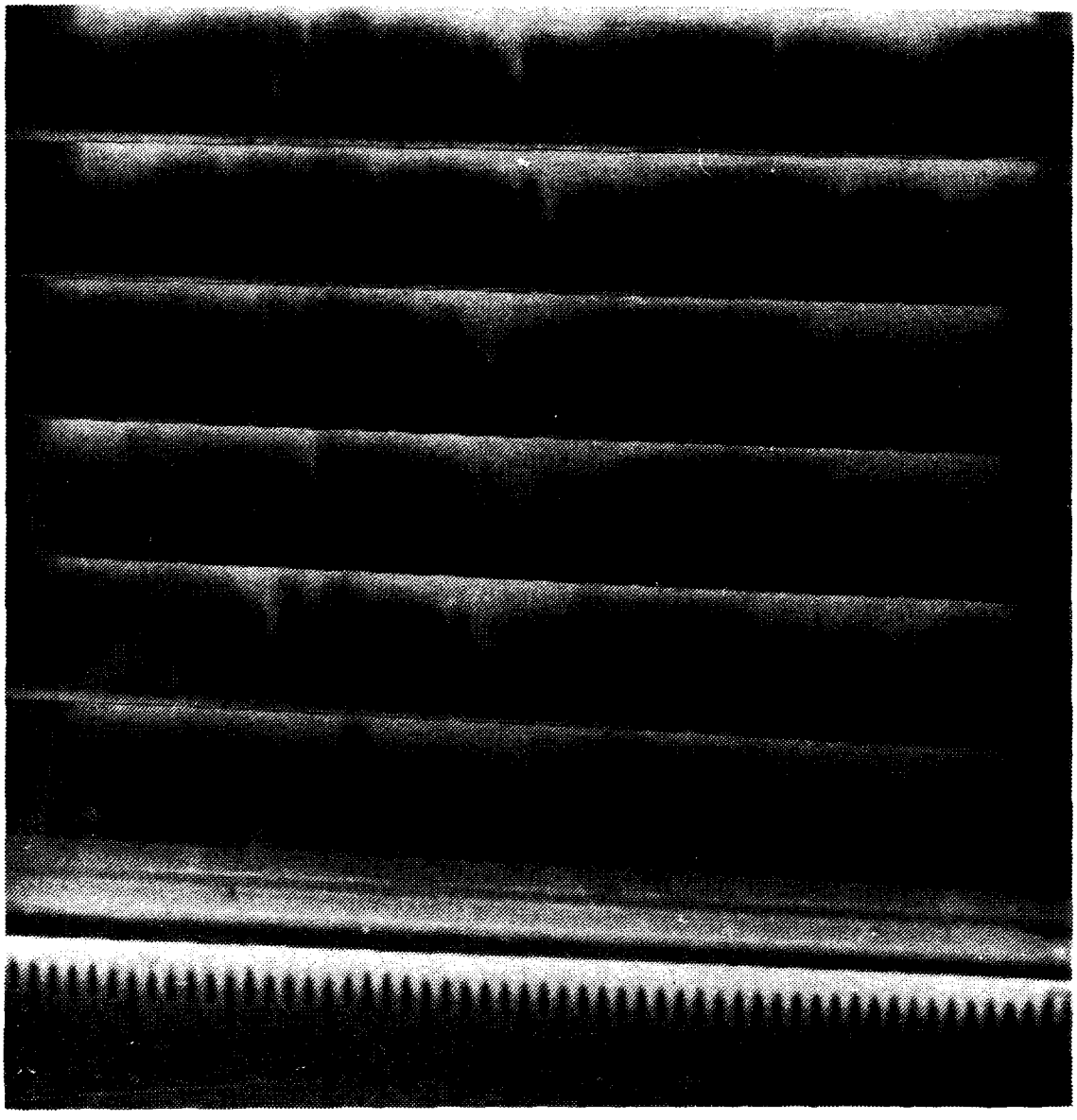

Figure 46 Flow Visualization At De=160 And 115 L Degrees From Start Of Curvature

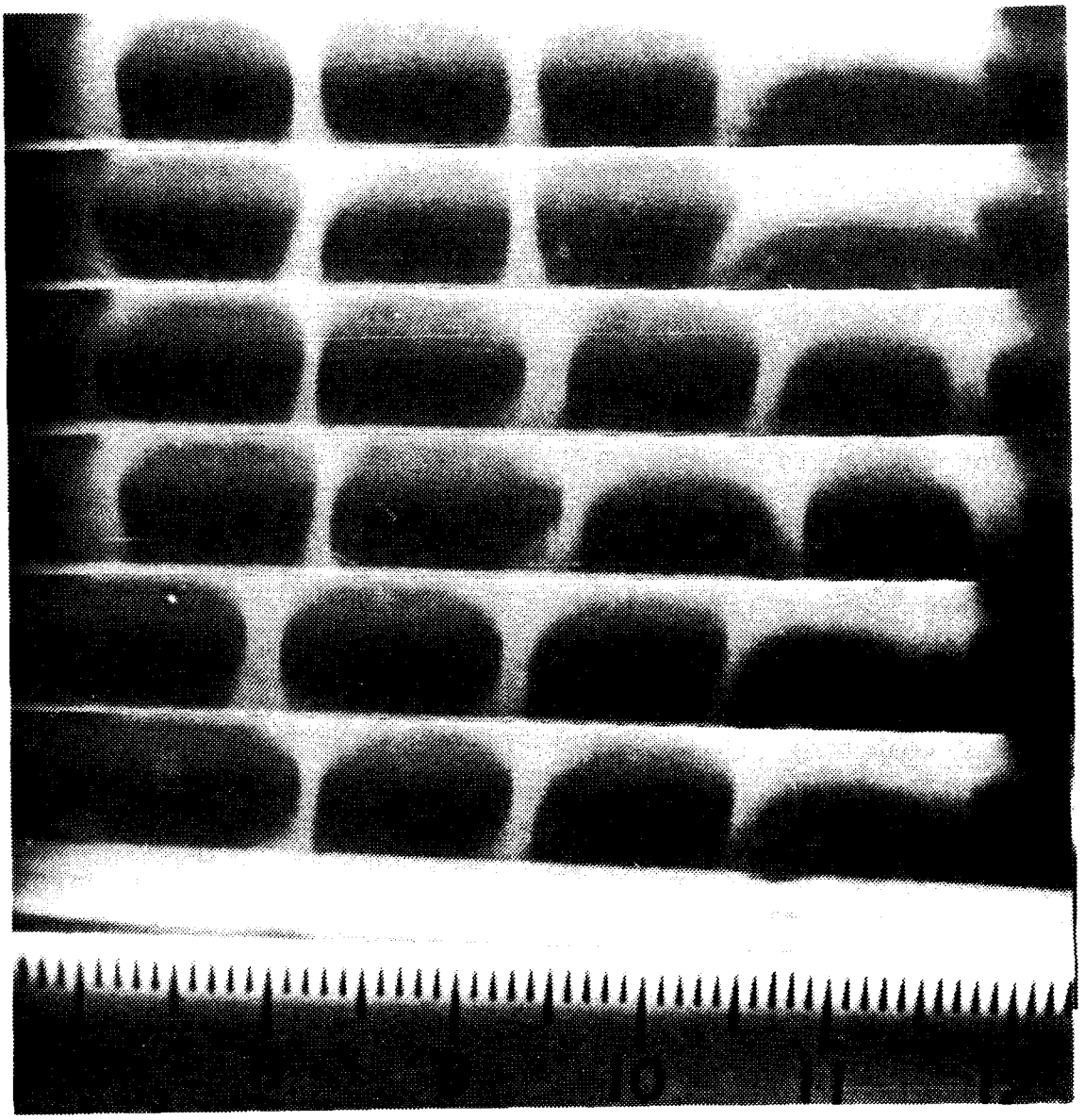

Figure 47 Flow Visualization At De=170
And 85 Degrees From Start
Of Curvature

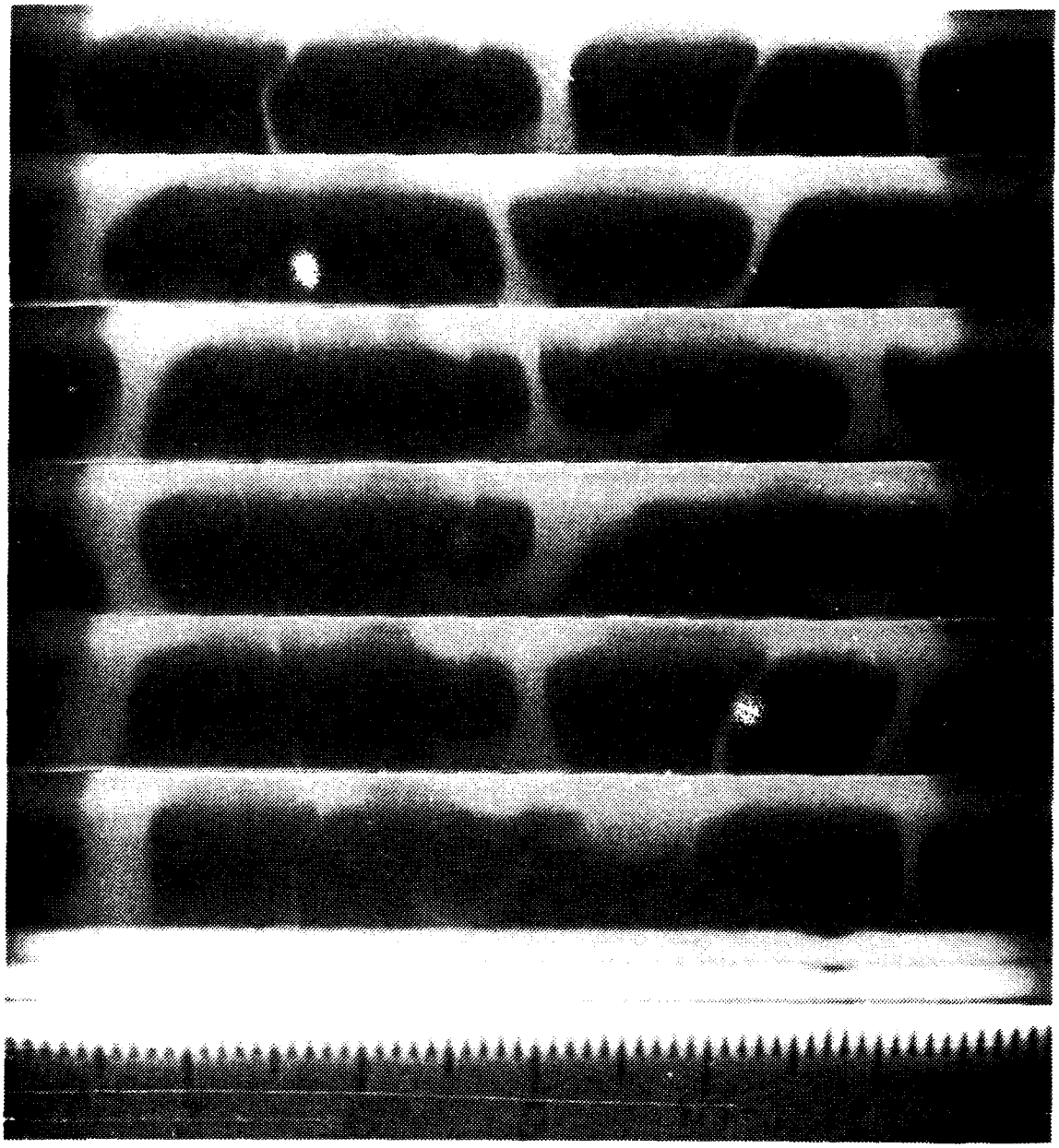

Figure 48 Flow Visualization at De=170
And 95 Degrees From Start
Of Curvature

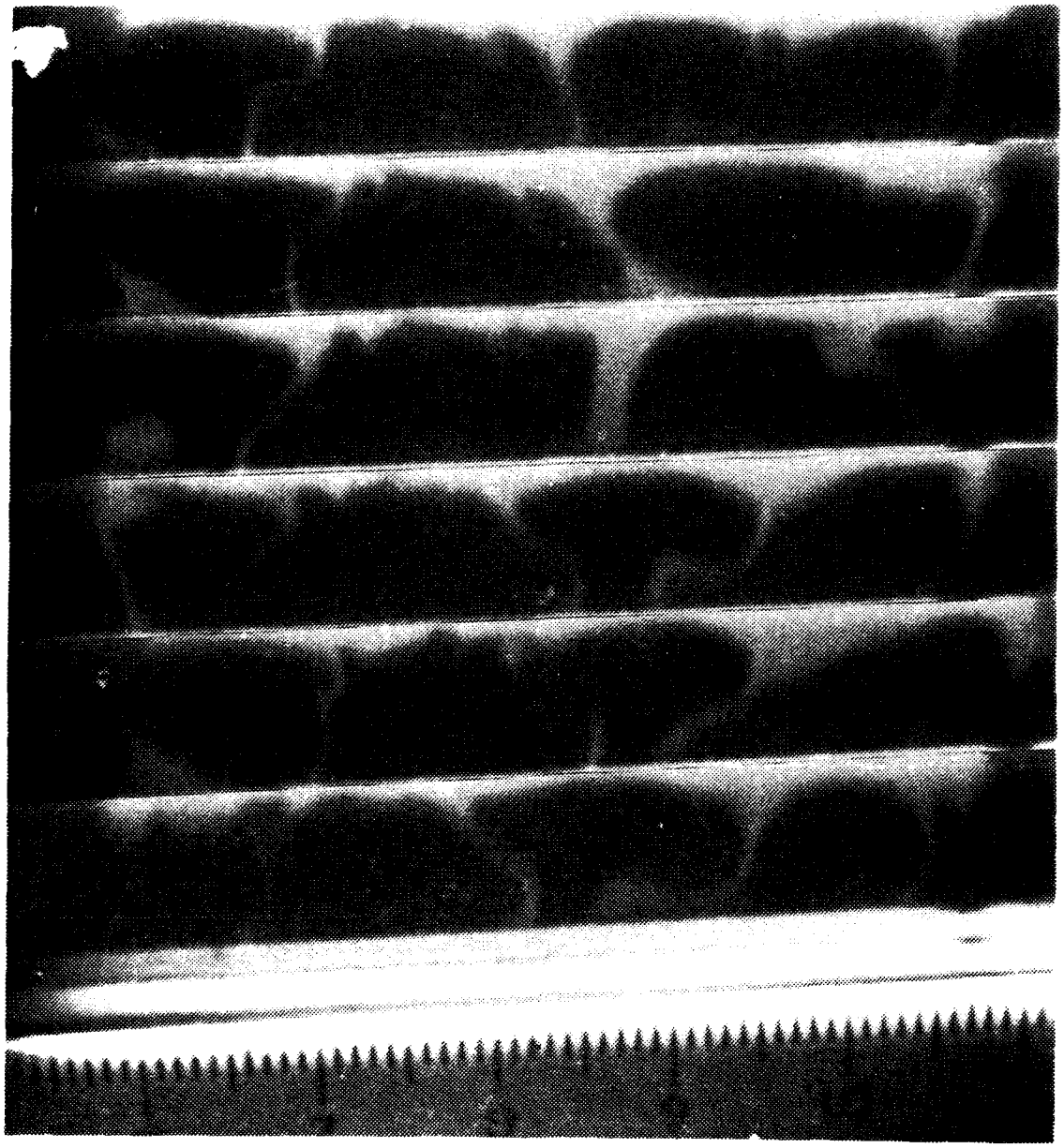

Figure 49 Flow Visualization At De=170
And 105 Degrees From Start
of Curvature

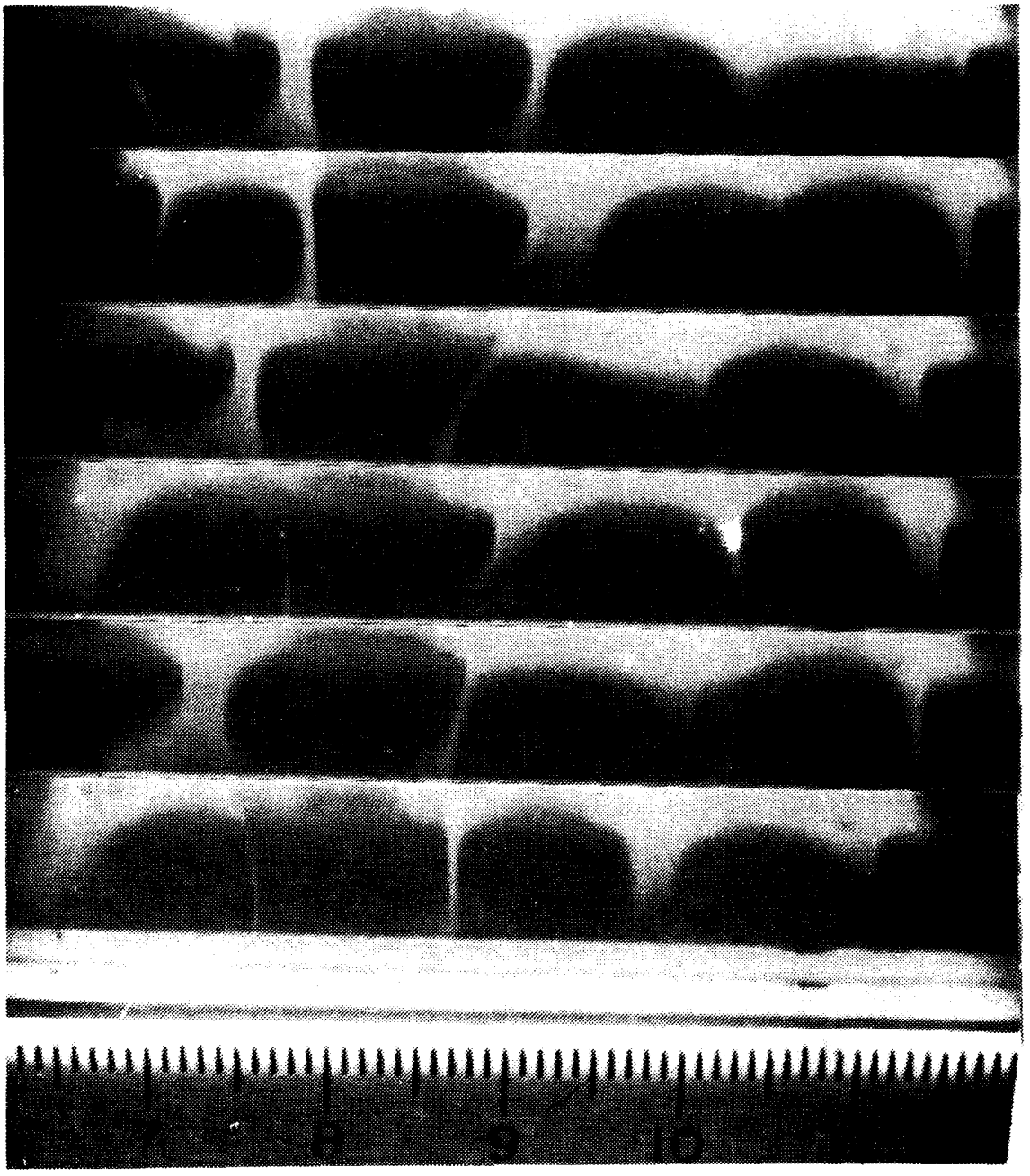

Figure 50 Flow Visualization At De=180
And 85 Degrees From Start
Of Curvature

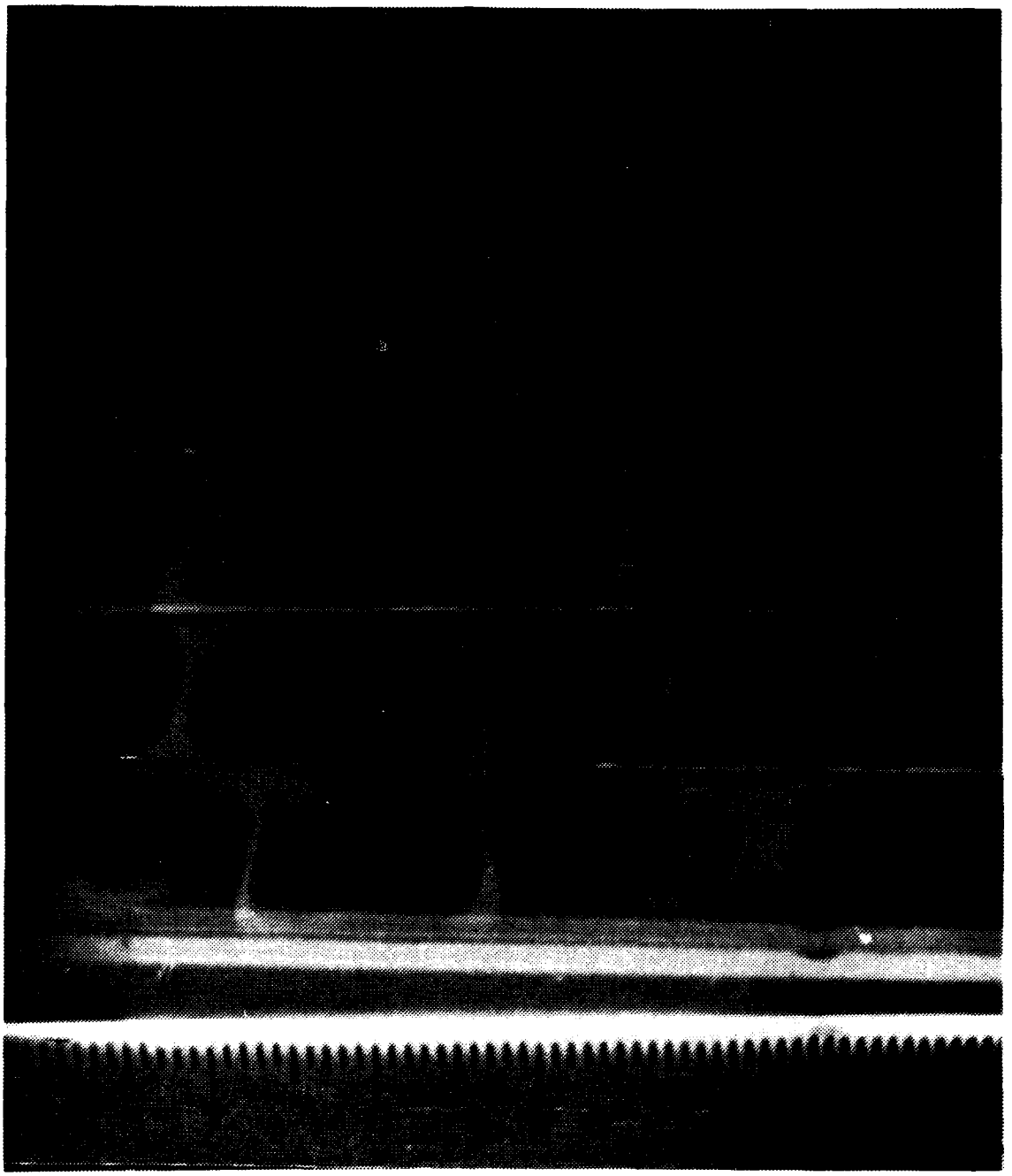

Figure 51 Flow Visualization At De=180 And 95 Degrees From Start Of Curvature

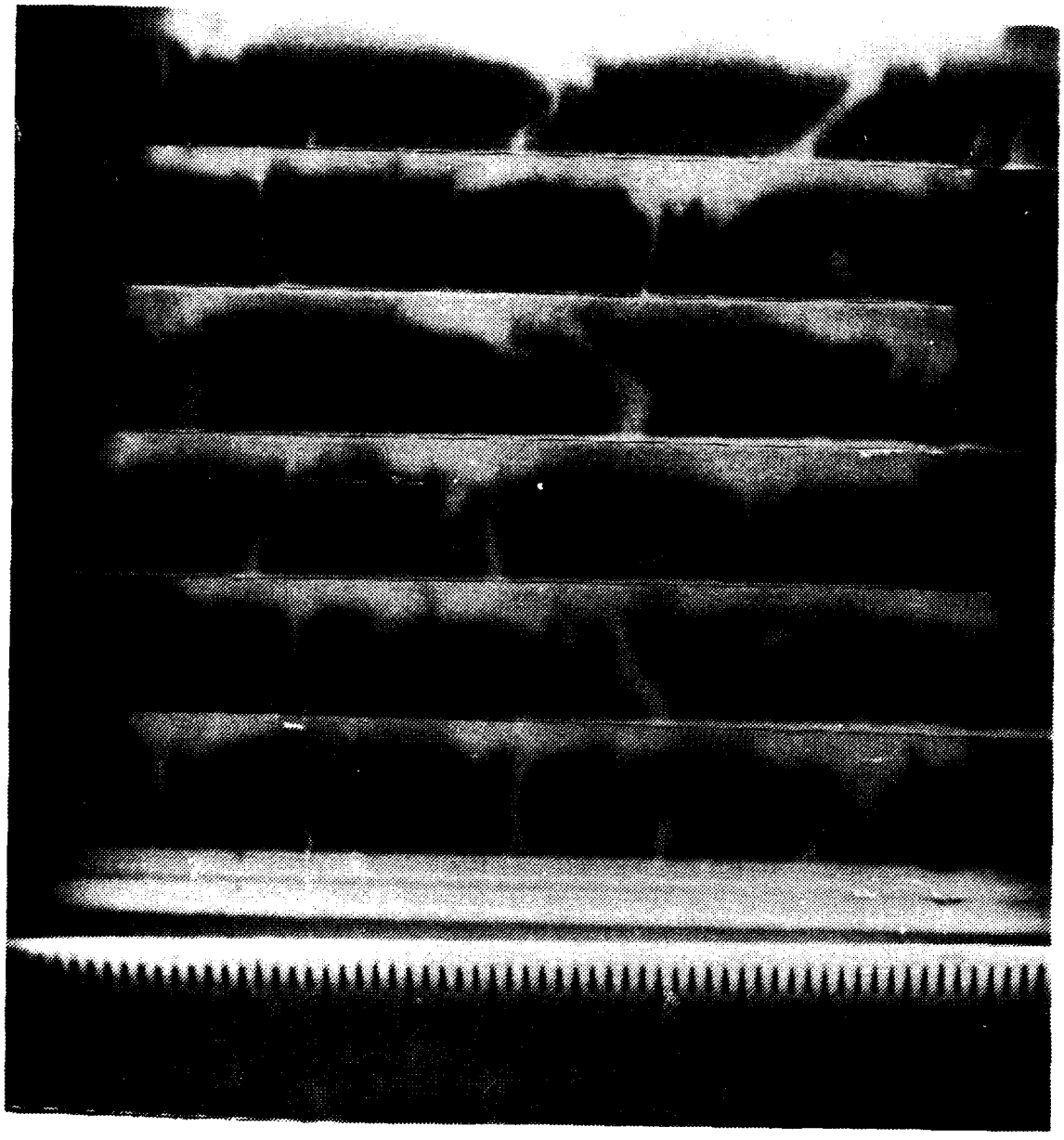

Figure 52 Flow Visualization At De=180
And 105 Degrees From Start
Of Curvature

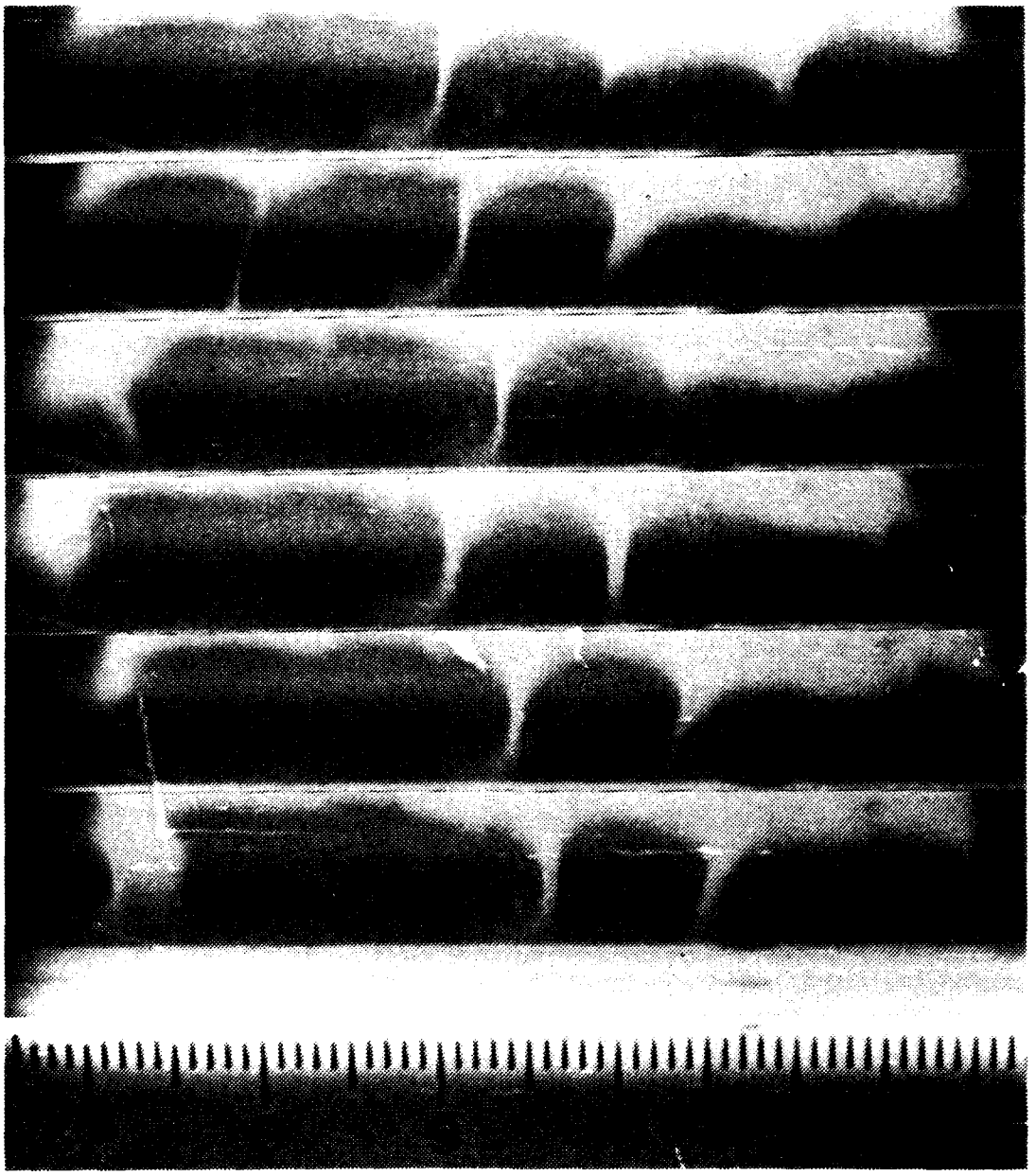

Figure 53 Flow Visualization At De=201
And 85 Degrees From Start
Of Curvature

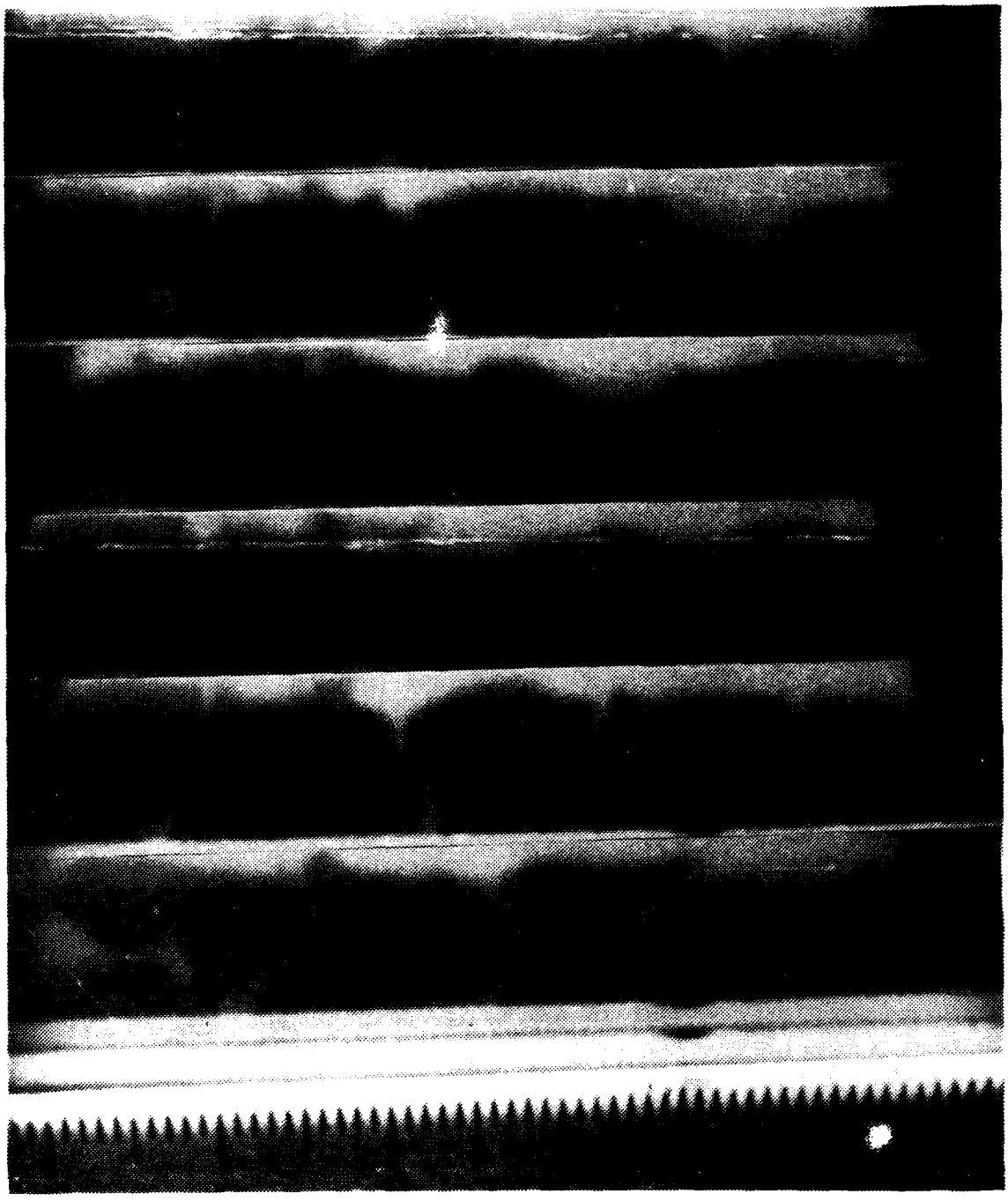

Figure 54 Flow Visualization At De=201
And 95 Degrees from Start
Of Curvature

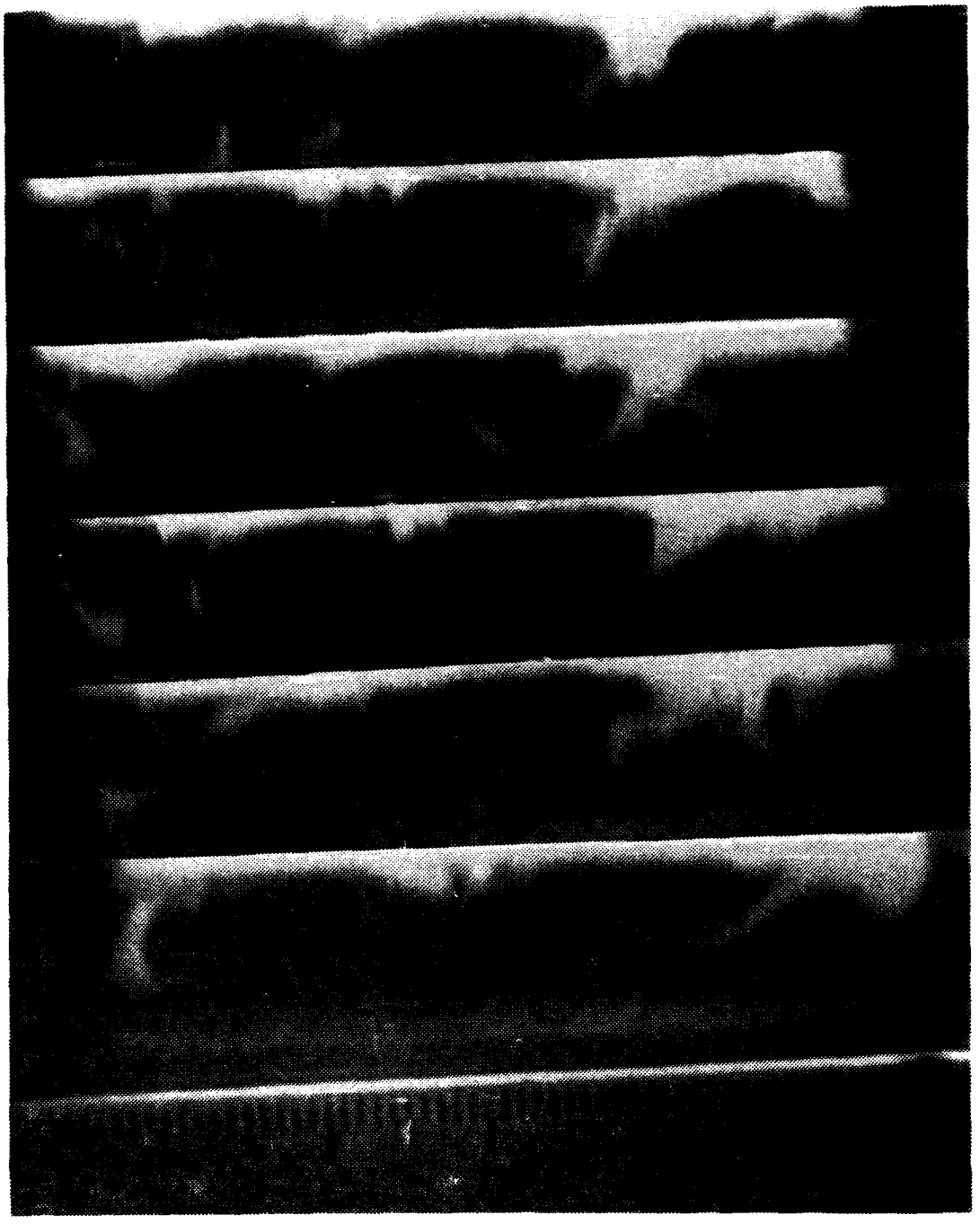

Figure 55 Flow Visualization At De=201
And 105 Degrees From Start
Of Curvature

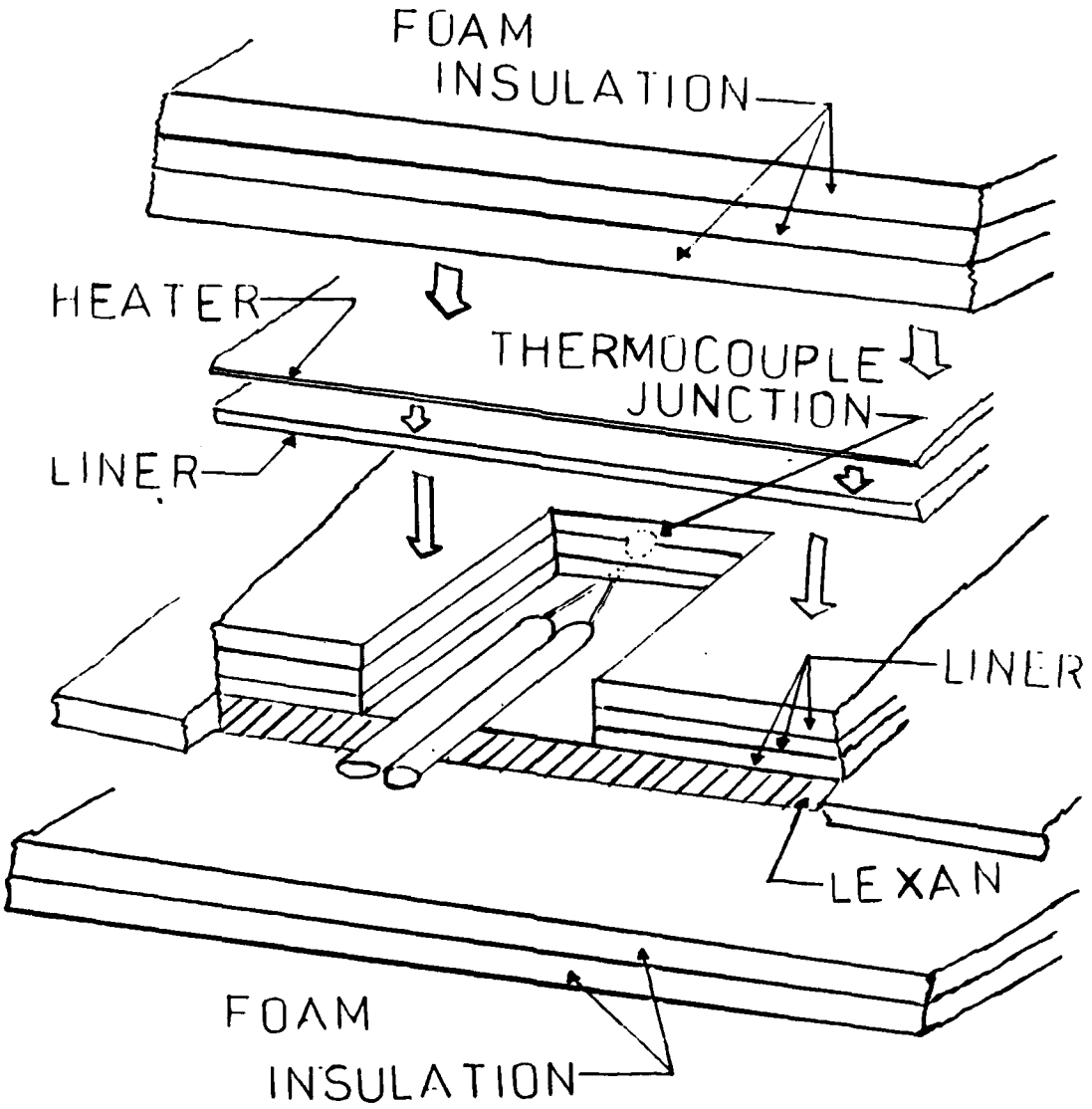

Figure 56 Thermocouple And Heat Transfer Surface For Curved Channel Heat Transfer Surface

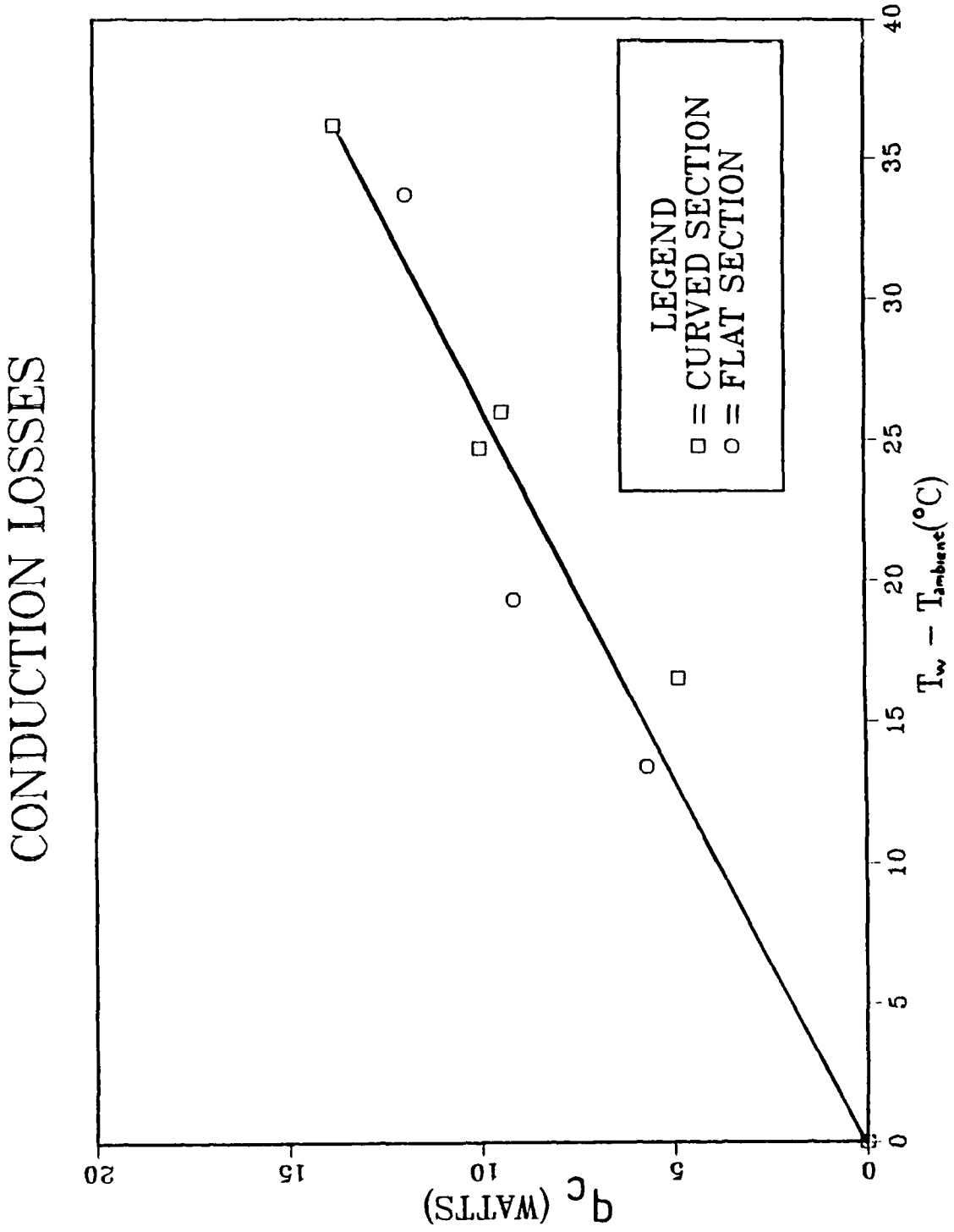

Figure 57 Conduction Losses

APPENDIX B

UNCERTAINTY ANALYSIS

1. Dean Number Uncertainty

Uncertainty in Dean number calculation is derived from factors affecting measurement uncertainties of the pressure drop accross an ASME standard orifice plate. A sample of the uncertainty quantities for De=150 is provided;

a. Celesco Transducer Calibration Uncertainty

$\delta P_{manometer} = \pm .002$ in. H_2O

$\delta \bar{E} = \pm .0007$ Volts

$\delta \bar{C} = \pm .0012$ in. H_2O/Volt

b. Pressure Drop Uncertainty

$\delta \bar{E} = \pm .047$ Volts

$\delta \Delta P_{or} = \pm .005$ in. H_2O

c. Mass Flow Rate Uncertainty

$\delta A_{or} = \pm .012$ in.^{2}

$\delta K = \pm .001$

$\delta Y = \pm .02$

$\delta \rho = \pm .002$ lbm/ft^3

$\delta \dot{m} = \pm .0004$ lbm/sec (95% confidence level)

$\delta A_{ch} = \pm .0052$ in.^{2}

δ De $= \pm 4.4$ (95% confidence level)

2. Conduction Loss Uncertainty

The uncertainty in calculation of the conduction loss (q_c) is derived from factors affecting the meassurement uncertainties involving power input and temperature measurement. A sample of uncertainty quantities for $T_w - T_{ambient} = 19.7$ is provided;

a. Power Unput Uncertainty

$\delta V = \pm .2$ volts

$\delta I = \pm .05$ amps

$\delta VI = \pm .63$ watts

b. Insulation loss Uncertainty

$\delta k = \pm .001$

$\delta A = \pm .0065\ m^2$

$\delta\Delta X = \pm .0015$ m

$\delta\Delta T = \pm .25\ ^\circ C$

$\delta q_w = \pm .70$ watts (95% confidence level)

c. Conduction Loss Uncertainty

$\delta q_c = \pm .94$ watts (95% confidence level)

3 . Contact Resistance Loss Uncertainty

The uncertainty in calculation of the Contact Resistance (CR) is derived from factors affecting the measurement of the temperature of the liquid crystals and the determination of the insulation losses. A sample of uncertainty quantities for the same conditions as in the Conduction Loss Uncertainty analysis is provided;

$\delta\Delta T = .283\ ^{\circ}C$

$\delta A = .0065\ m^2$

$\delta q_w = .70$ watts

$\delta CR = 4.7 \times 10^{-5}\ ^{\circ}Cm^2/watt$ (95% confidence level)

REFERENCES

1. nolihan, R. G. Jr., Investigations of Heat Transfer in Straight and Curved Rectangular Ducts for Laminar and Transition Flows, Master's Thesis, Naval Postgraduate School, Monterey, California, 1981.

2. Dean, W. R., "Fluid Motion in a Curved Channel," Proceedings of the Royal Society of London, Series A, V. 121, pp. 402-420, 1928.

3. Reid, W. H., "On the Stability of Viscous Flow in a Curved Channel," Proceedings of the Royal; Society of London, Series A, V. 244, pp. 186-198, 1958.

4. Hammerlin, G, "Die Stabilitat der Stromung in Einem Gekrummten Kanal," Archive for Rational Mechanics and Analysis, V. 1, pp. 212-224, 1958.

5. Brewster, D. B., Grosberg, P., and Nissan, A. H., "The Stability of Viscous Flow Between Horizontal Concentric Cylinders," Proceedings of the Royal Society of London, Series A, V. 251, pp. 76-91, 1959.

6. Cheng, K.C., Nakayama, J., Akiyama, M., "Effect of Finite and Infinite Aspect Ratios on Flow Patterns in Curved Rectangular Channels," Proceedings of the International Symposium on Flow Visualization, pp. 181-186, 1977.

7. Kelleher, M. D., Flentie, D. L., and McKee, R. J., "An Experimental Study of the Secondary Flow in a Curved Rectangular Channel," ASME Journal of Fluids Engineering, V. 102, pp. 92-96, 1980.

8. Thermosciences Division, Department of Mechanical Engineering, Stanford University Report TF-30, Instability and Transition in Curved Channel Flow,by W. H. Finlay, J. B. Keller and J. H. Ferziger, May 1987.

9. Finlay, W. H., Keller, J. B., and Ferziger, J. H., "Finite Amplitude Vortices in Curved Channel Flow," submitted to Journal of Fluid Mechanics, 1988.

10. Ligrani, P. M. and Niver, R. D., "Flow Visualization of Dean Vortices in a Curved Channel with 40 to 1 Aspect Ration," to appear in Physics of Fluids, 1988.

11. Niver, R. D., Structural Characteristics of Dean Vortices in a Curved Channel, Master's Thesis, Naval Postgraduate School, Monterey, California, June 1987.

12. Siedband, M. A., A Flow Visualozation Study of Laminar/Turbulent Transition in a Curved Channel, Master's Thesis, Naval Postgraduate School, Monterey, California, March 1987.

13. Baun, L. R., The Development and Structural Characteristics of Dean Vortices in a Curved Rectangular Channel, Engineer's Thesis, Naval Postgraduate School, Monterey, California, September 1988.

14. Morrison, G. A., On the Use of Liquid Crystal Thermography as a Technique of Flow Visualization, Master's Thesis, Naval Postgraduate School, Monterey, California, June 1984.

15. Holman, J. P. amd Gajda, W. J., Jr., Experimental Methods for Engineers, 4th Edition, pp. 238-247, McGraw-Hill, 1984.

16. ASME Power Test Committee, ASME Power Test Codes, (Supplement on Instruments and Apparatus), part 5, Chapter 4, p. 25, American Society of Mechanical Engineers, 1959.

17. Schwartz, G. E., Control of Embedded Vortices Using Wall Jets, Master's Thesis, Naval Postgraduate School, Monterey, California, September 1988.

18. Joseph, S. L., The Effects of an Embedded Vortex on a Film Cooled Turbulent Boundary Layer, Master's Thesis, Naval Postgraduate School, Monterey, California, December 1986.

INITIAL DISTRIBUTION LIST

		No. Copies
1.	Defense Technical Information Center Cameron Station Alexandria, Virginia 22304-6145	2
2.	Library, Code 0142 Naval Postgraduate School Monterey, California 93943-5002	2
3.	Professor P. M. Ligrani, Code 69Li Department of Mechanical Engineering Naval Postgraduate School Monterey, California 93943-5000	10
4.	Department Chairman, Code 69 Department of Mechanical Engineering Naval Postgraduate School Monterey, California 93943-5000	1
5.	Dr. K. Civinskas Propulsion Directorate U. S. Army Aviation Res. and Technology Activity AVSCOM NASA-Lewis Research Center Cleveland, Ohio 45433	10
6.	Naval Engineering Curricular Officer, Code 34 Department of Mechanical Engineering Naval Postgraduate School Monterey, California 93943-5000	1
7.	Professor C. S. Subramanian, Code 69Su Department of Mechanical Engineering Naval Postgraduate School Monterey, California 93943-5000	2
8.	LT David W. Bella 5435 Louise Street San Bernardino California 92407	2